

Structural Behavior of Connections between Tunnel Roof and Diaphragm Wall

FE-analysis of the connection in Korsvägen,
part of the West Link Project in Gothenburg

Master's thesis in Master Program Structural engineering and building technology

REBECKA PHILIPSSON FRANZÉN

TAREK ALTOUBAH

MASTER'S THESIS ACEX30

Structural Behavior of Connections between Tunnel Roof and Diaphragm Wall

FE-analysis of the connection in Korsvägen, part of the West Link
Project in Gothenburg

REBECKA PHILIPSSON FRANZÉN AND TAREK ALTOUBAH



Department of Architecture and Civil Engineering
Division of Structural Engineering
CHALMERS UNIVERSITY OF TECHNOLOGY
Gothenburg, Sweden 2022

Structural Behavior of Connections between Tunnel Roof and Diaphragm Wall:
FE-analysis of the connection in Korsvägen, part of the West Link Project in Gothen-
burg

REBECKA PHILIPSSON FRANZÉN AND TAREK ALTOUBAH

© REBECKA PHILIPSSON FRANZÉN AND TAREK ALTOUBAH, 2022.

Supervisors: Christoffer Svedholm, ELU. Anna Teike, Trafikverket. Karin Lund-
gren, Department of Architecture and Civil Engineering
Examiner: Karin Lundgren, Department of Architecture and Civil Engineering

Department of Architecture and Civil Engineering
Division of Structural Engineering
Chalmers University of Technology
SE-412 96 Gothenburg
Telephone +46 31 772 1000

Cover: Photos taken at Korsvägen (9/3-2022) and Centralen (16/3-2022), Gothen-
burg

Department of Architecture and Civil Engineering
Gothenburg, Sweden 2022

Structural Behavior of Connections between Tunnel Roof and Diaphragm Wall:
FE-analysis of the connection in Korsvågen, part of the West Link Project in Gothen-
burg

REBECKA PHILIPSSON FRANZÉN AND TAREK ALTOUBAH

Division of Structural Engineering
Chalmers University of Technology

Abstract

Due to densification of cities and strict demands regarding material use, permanent Diaphragm walls (D-walls) have become a more common option to use as supporting structures of underground tunnels. D-walls require less construction space than more traditional foundation methods and is currently being used in the West Link Project in Gothenburg. The tunnel is only connected to the D-walls through the tunnel roof and thus, the connections become a critical part of the structure. The aim of this project was to investigate a certain connection used in the West Link Project, the load effects on the connection and its behavior regarding cracks.

To study the behavior of the connection, three types of analyses were carried out: two global analyses (one elastoplastic and one elastic) and one local non-linear analysis. An idealized case of the structure in the sub-project Korsvågen in the West Link Project was chosen as a case study. First, a finite element model using plane strain-elements of both the surrounding soil and the structure was analyzed. This model was then compared to a beam model where the effect of the soil was modeled as applied loads. Section forces and moments from the beam model was inserted into a detailed local model, of the critical connection. The local model was analyzed to study the cracks and inelastic behavior of the concrete.

The results showed that the cracking in the connection was extensive, and a large crack developed in the upper corner between the D-wall and the tunnel roof. It was concluded that:

- A tunnel located at a large depth, built with a top-down method results in a critical situation with respect to the connection. The situation in Korsvågen is thus more critical than the other sub-projects in the West Link project.
- The earth pressure developed in the plane strain model, including the non-linear behavior of the soil, showed less mobilization of passive earth pressure than the analyses using a simplified beam model. One reason may be because the soil-structure interaction was included in the plane strain model.
- The assumption of elastic structure, and not including the soil-structure interaction in the simplified beam-model analyses result in too high mobilization of passive earth pressure, and thus the crack widths in the connection were overestimated.
- The FE-analyses indicated that the design of the connection at Korsvågen is not sufficient regarding allowable crack widths. Additional measures such as a haunch, additional struts or lighter backfill, may be used to reduce the crack widths.

Keywords: D-walls, tunnel, connection, The West Link Project, FE-analysis, ABAQUS, Non-linear FE-analysis, Concrete damage plasticity

Acknowledgements

This project was a study of a particular part of the current project, the West Link Project with focus on diaphragm walls and their connection to tunnels. As the last project at the master Structural Engineering and Building Technology, this Master's Thesis has been carried out during the spring term of 2022 at Chalmers University of Technology. The project was written at the division of Structural Engineering in collaboration with ELU and Trafikverket.

We want to thank our supervisor Christoffer Svedholm at ELU for your weekly support and help to push us forward through the FE-analyses. Thank you for being able to answer our never-ending stream of questions. We also want to thank Anna Teike at Trafikverket for your expertise regarding the West Link Project and input to the work. Also, for giving us the opportunity to visit the construction sites of the West Link Project, which was an extraordinary chance to get a better understanding. We want to thank our examiner Karin Lundgren at Chalmers University of Technology for the interesting discussions and important input on the report.

We also want to thank our opponents, Akash Roshan and Omar Darwish, for their feedback and the opportunity to read their work.

Finally, we want to thank our friends and families for their support during this last semester at Chalmers University of Technology.

Rebecka Philipsson Franzén and Tarek Altoubah, Gothenburg, June 2022

Contents

List of Figures	xv
List of Tables	xix
1 Introduction	1
1.1 Background	1
1.1.1 Diaphragm walls	1
1.1.2 The West link project	2
1.2 Problem description	3
1.3 Aim and Objectives	3
1.4 Limitations	3
1.5 Method	3
2 Theory	5
2.1 Geo-technique	5
2.1.1 Soil conditions	5
2.1.2 Earth pressure theory	6
2.2 Material models	7
2.2.1 Mohr-Coulomb	7
2.2.2 Soil-structure interaction	9
2.2.3 Concrete damaged plasticity	9
2.3 Element-types	10
2.3.1 Plane strain element	11
2.3.2 Beam-element	11
3 D-walls	13
3.1 Diaphragm walls	13
3.1.1 Use in Sweden and Worldwide/Previous projects	13
3.1.2 Construction of D-walls	13
3.1.3 Construction of the tunnel	15
3.1.4 Connections	15
3.2 Design code regulations	16
3.2.1 National	16
3.2.2 International	17
3.3 Connections in the West Link Project	17
3.3.1 Rigid connection	18
3.3.2 Hinged connection	20

4	FE-Analysis	23
4.1	FE-model	23
4.1.1	Dimensions and concrete types	23
4.1.2	Material properties	24
4.1.3	Construction phases	25
4.1.4	Assumptions	25
4.2	Two-dimensional plane strain model	26
4.2.1	Loading steps	26
4.2.2	Loads and boundary conditions	27
4.2.3	Interaction	28
4.2.4	Mesh size	28
4.2.5	Comparison with hand calculations	29
4.3	Two-dimensional beam model	29
4.3.1	Loading steps	30
4.3.2	Loads and boundary conditions	30
4.3.3	Interactions	30
4.3.4	Mesh size	31
4.3.5	Correspondence of deformation and stresses with plane strain model	31
4.4	Local FE-model of connection	32
4.4.1	Loading steps	33
4.4.2	Loads and boundary conditions	33
4.4.3	Interactions	34
4.4.4	Mesh type and size	34
4.4.5	Comparison of crack widths, equilibrium and stresses	35
5	Results	37
5.1	Earth pressure along D-wall	37
5.2	Deformations and stresses in D-wall	38
5.3	Crack widths and stresses in connection	41
6	Discussion	47
7	Conclusion	49
7.1	Further studies	49
A	Appendix A	I
A.1	Calculation methods	III
A.1.1	Total stability method	III
A.1.2	Rotation stability method	III
B	Appendix B	V
B.1	Earth pressure and load calculations	V
B.2	Water pressure in plane strain model	XIV
C	Appendix C	XV
C.1	Control of horizontal reaction forces in plane strain model	XV

C.2	Mesh convergence study of plain strain model	XVI
C.3	Complete verification of plane strain model	XVII
D	Appendix D	XIX
D.1	Control of horizontal reaction forces in the beam model	XIX
D.2	Mesh convergence study of beam model	XIX
D.3	Complete verification of beam model	XIX
E	Appendix E	XXXI
E.1	Material and element type of local model	XXXI
E.2	Material and element type of local model	XXXIV
F	Appendix F	XXXVII
F.1	Loads applied to local model	XXXVII
F.2	Mesh convergence study of local model	XXXVII
G	Appendix G	XXXIX
G.1	Verification of crack widths and steel stress at top slab	XXXIX
G.2	Verification of crack widths and steel stress at D-wall	XLII
H	Appendix H	XLV
H.1	Plastic strain in local model	XLVI
H.2	Compression stress in concrete in local model	XLVIII
H.3	Tensile stress in reinforcement in local model	L

List of Figures

1.1	A tunnel connected to D-walls by the tunnel roof	1
1.2	Map of the west link project, Modified by OpenStreetMaps 2015. CC BY-SA 2.0	2
2.1	Active and passive earth pressure acting on the D-wall	6
2.2	The horizontal and vertical stresses acting on a D-wall	7
2.3	The Mohr-Coulomb failure criteria, Modified by Taka2san 2012. CC BY-SA 3.0	8
2.4	Behavior of concrete subjected to uniaxial tension, redrawn from Hibbitt, Karlsson, Sorensen 2011	9
3.1	Machine used to excavate the trench of the D-wall, Photo from Korsvägen 9/3-2022	14
3.2	Construction sequence of D-walls, Modified, by Bertbau 2017. CC BY-SA 4.0	14
3.3	Vertical and horizontal connections of D-walls	15
3.4	Example on how horizontal reinforcement in between D-wall panels can be conducted, redrawn from Alén et al. 2006	16
3.5	Tunnel and D-walls at Korsvägen and Centralen, redrawn from Steffensen 2020 and COWI 2019	19
3.6	Reinforcement bars and couplers in reinforcement cage of a D-wall at Korsvägen, Photo from Korsvägen 9/3-2022	19
3.7	Wooden box covering the couplers at Korsvägen, Photo from Korsvägen 9/3-2022	19
3.8	Reinforcement layout of the rigid connection, redrawn from COWI 2021	20
3.9	Tunnel design with mezzanine slab at Kvarnberget, redrawn from SGS 2020	21
3.10	Shear box with steel plate cover during construction, redrawn from SGS 2020	22
3.11	Shear box with inserted mezzanine slab, redrawn from SGS 2021	22
4.1	Dimensions and concrete types	24
4.2	Construction phases in the top-down method, starting with excavation down to the level of the strut	25
4.3	Plane strain model showing the partitions, material and paths used for extraction of stresses	26

4.4	Boundary conditions and loads in the soil model in step 11	27
4.5	Connection between top slab and D-wall in the plane strain model . .	28
4.6	Connection between cross-wall and D-wall in the plane strain model .	28
4.7	Beam model in the permanent state	29
4.8	Connection between top slab and D-wall in beam model	31
4.9	Shapes and percentage needed for 50% and 100% mobilized passive earth pressure (SIS 2005b)	32
4.10	Dimensions of the submodel	32
4.11	Nodes in the beam-analysis used to gather section forces and moments	33
4.12	Boundary conditions and loads applied to the submodel	34
5.1	Comparison of the horizontal and vertical earth pressure between the plane strain model and hand calculated values	38
5.2	Deformation of D-wall when the top slab is inserted, step 4 in beam model analysis	39
5.3	Comparison of the deflection and vertical stresses in the D-wall be- tween the two models, having applied the mobilized passive earth pressure in the beam model	40
5.4	Comparison between the horizontal earth pressure applied in the beam model and the extracted earth pressure in the plane strain model	41
5.5	Concrete stresses in the permanent stage	42
5.6	Steel stresses at the permanent stage	42
5.7	Largest and second largest cracks in the permanent stage	43
5.8	Largest and second largest cracks marked in construction phase 5, excavation to bottom slab after backfilling	44
5.9	Different types of cracks in construction phase 5, excavation to bot- tom slab after backfilling	45
A.1	Figure of failure surface and slices in the total stability method	IV
A.2	Calculation properties of the rotational stability check	IV
B.1	Calculations steps in soil model with varying water pressure	XIV
C.1	The different reaction forces and force at the bottom of the D-wall used for the control	XV
C.2	Convergence study of different element-lengths in the D-wall, tunnel and soil	XVI
C.3	Complete verification of the horizontal earth pressure	XVII
C.4	Complete verification of the vertical earth pressure	XVIII
D.1	Convergence study of the 2D beam model	XIX
F.1	Convergence study of the 2D local model of the connection	XXXVIII
H.1	Plastic strain in submodel in construction phase 3-5	XLVI
H.2	Plastic strain in submodel in construction phase 6-7	XLVII
H.3	Compression stress in concrete in construction phase 3-5	XLVIII
H.4	Compression stress in concrete in construction phase 6-7	XLIX

H.5	Tensile stress in reinforcement in construction phase 3-5	L
H.6	Tensile stress in reinforcement in construction phase 6-7	LI

List of Tables

4.1	Elastic properties of the different materials	24
4.2	Soil properties	24
4.3	Loading steps in the plane strain model	27
4.4	Mesh size in soil model	29
4.5	Loading steps in beam model	30
4.6	Loading steps in local model analysis	33
4.7	Parameters defining the yield surface of the concrete in the submodel	34
4.8	Verification of equilibrium in the submodel	35
5.1	Crack widths and spacing in the different steps	44
A.1	National and international standards treating D-walls	II
C.1	Ratio between the horizontal force at the bottom of the D-wall and the different horizontal reaction forces along the symmetry line in the plane strain model	XV
D.1	Comparison between the horizontal force at the bottom of the D-wall and the different horizontal reaction forces along the symmetry line in the beam model	XIX
F.1	Section forces/moments inserted at the upper reference point in the D-wall	XXXVII
F.2	Section forces/moments inserted at the reference point in the top slab	XXXVII
F.3	Section forces/moments inserted at the reference point in the inner wall	XXXVII

1

Introduction

1.1 Background

1.1.1 Diaphragm walls

During excavation at construction sites support constructions are needed. One example is retaining walls which can be executed as sheet pile walls, secant pile walls or diaphragm walls. Diaphragm walls can, in addition to be used as retaining walls, also be used as deep foundation elements, cut-off walls or for slope stabilization (Scholz 2021). The D-walls can be temporary or permanent construction parts, in the latter case they are used as part of the permanent structure. The D-walls are often produced in concrete and cast in-situ (Alén et al. 2006). The casting of such a wall is often done panel-wise where each trench is excavated, filled with a supporting liquid, reinforced, and then casted. An example of a tunnel constructed with permanent D-walls is shown in Figure 1.1.

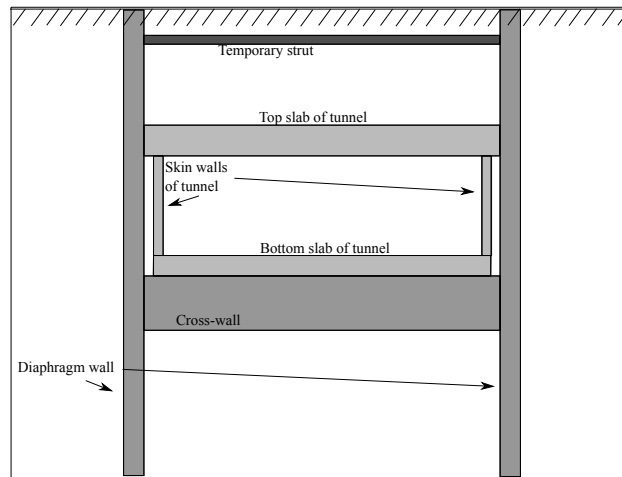


Figure 1.1: A tunnel connected to D-walls by the tunnel roof

Regulations regarding D-walls are today very few, especially when it comes to design (Alén et al. 2006). The European Standard EN 1538 contains regulations regarding the performance and execution of D-walls and is one of the regulations used in Sweden today. Regarding the design, some national regulations have been established, for example Krav TRVINFRA-00227 (Trafikverket 2021b) and Krav Tunnelbygande (Trafikverket 2016a) as well as additional documents regarding advises to the

two “krav”-documents. There is also some additional information and requirements regarding permanent D-walls in the Swedish Transport Administration document about geotechnics, TRVINFRA-00230 (Trafikverket 2022).

1.1.2 The West link project



Figure 1.2: Map of the west link project, Modified by OpenStreetMaps 2015. CC BY-SA 2.0

The West Link Project is a current railway-project in the city center of Gothenburg. The railway is mainly being built as a tunnel with three main stations, Centralen, Haga and Korsvägen, see Figure 1.2. The construction of the tunnel and stations is divided into four main contracts; Centralen, Kvarnberget, Haga and Korsvägen (Trafikverket n.d.). Since the four different sub-projects have different geotechnical conditions, local geotechnical variations and different contractors, the excavations and support constructions differ. At Korsvägen, Centralen and Kvarnberget the tunnel will be built using permanent D-walls reaching all the way down to bedrock or cut off in a deep clay layer. The tunnel itself will be connected to the D-walls through the roof of the tunnel, see Figure 1.1. Below the tunnel, cross-walls will in some locations be placed to increase the stability (Steffensen 2020). The cross-walls are similar to D-walls but are unreinforced and not casted up to the surface. To account for uncertainties related to the cross-walls they should be treated as temporary structures. With time, the cross-walls, which are not designed to be durable, are assumed to lose all their load-bearing capacity. Without cross-walls, the only contact between the tunnel and supporting structures will be the connection through the tunnel roof and D-walls. Thus, this connection becomes critical.

1.2 Problem description

The connection between the tunnel roof and the D-wall can be designed in several ways, acting as either rigid or hinged. With few requirements and previous projects using D-walls as permanent structures, the knowledge of modeling and designing of D-walls and the connection is limited. Different FE-analyses were carried out to find a way to model the structure and the connection based on the situation in Korsvägen in the West Link Project. In addition, the crack-pattern and widths but also the load transfer and FE-modelling techniques were analyzed to evaluate important aspects when designing D-walls.

1.3 Aim and Objectives

The aim of this project was to investigate the connection between a diaphragm wall and tunnel roof at Korsvägen. The specific objectives were:

- What specific conditions characterize the construction at Korsvägen and what differences exists compared to the other sub-projects?
- How can the soil, structure and soil-structure interaction be modeled and verified?
- Is it possible to analyze the load-effects of the connection without including the soil in a FE-model?
- How can the crack-pattern and crack widths in the connection be analyzed and how do they correspond to hand-calculations used for design?
- Is the design of the connection sufficient regarding crack-limits? If not, suggest possible modifications with the potential to meet the requirements.

1.4 Limitations

The focus of this work was the connections between D-walls and tunnel roof of an underground tunnel in an idealized soil profile. The limitations was summarized into the following points:

- The analyses were done in two dimensions. Thus, any three dimensional effects were not considered.
- The dimensions, construction method, connection type and foundation of the D-walls were kept constant, the analysis was limited to the conditions at Korsvägen.
- No time-dependent effects were considered and characteristic values were used.

1.5 Method

The project started by a literature review of D-walls, requirements, geotechnics, and the West Link Project. In addition to the literature reviewed about the West Link Project, three study visits were conducted. At Korsvägen, the 9:th of March 2022, at Centralen, the 16:th of March 2022 and at Kvarnberget, the 18:th of March 2022.

At Korsvägen the focus was the reinforcement cages of the D-walls, at Centralen the focus was on the reinforcement of the top slab and the couplers in the connection. At Kvarnberget, there was mainly focus on the construction site and D-walls. Inspired from Korsvägen in the West Link Project, the dimensions of the structure, an idealized soil profile and the connection was established. Three FE-analyses were conducted using the FE-software ABAQUS. The first model was a 2D plane strain model where the soil and D-wall were modelled using Mohr-coulomb material and plane strain elements. The second model was a 2D beam model in which the D-wall and tunnel were modelled with beam-elements and the horizontal earth pressure in the soil was introduced as loads. The two models were correlated by comparing the results regarding deformations and stresses in the D-wall and the tunnel roof. The local behavior of the connection was modelled by a local model using continuum elements in a non-linear 2D analysis, using results from the beam model as boundary conditions. A plastic- and damage behavior were used to analyze the concrete regarding the crack-pattern and crack widths. The method can be summarized into the following steps:

1. Literature review
2. Study visits
3. Linear analysis of 2D plane strain model
4. Comparison with hand-calculations of earth pressure
5. Linear analysis of 2D beam model
6. Correlation of deformations and stresses with the plane strain analysis
7. Non-linear analysis of 2D local model
8. Comparison of results with hand-calculated crack widths, spacing and stresses
9. Analysis of results
10. Draw conclusions

2

Theory

D-walls are underground structures, thus the soil conditions and properties become important to understand the loads acting on the structure. In addition, there are several material models and elements-types which can be used to analyse the load effects and behaviour of D-walls and tunnel.

2.1 Geo-technique

Diaphragm walls are in some cases used as supporting structures and thus considered to be part of the foundation. Since they are embedded in soil, the most essential loads acting on the structure will be the ones coming from the soil pressure. The geotechnical parameters and soil conditions often vary from one place to another which creates a large difference in load effects acting on D-walls. To account for these variations of situations some different parameters and conditions have to be specified.

2.1.1 Soil conditions

Soil is a three-phase material consisting of three different components, water, air and solid particles (Helwany 2007). To separate different types, the soil is divided with respect to particle size. The different types are, with a decreasing particle size, gravel, sand, silt and clay. Gravel, sand and silt is considered to be cohesionless since the particles do not adhere to each other in the presence of water. Clay particles start to adhere to other clay particles when water is present and is thereby considered to be a cohesive soil. The solid particles of the soil is weathered rocks (Helwany 2007). If water is present and all voids in the soil are filled, the soil is saturated and when the water is drained, the soil is unsaturated. In different locations the layers of different soil types are different regarding sequence and thickness of each layer. However, the most common sequence is some sort of sand followed by a clay or silt layer which reaches down to bedrock or moraine. The soil is assumed to be fully saturated beneath the groundwater level and fully drained above.

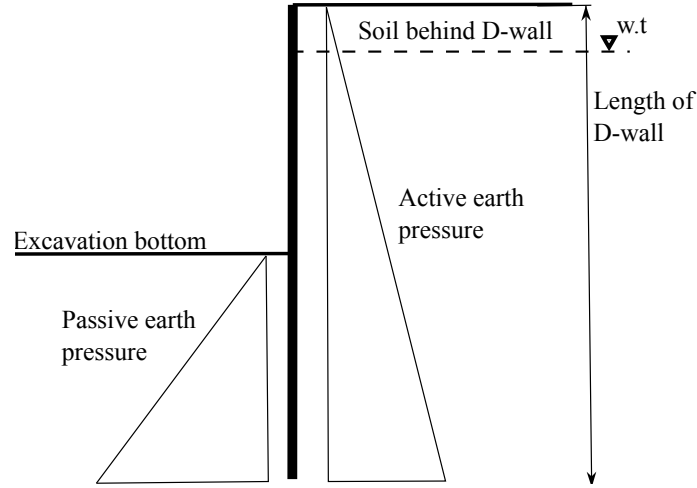


Figure 2.1: Active and passive earth pressure acting on the D-wall

The soil can also be divided into different states, at rest, active and passive (Helwany 2007). The at rest state will occur when the D-wall is restricted from any movement in the lateral direction. The active state occurs when the wall is allowed to move away from the soil, to the right in Figure 2.1, and is a destabilizing pressure. The active pressure is in that case developed at the right side of the D-wall. The passive earth pressure develops at the excavation side when the soil moves towards that soil, to the left in Figure 2.1. The movement required to mobilize passive earth pressure is larger than the movement required to mobilize active earth pressure (SIS 2005b). The most critical case occurs when complete active pressure is mobilized at the right side of the D-wall and complete passive pressure is mobilized on the left side.

2.1.2 Earth pressure theory

Stresses in the soil is depending on the density of the soil and can be separated into a vertical and horizontal component, see Figure 2.2 (Helwany 2007). The vertical stress, σ_v is calculated as:

$$\sigma_v = z * \gamma_{sat} \quad (2.1)$$

where z is the depth and γ_{sat} is the saturated soil density. The effective stress, σ'_v , is expressed in terms of the stress σ_v and the pore water pressure u according to:

$$\sigma'_v = z * (\gamma_{sat} - \gamma_w) = z * \gamma' = \sigma_v - u \quad (2.2)$$

Where γ' is the effective soil density, equal to the saturated soil density, γ_{sat} , reduced by the water density, γ_w .

When the soil is completely dry, the effective stress will be equal to the total stress. The pore water pressure, u , is:

$$u = H_w * \gamma_w \quad (2.3)$$

Where γ_w is the water density and H_w is the depth of the groundwater. The soil density is also referred to as the unit weight of the soil (Helwany 2007).

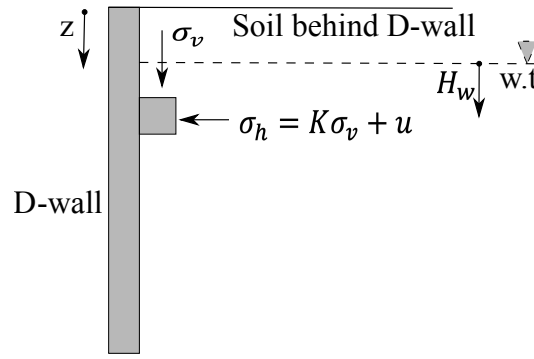


Figure 2.2: The horizontal and vertical stresses acting on a D-wall

To estimate the horizontal component of the stress, a lateral earth pressure coefficient has to be defined, K in Figure 2.2. This coefficient depends on which state the soil is in and is calculated according to Equation 2.4 to 2.6 where ϕ is the internal friction angle of the soil (Trafikverket 2011). K_0 is the at rest, K_a is the active and K_p is the passive lateral earth pressure coefficient. The horizontal stress-component is calculated according to Equation 2.7.

$$K_0 = 1 - \sin\phi \quad (2.4)$$

$$K_a = (1 - \sin\phi)/(1 + \sin\phi) \quad (2.5)$$

$$K_p = (1 + \sin\phi)/(1 - \sin\phi) \quad (2.6)$$

$$\sigma_h = K * \gamma_{sat} * z + u(z) \quad (2.7)$$

where the coefficient, K , vary between K_0 , K_a and K_p , depending on the current state of the soil.

2.2 Material models

There are several material models that can be used to describe the behaviour of soil and concrete. The two models used in this work, in addition to the elastic behaviour, is Mohr-Coulomb and Concrete damaged plasticity.

2.2.1 Mohr-Coulomb

The Mohr-Coulomb model is the most common material-model to use in geo-techniques (Jansson and Wikström 2006). The Mohr-Coulomb failure criterion is describing under which circumstances an isotropic material, such as soil, will fail. The failure criteria is the line denoted by τ in Figure 2.3.

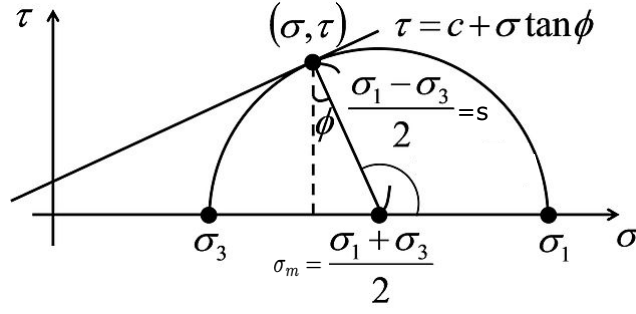


Figure 2.3: The Mohr-Coulomb failure criteria, Modified by Taka2san 2012. CC BY-SA 3.0

The criterion is expressed as a function of a major and minor principal stress, σ_1 , and, σ_3 , in Figure 2.3. It can also be expressed as a function of normal stress, σ_m , and shear stress, s , (Knappett 2012). The criterion is based on Mohr and Coulomb which each state different assumptions. The assumption of Mohr is that failure will only depend on the minor and major principal stresses and the location of the normal stress and shear acting on a failure plane. The terms of Coulomb are based on the assumption that the failure envelope is linear and is used to determine the critical combination of the normal stress and shear (Knappett 2012). The strength parameters of the soil is the cohesion and the internal friction angle, denoted as c and ϕ (Helwany 2007). These will, according to the Mohr-Coulomb failure criteria, together with the effective vertical stress define the shear strength of the soil, τ , Equation 2.8. The shear strength, the failure envelope, is thereby constructed in such way that if it is exceeded, the soil fails.

$$\tau = c + \sigma \tan \phi \quad (2.8)$$

From Mohr's circle we can then express the shear and stress as:

$$\tau = s * \cos \phi \quad (2.9)$$

and

$$\sigma = \sigma_m + s * \sin \phi \quad (2.10)$$

where

$$\sigma_m = \frac{\sigma_1 + \sigma_3}{2} \quad s = \frac{\sigma_1 - \sigma_3}{2} \quad (2.11)$$

In addition to the internal friction angle and cohesion, the dilation angle is also needed to define the yield stress criterion is the dilation angle. The dilation angle is calculated as.

$$\psi = \phi - 30^\circ \quad (2.12)$$

where both ψ , the dilation angle, and ϕ , the internal friction angle, is expressed in degrees (Bartlett 2012).

2.2.2 Soil-structure interaction

The interaction between the soil and the concrete must also be modeled. According to TK geo 11 (Trafikverket 2011) the friction coefficient between the soil and the D-walls should be:

$$\mu = \tan \phi \quad (2.13)$$

Where ϕ is the internal friction angle of the soil layer. When having an internal friction angle of 35° the friction coefficient is 0.7. Decreasing the internal friction angle also decrease the friction coefficient.

2.2.3 Concrete damaged plasticity

To describe the non-linear behavior of concrete it is possible to use a concrete damaged plasticity material model. The model is based on the assumptions that the concrete will fail by either cracking or crushing (Jankowiak and Lodygowski 2005). The mechanical behavior in uniaxial tension is described by Figure 2.4.

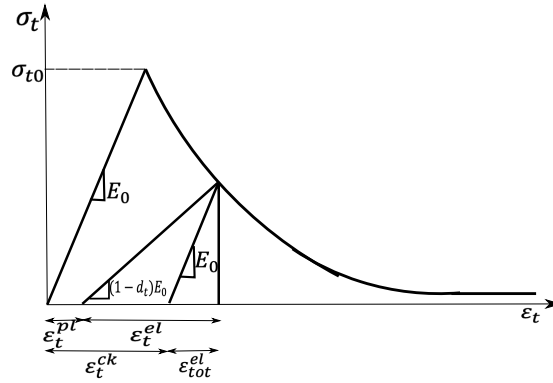


Figure 2.4: Behavior of concrete subjected to uniaxial tension, redrawn from Hibbitt, Karlsson, Sorensen 2011

The damage parameter in tension d_t is defined in terms of cracking strain ε_t^{ck} , modulus of elasticity of uncracked concrete, E_0 , tensile stress, σ_t , and b_t which is the relation between the plastic and cracking strain, often set to 0.7 (Zangeneh Kamali 2012). The cracking strain is calculated by:

$$\varepsilon_t^{ck} = \varepsilon_t - \frac{\sigma_t}{E_0} \quad (2.14)$$

Where ε_t is the total strain and σ_t/E_0 is the elastic strain, see Figure 2.4. The damage parameter is calculated for different tensile stresses and cracking strains with Equation 2.15.

$$d_t = 1 - \frac{\sigma_t * E_0^{-1}}{\sigma_t * E_0^{-1} + \varepsilon_t^{ck}(1 - b_t)} \quad (2.15)$$

From the damage parameter and cracking strain, the plastic strain can be estimated according to (Wahalathantri et al. 2011):

$$\varepsilon_t^{pl} = \varepsilon_t^{ck} - \frac{d_t}{1 - d_t} \frac{\sigma_t}{E_0} \quad (2.16)$$

In addition to the damage parameter, the tension softening behavior after cracking can be described by a stress-crack opening displacement relation:

$$\sigma_t(w) = \left(\left(1 + \left(\frac{c_1 * w}{w_c} \right)^3 \right) * e^{-c_2} * \frac{w}{w_c} - \frac{w}{w_c} * (1 + c_1^3) * e^{-c_2} \right) * f_{ctm}, \quad (2.17)$$

according to Hordjik (Zangeneh Kamali 2012). c_1 and c_2 are constants while w_c is the maximum crack opening based on the fracture energy and the mean tensile strength.

$$w_c = 5.14 \frac{G_f}{f_{ctm}} \quad (2.18)$$

w is the crack opening displacement for a certain tensile stress smaller than the mean tensile strength. The fracture energy, G_f is calculated according to Model code 2010 (fib special activity group, and Taerwe, Luc and Matthys, Stijn 2013).

To define the yield surface and plastic flow, the dilation angle, ψ , the eccentricity, ϵ , the relation between the equibiaxial and uniaxial compressive yield stress, f_{b0}/f_{c0} , a coefficient depending on the stress invariants, K_c and a viscosity parameter, μ , are needed. The plastic flow follows the equation (Lubliner et al. 1989):

$$G = \sqrt{(\epsilon * \sigma_{t0} * \tan\psi)^2 + q^2} - p * \tan\psi \quad (2.19)$$

The dilation angle ψ is measured in the p-q plane and σ_{t0} is the uniaxial tensile stress at failure. The dilation angle is often set to a value in-between 35-40 degrees (Malm 2009). The viscosity parameter is often set to 0.1. p is the hydrostatic pressure and q is the Mises equivalent effective stress (Lubliner et al. 1989). The yield stress function is:

$$F = \frac{1}{1 - \alpha} (q - 3\alpha p + \beta(\epsilon^{pl}) \langle \sigma_{max} \rangle - \gamma \langle -\sigma_{max} \rangle) - \sigma_c(\epsilon^{pl}) = 0 \quad (2.20)$$

Where:

$$\alpha = \frac{(f_{b0}/f_{c0}) - 1}{2(f_{b0}/f_{c0}) - 1} \quad (2.21)$$

$$\beta = \frac{\sigma_c(\epsilon_c^{pl})}{\sigma_t(\epsilon_t^{pl})} (1 - \alpha) - (1 + \alpha) \quad (2.22)$$

$$\gamma = \frac{3(1 - K_c)}{2K_c - 1} \quad (2.23)$$

σ_{max} is the maximum principal effective stress. The most common value of f_{b0}/f_{c0} is 1.16. K_c is ranged between 0.5 and 1 but most often set to 2/3. $\sigma_t(\epsilon_t^{pl})$ and $\sigma_c(\epsilon_c^{pl})$ is the tensile and compressive cohesion stress respectively (Zangeneh Kamali 2012).

2.3 Element-types

There are several element-types that can be used to model soil and concrete. The choice of element-type depends on which type of structure or material are modeled.

2.3.1 Plane strain element

Plane strain elements can be used in two-dimensional analyses combined with several material models (Helwany 2007). The type of element assumes that the strain in the part is only dependent on planar coordinates (SIMULIA 2022). Thus, the strain in the out of plane normal and shear direction is zero. The element-type can be used in combination with both Mohr-coulomb and concrete damage plasticity material models. When using plane strain elements, the part should be defined in the X-Y plane, including the loading, and the result in terms of deformations will also be confined to the same plane. The element-type is often used when having parts that have a large width in the out of plane direction compared to its width in the plane. For example, concrete dams, walls, and underground tunnels (Helwany 2007). The output when having plane strain elements does not allow extraction of section forces and moments directly but enable extraction of stresses and deformations in both x- and y-direction.

2.3.2 Beam-element

Beam-elements are a one-dimensional type of element and can be either an Euler-Bernoulli or a Timoshenko beam (SIMULIA 2022). The Euler-Bernoulli is often used when analyzing slender beams while Timoshenko can be used for both slender and thicker beams. Another difference between the two types is that the Timoshenko beam permit shear deformations while the Euler-Bernoulli does not. The behavior of the Timoshenko is assumed to be linear elastic in shear. When using the Timoshenko element type, a transverse shear stiffness is calculated by the FE-program and it is thus possible to subject the beam to axial strains (SIMULIA 2022). In addition, the modulus of elasticity defining the shear behavior is definite with no regard of bending or axial stretch. When using beam-elements, it is possible to extract the section forces and moments directly from the element-nodes.

3

D-walls

3.1 Diaphragm walls

Diaphragm walls are a common type of construction used as retaining walls and support construction when excavating (Alén et al. 2006). They have initially only been used as temporary structures in Sweden, but in many other parts of the world they are used as permanent structure. Diaphragm walls are built by rectangular panels connected into a complete wall through vertical joints. The most common material to use is reinforced concrete that is cast in situ (Alén et al. 2006).

3.1.1 Use in Sweden and Worldwide/Previous projects

Diaphragm walls have previously been used as temporary support structures during construction of Götatunneln in Gothenburg in 2001-2006 (Alén et al. 2006). This tunnel was, similarly to the current West Link Project, built in loose clay with cross-walls underneath the bottom of the tunnel. Another Swedish example where D-walls were used as temporary structures, was during construction of Citytunneln in Malmö. Citytunneln was, in contrast to the other projects, built in clay-moraine (Alén et al. 2006). Diaphragm-walls are in general used in dense city centers to lower the impact on the surroundings and take advantage of the limited space needed during construction. The use of D-walls as both temporary and permanent structures is very common in Europe and the USA (Technical Committee on Performance of Structures during Construction 2000).

Some examples where D-walls were used as part of the permanent structures are the railway-tunnel Studentertunden and SAS Radisson Hotel, both located in Oslo, Norway (Alén et al. 2006). The use of diaphragm walls, both as temporary and permanent, are more common for example in Germany where the first D-wall projects were executed already in 1959 in Berlin and Munich (Dausch 2020). Since then, the regulations, machines and construction of D-walls have been further developed and the construction of D-walls are nowadays quite different from the first projects (Dausch 2020).

3.1.2 Construction of D-walls

Diaphragm-walls, both permanent and temporary, are built before excavation of the construction site (Alén et al. 2006). The construction of the walls is done panel wise but not always subsequently, adjacent panels might not be built directly after one

another. The first step in the construction phase is to excavate a trench, which will act as formwork to the panel (Alén et al. 2006). The trench is being excavated using a special type of machine, see Figure 3.1, that will dig downwards while it collects the soil and carries it up, where it is collected and deported. When the trench is formed it is filled with a supporting liquid, either water or bentonite, which stabilizes it and ensures that it stays the wanted size. Into this liquid, a reinforcement cage is inserted, which also contains reinforcement bars used for the vertical and horizontal joints (Alén et al. 2006). The next step is to cast the actual wall which is done in place and from the bottom and up, while the support fluid is being pumped out. It is possible to use prefabricated elements as well, but the most common way is to cast in situ. Since there is no way to vibrate the concrete in the trench, it is important that the casting is done with proper speed. Also, the casting must be done before the concrete at the top hardens and closes the trench. With the casting being done from the bottom and up, the oldest concrete appears at the top (Teike 2022a). The speed is consequently important to make sure the wall gets the desired properties. The procedure of construction is summarized in figure 3.2. Since the casting is done into the supporting liquid, it is often considered as an underwater casting and should comply with the corresponding regulations (Alén et al. 2006).



Figure 3.1: Machine used to excavate the trench of the D-wall, Photo from Korsvägen 9/3-2022

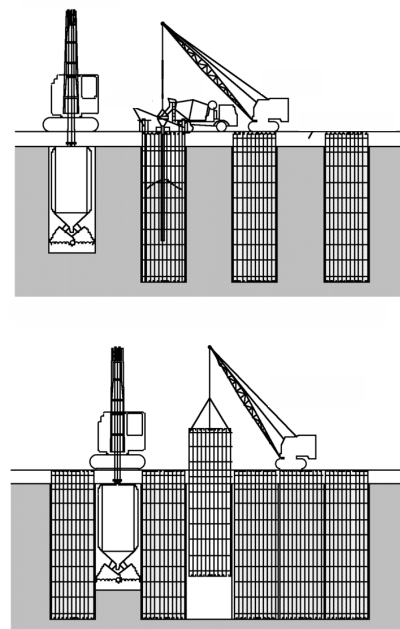


Figure 3.2: Construction sequence of D-walls, Modified, by Bertbau 2017. CC BY-SA 4.0

3.1.3 Construction of the tunnel

When the construction of the diaphragm wall is done, there are several ways to build the tunnel. One way is the top-down method (Teike 2022a). In this method, excavation is done down to the bottom of the tunnel-roof which then is casted and connected to the D-wall and the space above is backfilled. After this, excavation beneath the roof is done where the bottom slab and walls of the tunnel are installed. The underground excavation makes it possible to use the ground above the tunnel before the construction is complete. The tunnel is thereby built from the top down (Teike 2022a).

When D-walls are a permanent part of the tunnel, it can either act as the wall of the tunnel or be constructed as a two-part wall, with an inner wall called skin wall. The reasons to use a two-part wall are high requirements of water tightness, fire-safety, chloride-attacks or freeze. In some projects where there is risk of large deformations or extra stabilizing measures are needed, cross-walls can be built in between the D-walls (Alén et al. 2006). The cross-walls are in that case being built in a similar way as the D-walls but not casted all the way up. The casting of the cross-walls are done after casting the D-walls and before construction of the tunnel.

3.1.4 Connections

The connections in a tunnel supported by D-walls can be divided into two groups, vertical and horizontal. The horizontal type is between the D-walls and tunnel-structure, either the top and bottom slab or both and the vertical connections are between D-wall panels, see Figure 3.3.

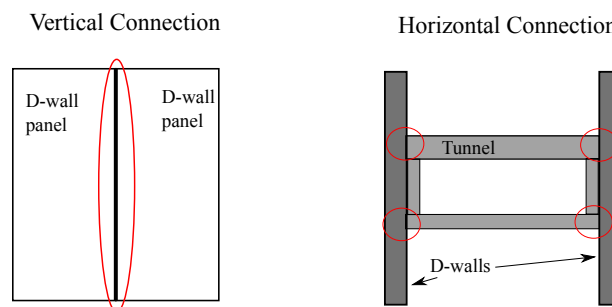


Figure 3.3: Vertical and horizontal connections of D-walls

The vertical joints between the panels are in most cases executed without reinforcement. Thus, moments and traction-forces are not transferred from one panel to another. Instead, each panel is designed to carry all forces acting on it and the joint will only be able to take shear forces and friction. In some special cases, horizontal reinforcement in between the panels might be necessary, but do often contribute to a more complex arrangement of the reinforcement cage and inferior quality of the casting (Alén et al. 2006). When using horizontal reinforcement between two panels the casting sequence of panels must be done in a certain order using a primary and secondary type of reinforcement cages, see Figure 3.4. The secondary reinforcement cage is placed in between two panels casted with primary reinforcement cages. The

trench of the primary panels must be larger than the primary panels being casted, such that some of the reinforcement is reaching out into the secondary panel.

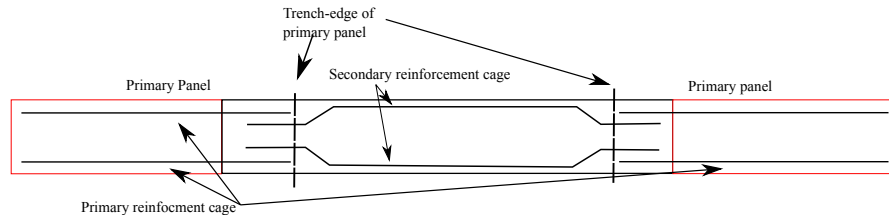


Figure 3.4: Example on how horizontal reinforcement in between D-wall panels can be conducted, redrawn from Alén et al. 2006

The horizontal connections are possible to design in several ways but act as either rigid or hinged. Both types are used in the West Link Project and is further described in Chapter 3.3. The horizontal joints are often reinforced when executed as rigid connections and, in such case, part of the reinforcement cage. The reinforcement cage of the D-wall then needs to be adapted and designed with a connection to the tunnel. This is often done by couplers which need to be strictly monitored when it comes to the depth in the ground, due to strict requirements for deviation in the concrete cover in the tunnel roof (Teike 2022b). The same applies for hinged connections where the designated box for the insertion of the top slab, or bottom slab, needs to be located at the correct height (Caster, Kendes, and Thunström 2022).

3.2 Design code regulations

Requirements regarding diaphragm walls are today quite few. D-walls have internationally been used for a long time and the use will likely increase as cities densify. Although, regulations regarding these types of retaining walls are not developing at the same pace. The regulations can be divided into national regulations, valid in Sweden, and international regulations.

3.2.1 National

The Swedish regulations for D-walls are mainly Krav TRVINFRA-00227 (Trafikverket 2021b) and Krav TRVINFRA-00230 (Trafikverket 2022). The documents Krav Tunnelbyggande (Trafikverket 2016a) and Råd Tunnelbyggande (Trafikverket 2016b) treat regulations regarding design and construction of tunnels in general but do not mention diaphragm walls explicitly. An overview of all the different regulations is presented in Table A.1. The document about bridge-building do mention diaphragm walls, but only briefly (Trafikverket 2021b). For example, the document advice that a two-part construction should be used if the structure is exposed to frost attack, chloride attack or fire. Krav TRVINFRA-00230 (Trafikverket 2022) is the document that contains the most with regard to D-walls and recently replaced the document TK Geo. It regulates the design methods of the D-walls in ultimate limit state, with

partial coefficients, with characteristic values and in service limit state (Trafikverket 2022). These documents are all produced by the Swedish Transport Administration.

3.2.2 International

In addition to the Swedish regulations there are also some international regulations. The European standard “EN 1538 Execution of special geotechnical work - Diaphragm walls”, is also valid in Sweden and referred to as SS-EN 1538 : 2010 + A1 : 2015 (Swedish Standards Institute 2015). This standard treat recommendations and requirements regarding geotechnical situations, materials and products, execution, and supervision, testing and monitoring. It also has a chapter about considerations during design. Whenever some of the national documents have a stricter requirement than SS-EN 1538, the national should be applied. The SS-EN 1538 does not contain any direct requirements regarding the horizontal joints between the roof and the D-wall but does specify some requirements regarding the vertical joints between panels. Although, the SS-EN 1538 regulates the rebar-spacing which might be interpreted as a requirement of the layout of a rigid connection. These other requirements can, however, in some way affect the joints between the D-walls and top slab of the tunnel. In addition to SS-EN 1538, the European standard regarding design of concrete structures, Eurocode 2, is valid (SIS 2005a). In Germany it is significantly more common to build with D-walls, both as temporary and permanent structures. As a result, Germany has its own national regulations (Dausch 2020). The first versions of these national regulations, called DIN 4127 and DIN 4126, were published already in 1986.

3.3 Connections in the West Link Project

There are several parameters that differ between the different sub-projects in the West Link Project. These parameters affect the D-wall and the behavior of the connection between the tunnel roof and D-walls. Example of such parameters are:

- Foundation of D-wall
- The depth of the tunnel
- Construction method of tunnel
- Type of connection

The insertion ratio, the length of the D-wall underneath the excavation bottom to the excavation depth, have a large impact on the maximum horizontal displacement of the D-wall and settlements of the surrounding soil (Feng et al. 2022). Both the settlements and deformations decrease for a higher ratio. Having the same length of a D-wall, the ratio decreases with an increasing depth of the tunnel. Although, when the ratio exceed 0.6 the impact of the insertion ratio is smaller than for lower ratios (Chen et al. 2020). A larger depth of the tunnel also results in a larger weight from the backfill on top of the tunnel, resulting in a larger load in the connection between the D-wall and tunnel roof.

The two different types of construction methods that can be used to build the tunnel is the top-down and bottom-up method. According to Xu, Zhu, and Ding 2021

the construction method affects the deflection of the D-walls. In general, using a top-down method lead to smaller deflections of the walls compared to using the bottom-up method. In the bottom-up method, the top slab is supported on the skin wall, and the bottom slab, before backfilling. Thus, the weight from the backfill does not have to be carried entirely through the connection. Each phase in the top-down method is further described in Chapter 4.1.3.

The two types of connections, hinged and rigid, have large differences and thus different advantages and disadvantages. The hinged connection has no reinforcement through the connection which leads to a reduced risk of bentonite inclusion (Mortier et al. 2013). Although, it might lead to larger deflections of the D-wall and thereby larger settlements in the surrounding soil. This might be a decisive point since D-walls are often used in dense city areas. The use of a hinged connection also creates a demand to control every load case and fatigue. Having a hinged connection will result in a larger field moment in the top slab. The rigid connection, on the other hand, requires more reinforcement but often leads to less settlements in the soil (Mortier et al. 2013). The disadvantage with more reinforcement is that the casting of the concrete becomes more critical due to the difficulties getting the concrete in between the rebars. The rigid connection also has a higher risk of resulting in large cracks at the top of the tunnel roof near the connection due to larger moment in the upper edge. This may lead to deterioration and reduced service life or need of repair.

3.3.1 Rigid connection

The sub-projects of the West Link Project using a rigid connection between the tunnel roof and D-walls, are Korsvägen and Centralen. The sub-project Korsvägen is located southeast from the city center of Gothenburg. The tunnel is going through a varying landscape, located in either rock or clay, whereas the parts located in clay are supported by D-walls (Steffensen 2020). The design of the tunnel, including the D-walls and connection is shown to the left in Figure 3.5. The height above the top slab needed to be backfilled is 9.2m. The connection between the top slab and D-walls is a rigid connection with reinforcement going through the connection. The sub-project Centralen, to the right in Figure 3.5, also has a rigid connection with couplers but have a smaller total depth and is only backfilled approximately 4 m (COWI 2019). Another difference between the two locations is that the D-walls at Korsvägen is founded at bedrock while the D-walls at Centralen ends in clay. The construction method in Korsvägen is a top-down method while the tunnel is built from the bottom up in Centralen. When comparing the two locations, Korsvägen and Centralen, it can be argued that Korsvägen is more critical regarding the connection, mainly due to the construction method and the depth of the tunnel.

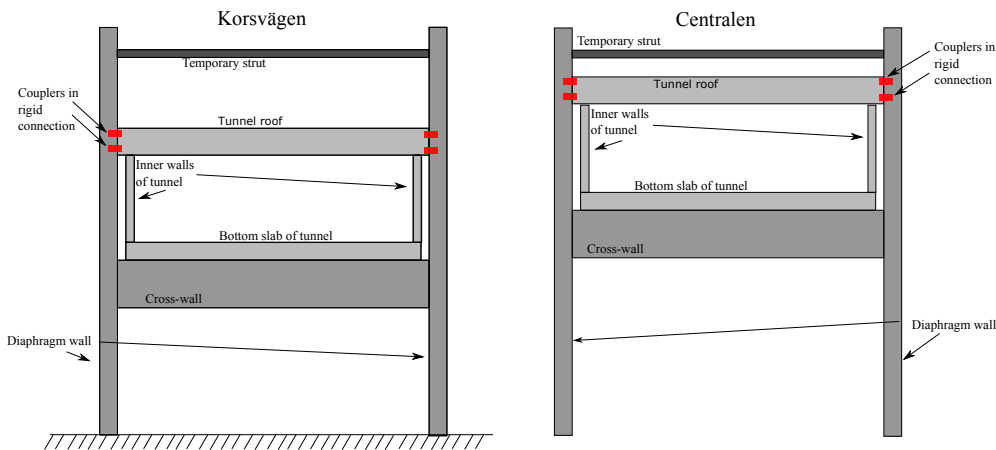


Figure 3.5: Tunnel and D-walls at Korsvågen and Centralen, redrawn from Stefensen 2020 and COWI 2019

The rigid connections used in Korsvågen and Centralen are designed to transfer moments and transversal forces from the tunnel roof into the D-wall. The reinforcement in the tunnel roof needs to be connected with full anchorage length in the D-wall. The anchorage length ends with a coupler, seen at the upper left in Figure 3.6. The coupler is needed since the two parts, the D-wall and tunnel roof, are casted at different times. The couplers are covered by a wooden box when the reinforcement cage of the D-wall is lowered into the excavation trench, see Figure 3.7, and then uncovered after the casting of the D-wall is done.



Figure 3.6: Reinforcement bars and couplers in reinforcement cage of a D-wall at Korsvågen, Photo from Korsvågen 9/3-2022



Figure 3.7: Wooden box covering the couplers at Korsvågen, Photo from Korsvågen 9/3-2022

The reinforcement layout of the connection is shown in Figure 3.8, showing both shear and longitudinal reinforcement. The couplers have a radius of 45mm and a length of 108mm, based on the coupled rebars having a diameter of 32mm. The limited crack widths in the top slab and D-wall is according to the RKF 0.2 mm and 0.3 mm respectively, (Steffensen 2020). The construction company which designed the connection could not meet the requirements regarding crack widths in the top slab during construction. However, an exception was allowed, accepting a crack width of 0.55mm during construction. This was accepted if provided additional measures were taken to prevent the connection to deteriorate and measuring of the crack width.

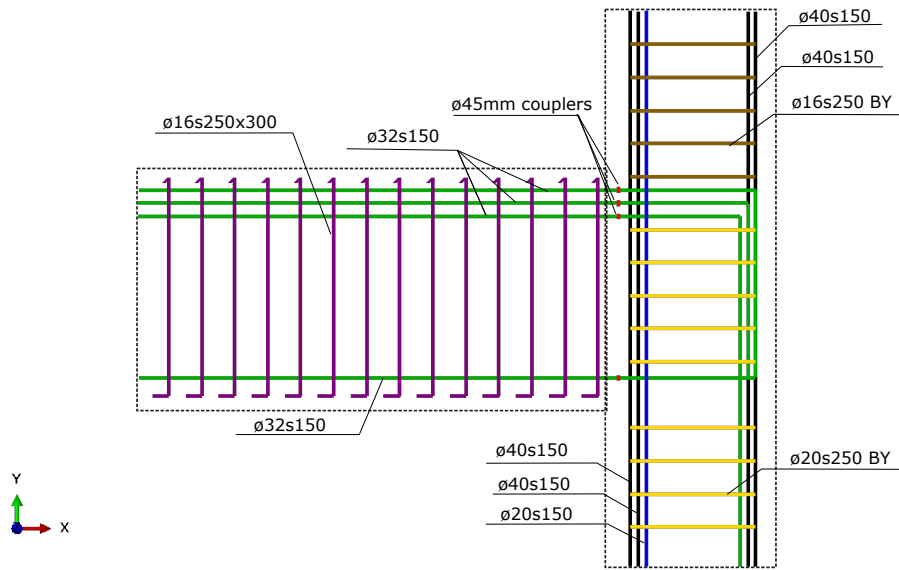


Figure 3.8: Reinforcement layout of the rigid connection, redrawn from COWI 2021

3.3.2 Hinged connection

In the sub-project Kvarnberget, a hinged connection is used to connect the tunnel roof to the D-walls instead of a rigid connection, as in Korsvägen and Centralen. Kvarnberget is also different regarding the design of the tunnel compared to Centralen and Korsvägen, see Figure 3.9. The tunnel has two levels, one mezzanine slab, acting as the tunnel roof, and one upper, fixed at the top of the D-walls. The space in between is an installation space. Both the mezzanine slab and the bottom slab is connected to the D-wall through hinged connection types (SGS 2020). Similar to Korsvägen, the D-walls are founded at bedrock and built with top-down method. Since the tunnel at Kvarnberget has an upper level, the load from backfilling is not imposed onto the tunnel-roof, mezzanine slab which results in lower loads on the connection. The bottom slab is also connected to the D-walls; in other words, the connection through the tunnel roof is not the only connection between the tunnel and D-walls. The tunnel roof at Kvarnberget is significantly thinner than the one at Korsvägen, 0.8m and 1.8m, respectively, implying smaller loads acting on the roof. Due to the lack of backfill and the additional connection to the D-walls in the

bottom slab, it can be established that the connection in Korsvägen is more critical than the one in Kvarnberget.

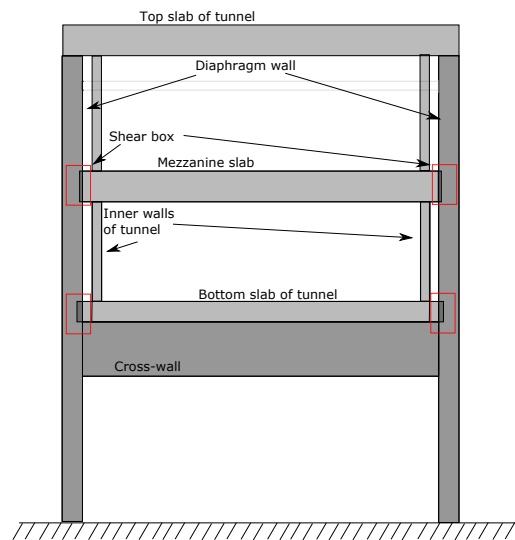


Figure 3.9: Tunnel design with mezzanine slab at Kvarnberget, redrawn from SGS 2020

The connection used in Kvarnberget has no reinforcement going through the joint, thus it acts as a hinged connection, transferring vertical and horizontal forces. The mezzanine slab is connected to the D-wall through shear boxes (SGS 2020). The shear boxes are openings in the inner edge of the D-wall which are covered by steel plates during casting of the D-wall, see Figure 3.10. The steel is later removed, and the top slab is casted into the opening. The same type of connection is used to connect the bottom slab to the D-walls. Between the slabs and D-walls, a waterproofing membrane is attached to ensure that the connection is waterproof, see Figure 3.11. The membrane is in a first phase only covering the connection, ending in waterbars. The membrane is in later phases welded together with the rest of the waterproofing membrane along the D-wall (SGS 2020). The depth of the shear box into the D-wall is 0.4m and the width 0.8m. The tunnel roof is 0.8 m high but widens at the shear box where the height is 1.2 at the inner edge and 1.3m at the outer. The metallic formwork used to cover the shear box is slightly larger than the wanted dimensions of the opening, requiring a leveling of concrete after excavation down to the connection.

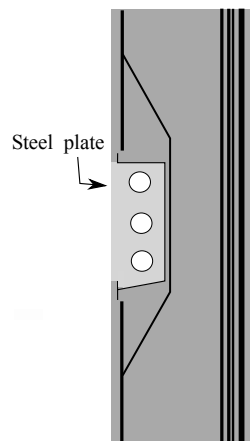


Figure 3.10: Shear box with steel plate cover during construction, redrawn from SGS 2020

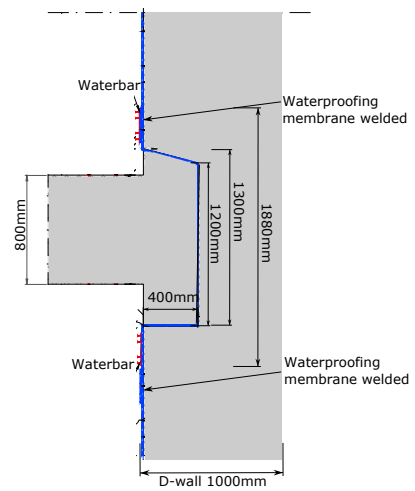


Figure 3.11: Shear box with inserted mezzanine slab, redrawn from SGS 2021

4

FE-Analysis

In this work, two methods were used to model the whole D-wall, either using plane strain elements or elastic beam elements. The first method was used in a 2D plane strain model where the D-wall and soil were parts of the model. The second method was used in a 2D beam model of the structure where the soil was inserted as loads. Both analyses were linear with regard to the structure and assumed elastic behavior of the tunnel and D-walls. The advantages of the plane strain model were that it gave a better approximation of the deflections of the D-wall and more accurate stresses in the soil, but on the other hand it was harder to extract sectional moments and forces (Everaars and Peters 2013). In the beam model it was possible to extract sectional forces and moments directly from the structural parts, but it was not possible to see the deformations of the soil which could be crucial in a dense city region. The third analysis was a non-linear analysis of the connection, using elastoplastic material and the damage behavior of the concrete. The FE-analysis was performed in the software Abaqus FEA 2020.

4.1 FE-model

The conditions, dimensions and construction phases used in the different FE-analyses was based on Korsvägen, the most critical case regarding the connection, see Chapter 3.3.1 and 3.3.2.

4.1.1 Dimensions and concrete types

The dimension of one D-wall panel is 1.2x7x29 m, the top slab has a thickness of 1.8m and a span length of 22m, see Figure 4.1. The bottom slab is 1.4m thick and the skin walls have a thickness of 1m. The cross-walls are 1m thick and 3m high with a center to center distance of 7 m. The D-walls and cross-walls are concrete class C40/50 while the top slab, bottom slab and skin walls are C35/45. The difference between the D-walls and cross-walls is that the D-walls are reinforced, and the cross-walls are unreinforced. In addition to the permanent structure, temporary struts are installed during the construction. The strut and the top slab are located 3.5 m and 11 m respectively from the top of the D-walls. The height of the tunnel is 11.5 m, including the bottom and top slab.

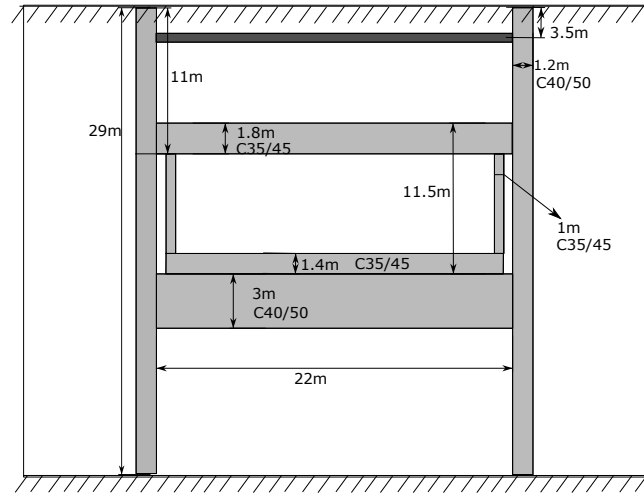


Figure 4.1: Dimensions and concrete types

4.1.2 Material properties

The elastic properties used to model the elastic behavior of the different materials are listed in Table 4.1.

Table 4.1: Elastic properties of the different materials

Material	ρ [kg/m^3]	Modulus of elasticity [GPa]	ν [-]
C40/50	2500	23.8	0.15
C35/45	2500	34	0.15
Reinforcement	7850	200	0.4
Cross-wall	2400	23.8	0.2

The soil profile at Korsvågen has the following sequence: a top layer with fill, an underlying layer of clay with varying properties and a layer of friction material down to bedrock. The D-wall is grouted to the bedrock and thus supported in the vertical direction (Steffensen 2020). The properties of the soil are summarized in Table 4.2. Beside the soil profile, the space above the tunnel is backfilled with two types of fill-material after installation of the top slab. One standard material and one lightweight to reduce the weight on top of the tunnel roof.

Table 4.2: Soil properties

Material	Thickness [m]	γ_k [kN/m^3]	ϕ [°]	c [kPa]	Modulus of elasticity [MPa]	ν [-]
Fill	1.5	18	30	0.1	25	0.3
Clay 1	5.5	14.7	35	1	25	0.2
Clay 2	8	15	35	1	25	0.2
Clay 3	3	15	35	1	25	0.2
Silty clay (SiCl)	5	18.7	35	1	25	0.2
Silty sand (SiSa)	6	19	32	0.1	17	0.3
Backfill lightweight (LW)	8.5-9.5	11	40	0.1	20	0.3
Backfill standard	1.5-2	21	35	0.1	25	0.3

4.1.3 Construction phases

After excavation of the trenches and casting of the D-walls as described in Chapter 3.1.2, the tunnel was built using the top-down method. Each phase of the construction is shown in Figure 4.2.

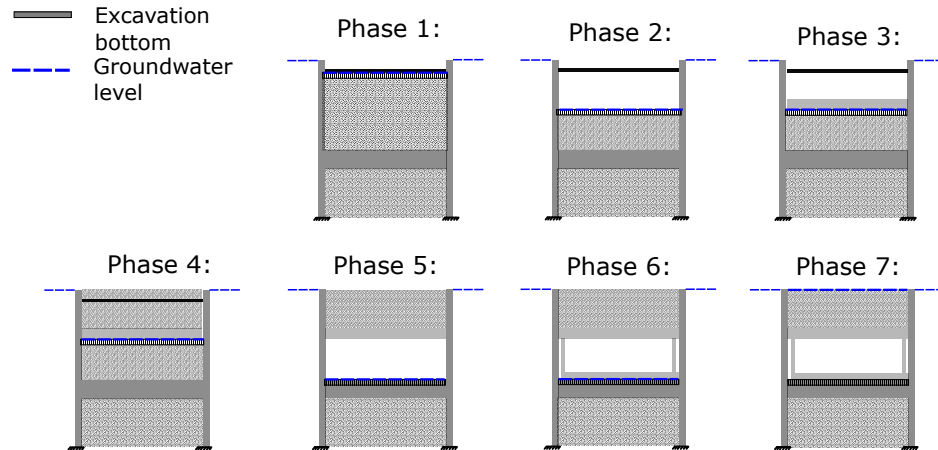


Figure 4.2: Construction phases in the top-down method, starting with excavation down to the level of the strut

Construction phase 1 is excavation and installation down to the level of the strut, to 3.5 m below the ground surface. Phase 2 is excavation down to the bottom of the top slab, 11 m below ground followed by casting of the top slab in phase 3. The space above the top slab is then filled with the two backfill-materials, phase 4, followed by removal of the strut. Phase 5 is excavating below the top slab down to the lower level of the bottom slab, 20.7m below ground. In Phase 6, the bottom slab and skin walls are casted which results in the complete structure after construction. In the permanent stage, phase 7, the water pressure is restored.

4.1.4 Assumptions

To be able to analyze the conditions at Korsvågen, some assumptions are made. The strut is assumed to have a strength large enough to resist deflection of the D-wall in the lateral direction. Hence it is modeled as a boundary condition constrained in the x-direction. The force at the bottom of the D-wall is assumed to be small enough to have a soft spring as support in the horizontal direction to model the mounting of the D-wall to bedrock. The magnitude of the horizontal forces are verified to be of reasonable size in Appendix C.1 and D.1. Since the tunnel is symmetric around the y-axis in the middle, only half the tunnel and one D-wall need to be modeled. The nodes along the symmetry line are constrained from moving in the horizontal direction. The cross-wall is assumed to act as a beam and thus modeled with beam-elements. The excavation pit is assumed to be watertight in a way such that it is possible to have a continuous dewatering of the pit during the excavation phase. Therefore as dewatering occur inside the pit, the water pressure is decreased simultaneously. All elements are assumed to have a one meter out of plane thickness.

4.2 Two-dimensional plane strain model

The 2D plane strain model, had five parts: the soil, the backfill, the D-wall, the tunnel and the cross-wall. The soil as well as the structure was modeled with plane strain elements. The soil was partitioned into layers according to Table 4.2, see Figure 4.3. The material model of the soil and backfill was an elastic-perfectly plastic model with Mohr-Coulomb yield surface, defined by the friction angle, the dilation angle, and the cohesion yield stress. To model the elastic behavior, the modulus of elasticity and Poisson's ratio was used as input. The D-wall and tunnel was modeled to have a fully elastic material behavior. The cross-wall was modeled by beam-elements with a fully elastic material model.

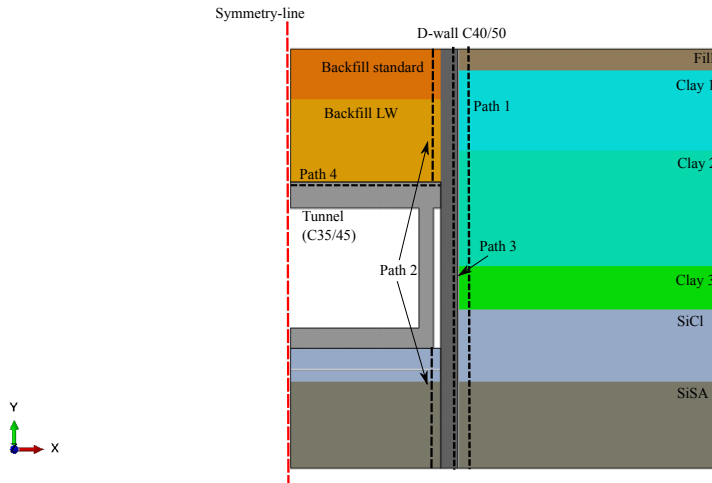


Figure 4.3: Plane strain model showing the partitions, material and paths used for extraction of stresses

4.2.1 Loading steps

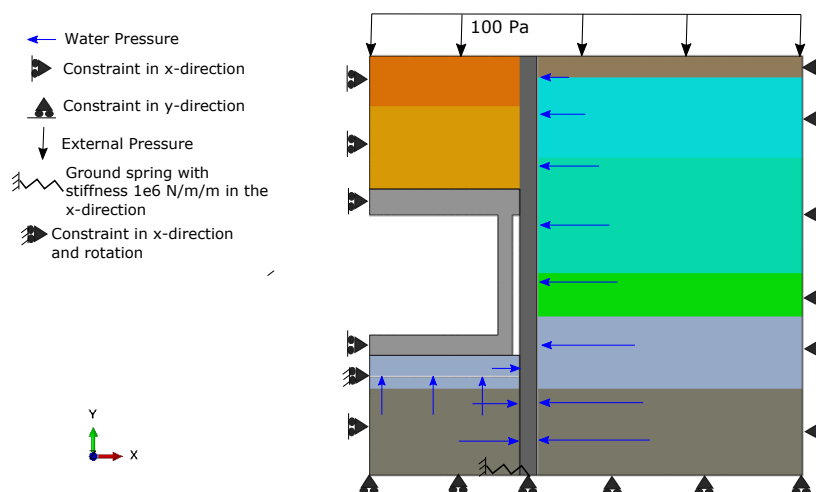
The construction phases were simulated by different loading steps. The first step was a geostatic step where the earth pressure in the soil was established without any structural parts inserted. In step 2, which was of type static general, the D-wall and cross-wall were inserted and soil in their place excavated. To avoid issues of convergence the insertion of the backfilling was made in several steps. The steps and what they simulate is presented in Table 4.3. The insertion of structural parts and excavation were made using the ability to de- and reactivate parts in the interaction module.

Table 4.3: Loading steps in the plane strain model

Step	Step Type	Construction phase	Activities
Step 1	Geostatic	None	Only soil
Step 2	Static, general	None	Excavation and casting of D-wall and Cross-wall
Step 3	Static, general	Phase 1	Excavation down to -3.5m and insertion of strut
Step 4	Static, general	Phase 2	Excavation down to bottom top slab, -11m below ground level
Step 5	Static, general	Phase 3	Casting of top slab
Step 6-9	Static, general	Phase 4	Backfilling above top slab
Step 10	Static, general	Phase 5	Removal of strut and excavation down to bottom slab, -20.7m
Step 11	Static, general	Phase 6	Installation of bottom slab and inner walls
Step 12	Static, general	Phase 7	Permanent stage, restored water pressure below bottom slab and in backfill

4.2.2 Loads and boundary conditions

Boundary conditions of the soil and the backfill were established along the outer edges, both vertical and horizontal, see Figure 4.4. Along the vertical edges, the soil was constrained from moving in the horizontal direction. Along the horizontal edge at the bottom, the soil was stopped from moving in the vertical direction. The bottom boundary conditions simulate the interaction the soil had with the rock underneath. The D-wall was locked in the vertical direction at the structural line bottom node. The D-wall was also constrained by a ground spring with a stiffness of 1 MN/m/m in the horizontal direction at the bottom node.

**Figure 4.4:** Boundary conditions and loads in the soil model in step 11

The applied loads on the model were the water pressure, the gravity, and a surface load on the soil which was a uniform load of 0.1 kPa, added to improve the convergence rate of the soil and prevent it from rising too much. The groundwater level was located right below the ground level and decreased along with the excavation

depth at the inside of the D-wall due to dewatering. The water pressure was defined separately, as a pressure acting towards the edge of the D-wall increasing with depth. An uplifting pressure from the water was also added below the cross-wall and bottom slab of the tunnel. In addition, the weight of the water needed to be added above the top slab and cross-wall. The water pressure varied according to Figure B.1 and values of the water-loads is shown in Appendix B. In the permanent stage, after a long time, the water pressure on the inside of the D-wall was assumed to be restored to its initial value. This resulted in an uplift force on the tunnel, due to the restored water pressure under the tunnel. The backfill was also assumed to be fully saturated after a long time. Gravity was applied to the whole model in all steps.

4.2.3 Interaction

The soil-structure interaction was used to simulate skin friction between the D-wall and soil and was defined as a node-surface interaction with tangential and normal behavior. The friction coefficient was calculated according to Equation 2.13, using an estimated mean friction angle of 35° . The connection between the tunnel roof and the D-wall was modeled with two couplings and a stiff link, see Figure 4.5. The horizontal center line in the D-wall was locked to a reference point, RP, in the middle by a coupling. The right edge of the top slab was, similarly, locked to a reference point in the middle of the top slab's inner edge. The two reference points were then connected by a cartesian wire with all degrees of freedom constrained. The connection between the cross-wall and D-wall were executed in a similar way, see Figure 4.6.

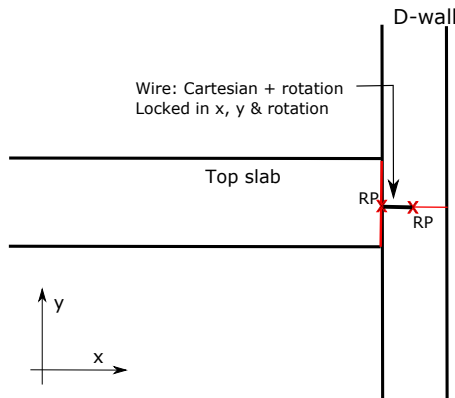


Figure 4.5: Connection between top slab and D-wall in the plane strain model

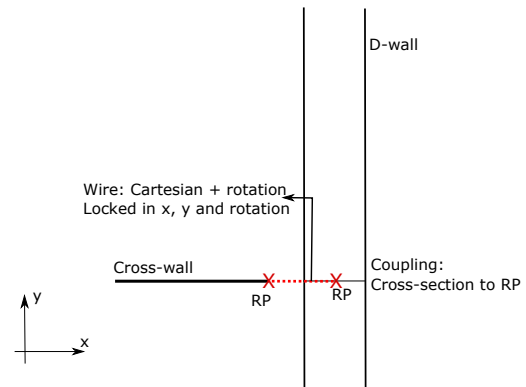


Figure 4.6: Connection between cross-wall and D-wall in the plane strain model

4.2.4 Mesh size

The chosen mesh in the plane-strain model was elements with mesh-sizes listed in Table 4.4. To ensure the mesh-size was small enough to give accurate results, a convergence study of different elements-sizes was conducted, see Appendix C. The

element-type was a 4 node bilinear plane strain quadrilateral elements with reduced integration.

Table 4.4: Mesh size in soil model

Soil	D-wall	Tunnel	Backfill	Cross-wall
500mm	200mm	150mm	200mm	500mm

4.2.5 Comparison with hand calculations

The vertical and horizontal earth pressure in every construction phase was calculated analytically according to Chapter 2.1.2, see Appendix B. The calculated at rest pressure was compared to the obtained soil stresses from the plane strain model analysis. The vertical and horizontal stress was extracted along path 1 and 2 in Figure 4.3. The soil was assumed to be normally consolidated and the at rest coefficient, K_0 , was thus calculated the same way in the friction and cohesion material.

4.3 Two-dimensional beam model

The structural parts, in the beam model, were modeled with 2D Timoshenko beam-elements, and the soil was inserted as loads, see Figure 4.7. The load was calculated according to earth pressure theory, see Chapter 2.1.2. The model was divided into three parts: the tunnel, the D-wall, and the cross-wall, all modeled with beam-elements. The beams were given fully elastic properties defined by the modulus of elasticity and Poisson's ratio.

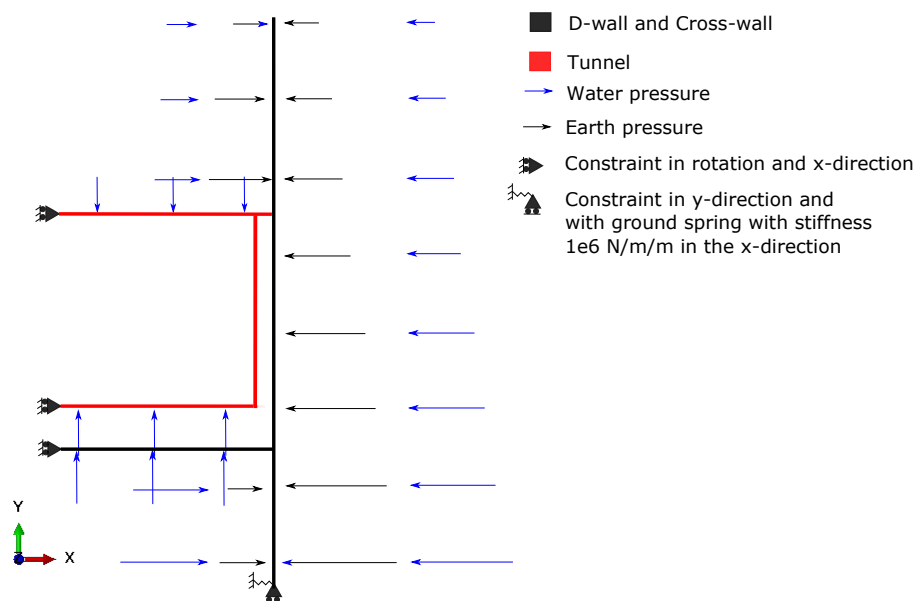


Figure 4.7: Beam model in the permanent state

4.3.1 Loading steps

The calculation steps in the beam model are similar to the ones in the plane strain analysis. The main difference is that the first step is not a geostatic step and that the backfilling was not divided into several steps. The resulting 8 steps are presented in Table 4.5.

Table 4.5: Loading steps in beam model

Step	Step Type	Construction phase
Step 1	Static, general	Start
Step 2	Static, general	Excavation down to -3.5m and insertion of strut
Step 3	Static, general	Excavation down to bottom top slab, -11m below ground level
Step 4	Static, general	Casting of top slab
Step 5	Static, general	Backfilling above top slab
Step 6	Static, general	Removal of strut and excavation down to bottom slab, -20.7m
Step 7	Static, general	Installation of bottom slab and inner walls
Step 8	Static, general	Permanent stage, restored water pressure below bottom slab and in backfill

4.3.2 Loads and boundary conditions

The applied loads on the D-wall were the at rest horizontal earth pressure component, the water pressure, and the gravity. The loads can be seen in completeness in Appendix D. The result of the analysis with the at rest pressure was used in combination with the direction in Eurocode 7 for mobilization of active/passive earth pressure (SIS 2005b). The soil was assumed to be compact and only the passive earth pressure was considered. The mobilization of passive earth pressure had to be evaluated in every loading step. The water pressure was inserted the same way as in the plane strain model, increasing with depth, and reduced with an increasing excavation depth.

4.3.3 Interactions

In the beam-model, the loads were used to simulate the different construction phases, instead of the de- and reactivation used in the plane strain model. No interaction between the structural parts were defined, hence no skin friction was assumed. The connection between the D-wall and top slab of the tunnel was defined as in Figure 4.8. A length, along the D-wall, equal to the thickness of the top slab was locked in all degrees of freedom to a reference point, RP, in the middle by a coupling. The innermost node of the top slab was connected to the same reference point by a coupling also locked in all degrees of freedom. The connection between the cross-wall and the D-wall was done in the same way but with only the horizontal and vertical degrees of freedom constrained.

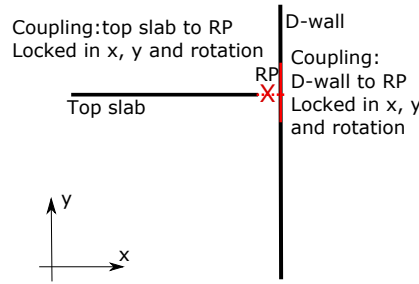


Figure 4.8: Connection between top slab and D-wall in beam model

4.3.4 Mesh size

A convergence study of the 2D beam model is presented in Appendix D. The result compared in the convergence study was the deformations in the D-wall and moments in the top slab. The study showed that a mesh-size of 50 mm is sufficient. The element-type used was a 2-node element, linear in a plane.

4.3.5 Correspondence of deformation and stresses with plane strain model

The results of the beam model analysis regarding deformations and stresses in the D-wall and top slab were compared with the results of the plane strain model analysis. Comparisons were done for the stress in the normal direction along the upper edge of the top slab and the outer edge of the D-wall, see path 3 and 4 in Figure 4.3. Using beam-elements meant that the stress could not be extracted directly. Instead, the normal force and moment was retrieved and used to calculate the stress with Navier-Stokes equation (Al-Emrani et al. 2011):

$$\sigma = \frac{N}{A} + \frac{M}{I} * z, \quad (4.1)$$

where A is the cross-sectional area, and I is the moment of inertia of the cross-section, N is the normal force, M is the moment extracted from the beam model, z is the internal leverarm. The verification had to be done in several steps. First, the analysis was run having the at rest earth pressure applied to the structure. The resulting deformations of the D-wall were then used to estimate the amount of mobilized passive earth pressure according to Eurocode 7 (SIS 2005b). The mobilization depends on the value of the deformation, v , and the corresponding height, h , of a specific shape which is determined from the analysis of the deformation curve, a , b or c , see Figure 4.9. Where a is a decreasing deformation, b is an evenly distributed deformation, and c is an increasing deformation in relation to depth.

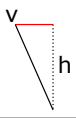
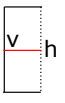
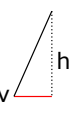
a)		v/h for 50%: 1.1% v/h for 100%: 5%
b)		v/h for 50%: 0.5% v/h for 100%: 3%
c)		v/h for 50%: 0.5% v/h for 100%: 5%

Figure 4.9: Shapes and percentage needed for 50% and 100% mobilized passive earth pressure (SIS 2005b)

4.4 Local FE-model of connection

The local FE-model, submodel, was a model of the connection between the D-wall and top slab. This was analyzed to study to see how the construction phases affect the connection in terms of stresses, crack-patterns, and crack widths. To simulate the different construction phases, loads in terms of section forces and moments were extracted from the beam model in the different steps. The submodel included the connection and 1 or 2 widths out in each direction to include the entire discontinuity region resulting in a total height of 4.2 m and a width of 4.8 m, see Figure 4.10.

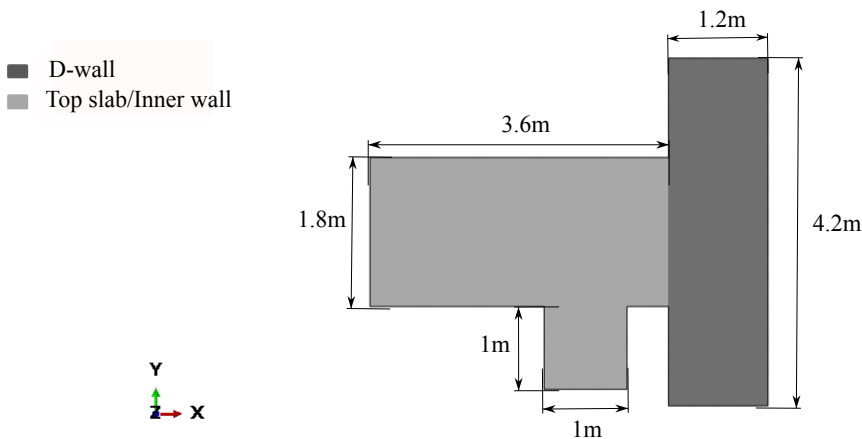


Figure 4.10: Dimensions of the submodel

4.4.1 Loading steps

The submodel-analysis was divided into 5 steps, all of type static general. The first step was installation of the top slab and the last step was the permanent stage. Table 4.6 lists the steps and corresponding construction phases. The first two steps used in the two other analyses, excavation to strut level and bottom top slab were disregarded since the connection is not included in those phases.

Table 4.6: Loading steps in local model analysis

Step	Step Type	Construction phase	Step in Beam model analysis
Step 1	Static, general	Casting of top slab	Step 4
Step 2	Static, general	Backfilling above top slab	Step 5
Step 3	Static, general	Removal of strut and excavation down to bottom slab, -20.7m	Step 6
Step 4	Static, general	Installation of bottom slab and inner walls	Step 7
Step 5	Static, general	Permanent stage, restored water pressure below bottom slab and in backfill	Step 8

4.4.2 Loads and boundary conditions

The loads of the local model were retrieved from nodes in the beam-model analysis, corresponding to the concrete edges of the submodel, see Figure 4.11. The normal and tangential force and moment of each node was applied to the corresponding reference point in the local model. The lower reference point of the D-wall was constrained from moving or rotating in any direction, see Figure 4.12. The load in each step was retrieved from different steps in the beam-model analysis to simulate the different construction phases, listed in Table 4.6. The direction of the forces and moments in Figure 4.12 is an example and do not correspond to any particular step. The loads of each step and reference point is presented in Appendix F.

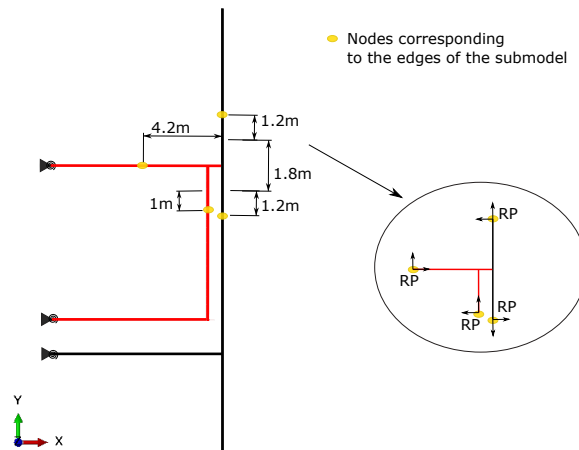


Figure 4.11: Nodes in the beam-analysis used to gather section forces and moments

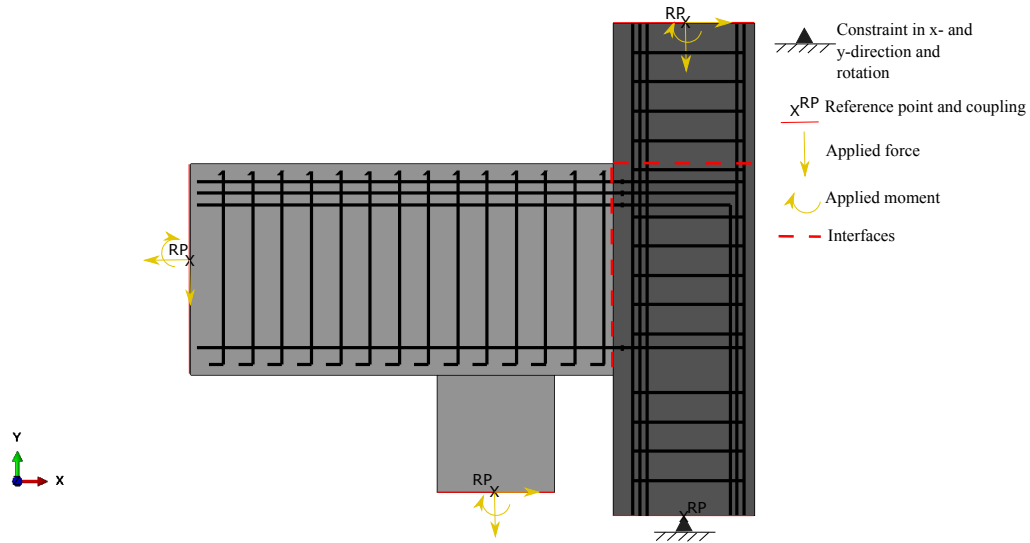


Figure 4.12: Boundary conditions and loads applied to the submodel

4.4.3 Interactions

The outer edges were locked to a reference point, RP, in the middle of each edge by a coupling. That way, the load could be applied to the reference point and transferred to the entire edge. The couplings were locked in translation and rotation. The interaction between the reinforcements and the concrete was done using embedded constraint, where the reinforcements selected as embedded region and the concrete as host region. Thus, full interaction between reinforcement and concrete was assumed. The inner wall was deactivated in the first step and then reactivated in the step corresponding to construction phase 6, see Figure 4.2.

4.4.4 Mesh type and size

The concrete was modeled using plane strain element with the concrete damage plasticity material-model to describe cracking. In compression, the concrete was assumed to behave elastic. The yield surface and plastic flow was defined by the parameters in Table 4.7, all set to recommended values (Zangeneh Kamali 2012).

Table 4.7: Parameters defining the yield surface of the concrete in the submodel

ψ	ϵ	f_{b0}/f_{c0}	K_c	μ
37	0.1	1.16	2/3	1e-06

Since there are different concrete classes in the D-wall and the top slab, the tension softening and damage behavior was estimated for both concrete types, see Appendix E.

The reinforcement layout can be seen in Figure 3.8 and was modeled as solely elastic using truss-elements. The area per effective length of each layer was calculated as:

$$A = \frac{\pi}{4} * d^2 * \frac{1m}{s} \quad (4.2)$$

Where s was the spacing of reinforcement bars out of the plane and d was the diameter of each bar. The couplers were modeled with beam-elements across the rebars. The additional area in the transversal direction will result in an enhanced area in contact with the concrete and thus a larger attachment between the reinforcement and concrete.

A convergence study was done for the local model as well, comparing the reaction force in the lower node of the D-wall. The convergence study is presented in Appendix F. The final mesh used in the analysis had an element-length of 20 mm in both the reinforcement and concrete. The element-type of the concrete was 4-node bilinear plane strain quadrilateral elements with reduced integration. The reinforcement was modeled with 2-node linear 2D truss elements.

4.4.5 Comparison of crack widths, equilibrium and stresses

The verification of the submodel was done by verifying the forces, moments, stresses, and cracks. The entire verification of the submodel was performed on the permanent stage, the last step. To verify the reaction forces and moments in the lower node of the D-wall, the section forces and moments inserted were summed up, see Table 4.8. The sum was thus compared to the obtained reaction forces and moments in the submodel to ensure equilibrium. In addition, the global equilibrium was controlled by summing up the external loads and comparing the result with the sum of the reaction and section forces and moments.

Table 4.8: Verification of equilibrium in the submodel

Node	Rx [kN/m]	Ry [kN/m]	Mz [kNm/m]
Upper D-wall	665.8	-240.1	-1775.7
Top slab	96.3	-2014.4	-2376.9
Inner wall	427.7	1519.9	-202.0
Calculated value of reaction	-1189.8	734.6	1409.9
Difference to obtained reaction in analysis	0.01%	0.02%	0.04%
Difference to external loads	4 %	3 %	3 %

The steel stress in the upper rebars in the top slab was calculated by Navier-Stokes equation, Equation 4.1, of concrete cracked section. The hand-calculated value was compared to the obtained steel stress in the rebars which in turn also was compared to the tensile strength of the reinforcement. This, to ensure that the rebars had an elastic material behavior as assumed. To ensure that no crushing occurs, the compression stress was compared to the limit of $0.6 f_{ck}$ for short-term load and $0.45 f_{ck}$ for long-term load (SIS 2005a). In terms of cracks, the anticipated crack width and crack-spacing was calculated according to Eurocode 2, see Appendix G (SIS 2005a). The crack width in the submodel was obtained by multiplying the plastic strain with the element length. In the calculation of the crack widths, spacing and steel stresses was calculated with the normal force and moment obtained from the beam model analysis at the interfaces between the top slab and D-wall, see Figure 4.12.

5

Results

5.1 Earth pressure along D-wall

The result of the plain strain model analysis in terms of earth pressure, vertical and horizontal, was compared to hand-calculated values of the at rest earth pressure, see Figure 5.1. It could be seen that the results of the two methods were similar. The calculated at rest pressure was slightly higher than the obtained values from the FE-analysis but the shape of the curves was very similar. The lower horizontal earth pressure behind the D-wall is most likely mobilization of active earth pressure due to movement of the D-wall. The vertical earth pressure, from the FE-analysis and hand-calculated, were almost identical. The horizontal earth pressure is a multiple of the vertical pressure, validating that the difference depend on the state of the soil. Overall, the earth pressure in the plane strain analysis agreed well with hand-calculated values. The complete comparison is presented in Appendix C. The plateau at 24 m depth is due to the change of material from silty clay to silty sand. The two different layers have different internal friction angles and thereby different lateral earth pressure coefficients.

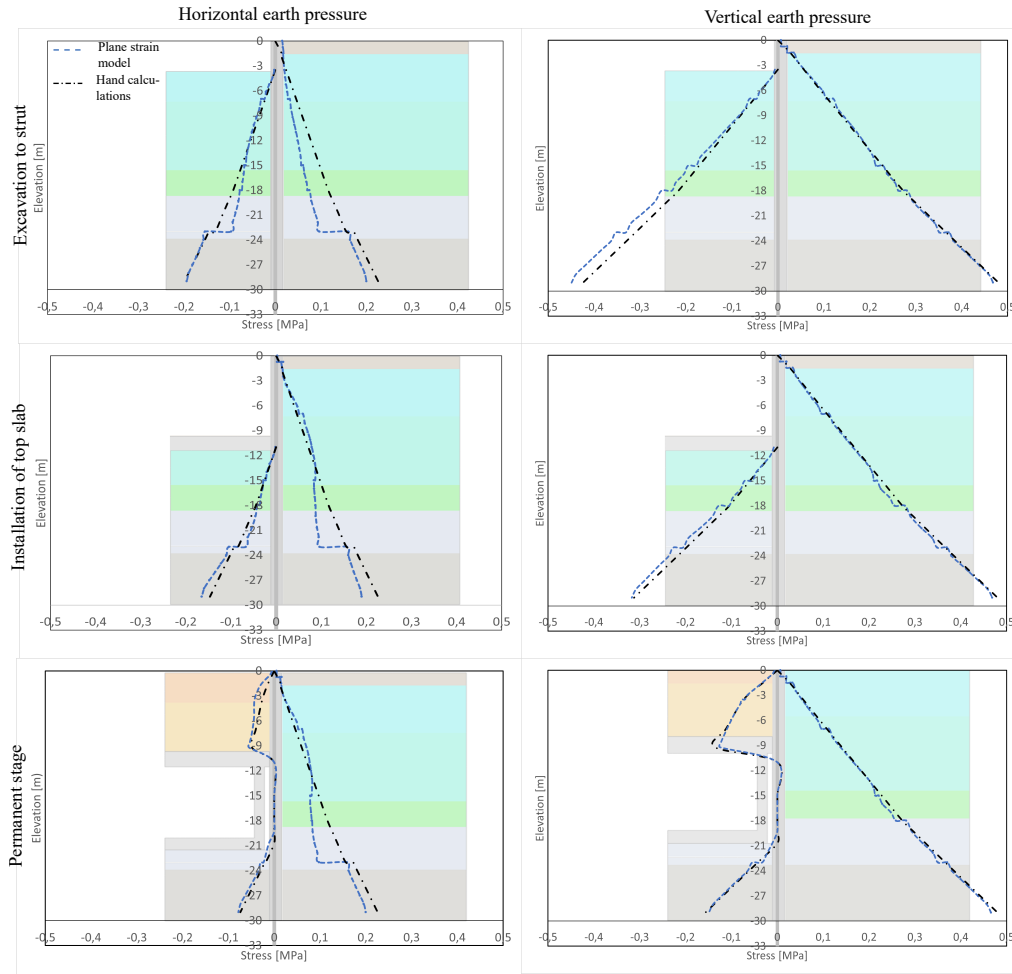


Figure 5.1: Comparison of the horizontal and vertical earth pressure between the plane strain model and hand calculated values

The plane strain model had some convergence problems which were strongly related to the parameters defining the Mohr-Coulomb yield surface. During excavation, the self-weight from the soil above was lifted and the soil wanted to rise. Thus, to improve convergence a small amount of cohesion yield stress was added to the non-cohesive soil layers, 0.1 kPa. The insertion of the backfill material took place in 4 steps to avoid convergence problems due to the high load caused on the top slab. In this model, there was no need to calculate the earth pressure or the amount of mobilized active/passive earth pressure (due to the use of a Mohr-Coulomb material model).

5.2 Deformations and stresses in D-wall

The deformation of the D-wall in the beam model analysis when having applied the at rest earth pressure is represented by the black line in Figure 5.2 which shows the deformation in loading step 4, casting of the top slab. The maximum deformation was 34.3mm, and the shape in the region was almost rectangular (shape b in Figure 4.9) and the corresponding height, h , was 12m. The resulting deformation-height

ratio was then 0.29%. According to Eurocode 7 (SIS 2005b) and the values stated in Figure 4.9, the amount of mobilized passive earth pressure along the height was estimated to 40%. The maximum deformation, corresponding height and assumed shape of the deformation was estimated in a similar manner in each loading step. The resulting degree of mobilization in each soil-layer is together with the resulting earth pressure presented in Appendix D. Since there is no defined relation between the mobilization and deformation in Eurocode 7, the amount of mobilization, 40% in step 4, was an estimated value. The new earth pressure, the partly mobilized passive earth pressure, was applied to the beam model in every step and the new deformation is shown as the orange line in Figure 5.2.

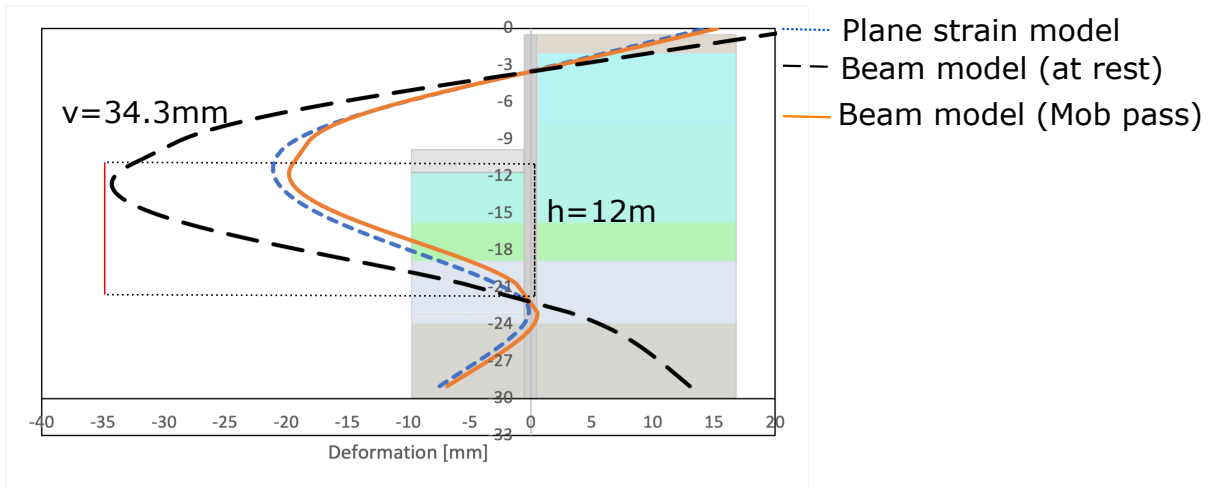


Figure 5.2: Deformation of D-wall when the top slab is inserted, step 4 in beam model analysis

The result regarding deformation and stresses of the D-wall after mobilization was compared to the result of the plane strain analysis, the blue line in Figure 5.3. The result of the beam model analysis with partly mobilized passive earth pressure, the orange line in Figure 5.3, corresponded well with the result of the plane strain analysis. When the partly mobilized earth pressure was applied, the stresses and deformations of the top slab also corresponded well with the result of the plane strain analysis, see Appendix D. The peak or rounded peak at 23 m depth is due to the cross-wall and the large vertical load transferred from the cross-wall into the D-wall. The same occurs at a depth of 11 m, at the top slab, caused by the same situation, but with an additional moment transfer as well. The stresses in the second row in Figure 5.3, corresponding to construction phase 5, excavation to bottom slab after backfilling, shows the largest stresses. This confirms that construction phase 5 is the most critical phase, see discussion in Chapter 3.3.1.

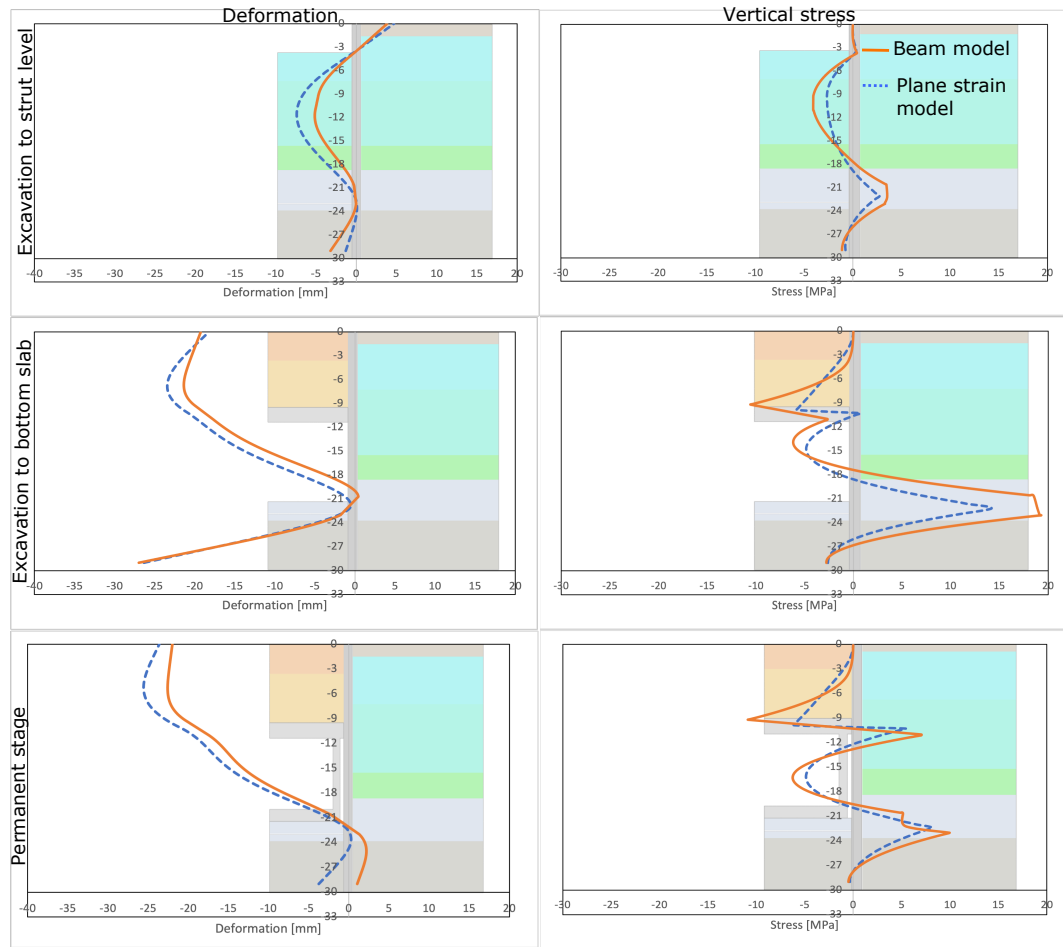


Figure 5.3: Comparison of the deflection and vertical stresses in the D-wall between the two models, having applied the mobilized passive earth pressure in the beam model

When the mobilized passive earth pressure is applied, the earth pressure applied to the structure is higher than the pressure acting on the structure in the plane strain model, see Figure 5.4. The earth pressure on the right side, behind the D-wall, is slightly lower. This might be an indication that active earth pressure is mobilized behind the D-wall. A reason why the mobilization of passive earth pressure is higher in the beam model might be because the earth pressure behind the D-wall is kept the same, the at rest earth pressure, in all steps. In the plane strain model analysis, movements of the D-wall automatically lead to mobilization of the soil and the stiffness of the soil might interfere. The boundary condition, restricting the soil from moving in the horizontal direction along the vertical edge, see Figure 4.4, is assumed to be far enough to not influence the structure but might add some additional stiffness to the soil in the horizontal direction. This result in smaller deflection of the D-wall and thus less mobilized passive earth pressure. The result in Figure 5.3 shows larger stresses in the D-wall in the beam model analysis compared to the plane strain model. The deviations between the deformations and stresses in the two models depend most likely on the differences in loads, see Figure 5.4. Overall, the result shows that the mobilization of earth pressure must be considered

when using a model without the soil to capture the real behavior of an underground tunnel supported by D-walls.

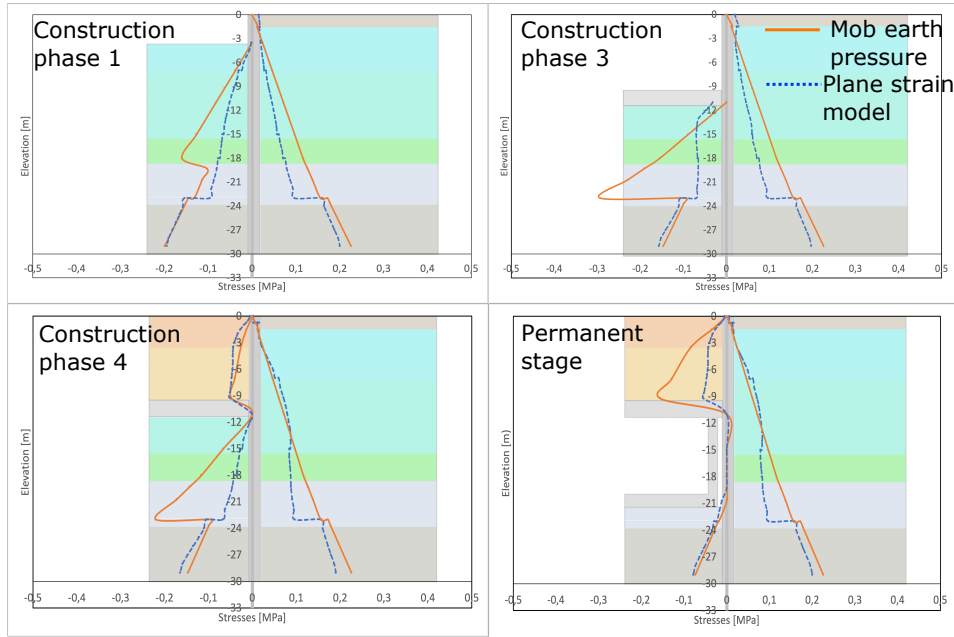


Figure 5.4: Comparison between the horizontal earth pressure applied in the beam model and the extracted earth pressure in the plane strain model

The degree of mobilized passive earth pressure also affected the section forces in the structure. Due to the higher load, the section forces in the reference points used as input to the local model also became higher. The expected crack widths would in such case become smaller, especially in the D-wall which is the part of the structure most exposed to the horizontal earth pressure. The lower load in the D-wall would also be expected to lower the crack width of the crack in the upper corner between the D-wall and top slab. The assumption of fully elastic behavior also contributes to higher loads in the structure than if the plastic behavior would be included. The fully elastic behavior is in such case assumed even if the loads in fact are large enough to govern a cracking or plastic behavior. The plastic behavior would force the loads in the structure to redistribute to parts with higher stiffness and possibly thereby also result in smaller section forces in the connection.

5.3 Crack widths and stresses in connection

The stress in the reinforcement and concrete did in some parts exceed the yielding strength of 500 MPa and limit of compression of $0.45 f_{ck}$, 15.75MPa in the top slab and 18MPa in the D-wall, respectively, see Figure 5.5 and 5.6. Although, there is only small parts of the model that exceed the limits. The limit is set to be on the safe side during design of structural parts according to Eurocode 2 (SIS 2005a). The parts exceeding the limit in the reinforcement was mainly small local parts in the horizontal rebars, red parts in Figure 5.6. In the concrete, the only parts exceeding the limit was the upper and lower corner, and a small part of the outer

5. Results

edge. Because of this, only small parts and limit on the safe side, the reinforcement and concrete are still assumed to behave elastic and not crush. The steel stress in the upper rebar-layer at the interface between the top slab and D-wall was according to hand-calculated values 375 MPa which is significantly higher than the obtained value from the analysis, which was 208 MPa.



Figure 5.5: Concrete stresses in the permanent stage

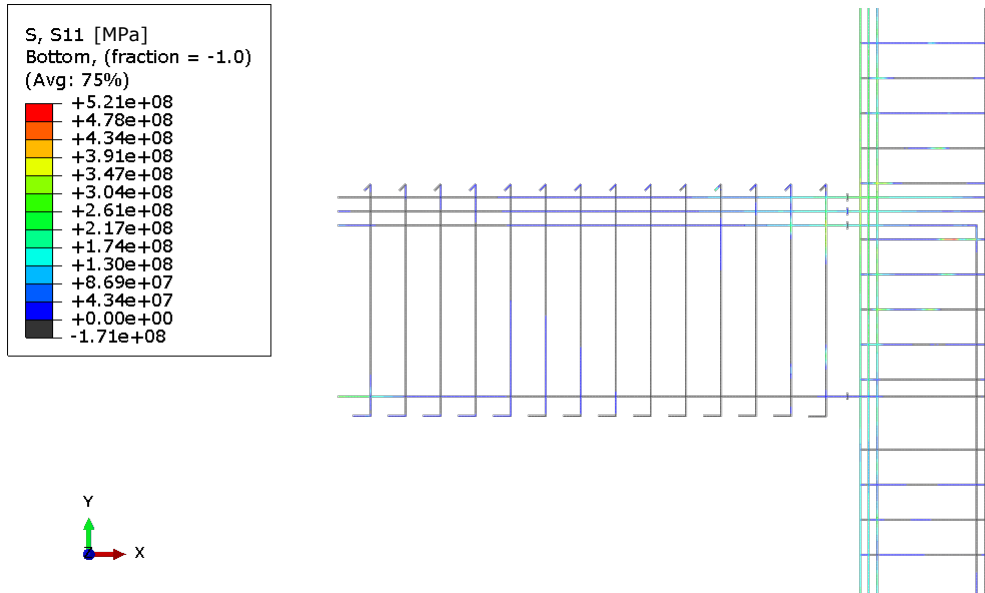


Figure 5.6: Steel stresses at the permanent stage

The crack width in the upper corner of the top slab becomes very high, 1.89 mm. The entire crack pattern in the permanent stage is shown in Figure 5.7, where the

largest and second largest cracks in the D-wall and top slab are marked. The largest crack, in the corner, becomes significantly larger than the calculated crack width. It can be argued that the obtained crack width in the corner should be compared to the sum of the two calculated crack widths since it appears at the intersection of the interfaces which the cracks are calculated for. The sum of the two hand-calculated cracks at the corner is 1.2 mm, significantly smaller than the obtained crack width in the FE-analysis. A reason why the crack width from the hand-calculation does not comply with the crack width from the FE-analysis, might be because the procedure to calculate crack widths in Eurocode 2 does not consider the impact of two intersected cracks. The choice of constants in terms of, k_1 , k_2 and k_3 also affects the calculated crack width. The crack width of the second largest crack in the top slab is 0.12 mm and the distance to the corner is 140 mm. The limit of allowable crack width, 0.2 mm in the top slab, is thereby not exceeded. The second largest crack in the D-wall has a width of 0.3 mm and appear 360 mm away from the first crack. The allowable crack width in the D-wall is 0.3 mm; the obtained crack width is thus on the limit.

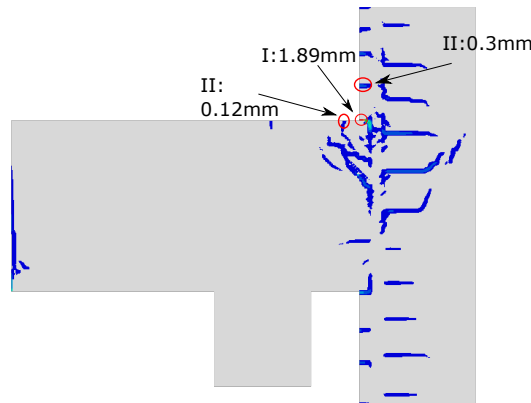


Figure 5.7: Largest and second largest cracks in the permanent stage

The behavior of the connection in the different loading steps is presented in Appendix H. The most critical step was construction phase 5 where excavation is done down to the bottom of the bottom slab, backfill is done above the top slab and the strut is removed. From the analysis results, it seems like the largest cracks appeared in the step representing construction phase 5 as expected. The crack-pattern and widths are almost identical in step 3, construction phase 5, and 5, permanent stage, see Figure 5.7 and 5.8. The restored water pressure in the permanent stage was expected to close the cracks in the top slab due to the uplifting force. However, this cannot be seen in the results of the local model analysis. Thus, may be because the crack in the corner becomes too large for the defined damage behavior to be effective. The crack widths and spacing of cracks one and two in the top slab and D-wall are listed in Table 5.1.

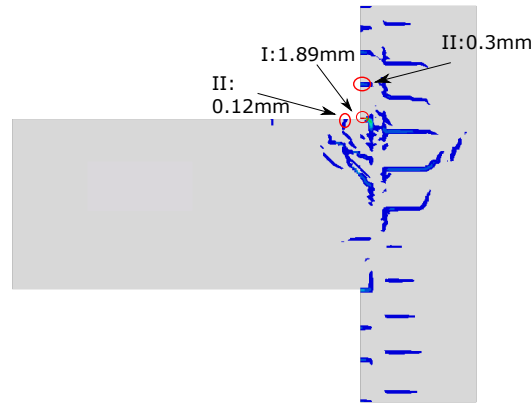


Figure 5.8: Largest and second largest cracks marked in construction phase 5, excavation to bottom slab after backfilling

Table 5.1: Crack widths and spacing in the different steps

Step	Crack I	Crack II (Top slab)		Crack II (D-wall)	
	Width [mm]	Width [mm]	Spacing [mm]	Width [mm]	Spacing [mm]
Step 1: Installation top slab	1	0.09	140	0.2	360
Step 2: Backfilling	1.88	0.12	140	0.29	360
Step 3: Excavation to bottom slab	1.89	0.12	140	0.3	360
Step 4: Installation of bottom slab	1.89	0.12	140	0.3	360
Step 5: Permanent stage	1.89	0.12	140	0.3	360

Overall, looking at the results with regard to crack-pattern and stresses it can be established that the connection is subjected to very high loads. The skew cracks in the dotted circle in Figure 5.9, is most probably due to shear forces and appear in both the top slab and D-wall. The changing direction of the horizontal crack in the middle of the D-wall, marked crack III in Figure 5.9, indicates that shear force affects the part, possibly due to horizontal forces and imposed rotation. The vertical cracks in the top slab and horizontal cracks in the D-wall are most likely bending cracks, in the longdashed circle in Figure 5.9. It can be noted that horizontal cracks are visible on both sides of the reinforcement, but not at the location of the reinforcement of the D-wall. This is most likely due to the full interaction between the reinforcement and concrete; at the rebar location, all elements were cracked, but with smaller strains than the other cracked elements. These cracks were therefore not visible in the contour plots. These cracks were therefore not visible in the contour plots. The crack widths and spacings in the D-wall were approximately the same along the inner edge with a crack width of 0.3 mm and a spacing of 360 mm. A smaller crack, 0.9 m out into the top slab, appeared in the top slab, crack IV, and had a width of approximately 0.08 mm.

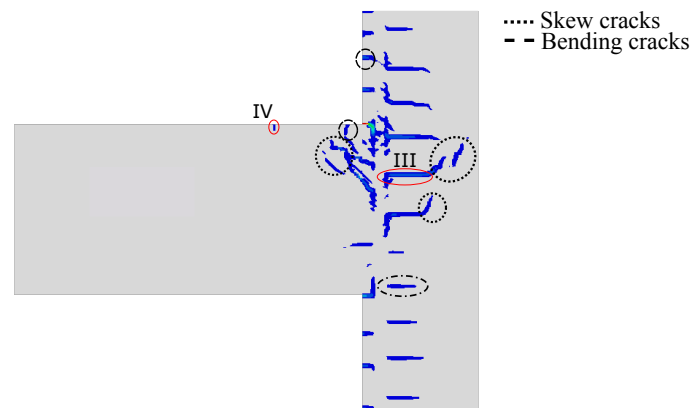


Figure 5.9: Different types of cracks in construction phase 5, excavation to bottom slab after backfilling

6

Discussion

Comparing the situations in Centralen and Korsvågen, it can be seen that the connection in Korsvågen is subjected to significantly higher loads. The higher loads are mainly due to the choice of building method, and the chosen depth of the tunnel. When using a top-down method, the amount of backfill will be a critical parameter governing the most severe load situation, construction phase 5, when excavated down to the bottom slab after backfilling. The backfill itself is directly dependent on the depth of the tunnel. In other words, the larger the depth of the tunnel, the more backfill and the higher loads on the connection. By reducing the depth of the tunnel, or by modifying the building method from top-down to bottom up, it is possible to reduce the loads on the connection. Another solution might be to use lightweight backfill all the way up to ground surface, which would reduce the weight on the top slab. The effect of the backfill can clearly be seen when comparing the design of the tunnel in Korsvågen versus Kvarnberget. The top slab in Kvarnberget is a lot thinner than the top slab in Korsvågen, indicating a smaller load acting on the slab due to the lack or smaller amount of backfill.

The use of a hinged connection results in a larger field-moment in the top slab while a rigid connection creates higher support-moments. This creates different demands on the design of the top slab and connection. Higher rebar area in the middle and bottom of the top slab would be required when using a hinged connection. A rigid connection requires more reinforcement at the top of the tunnel roof near the connection. If a hinged connection were to be used in Korsvågen, the field-moment at the middle of the top slab would probably become too high for the current height of the top slab. A thicker top slab will give an even higher load acting in the connection due to self-weight. Thus, a hinged connection is not to be preferred in Korsvågen. However, the load during construction is very high and can be reduced by having more lightweight backfill.

If the tunnel in Korsvågen were to be built with a bottom-up method, additional struts would be required due to the large depth of the tunnel. However, larger deformations would be expected, according to Chapter 3.3, due to the larger excavation depth without the horizontal support by the top slab. Larger horizontal deformations of the D-wall would result in a higher degree of mobilized passive earth pressure and thus larger section forces and moments in the D-wall. The anticipated crack widths in the D-wall in the connection would then increase as well. The larger deformations of the D-wall, compared to a top-down construction, could be reduced by additional strut-levels. An important difference between the two methods regard-

ing the connection is that construction phase 5 (excavation down to the bottom slab after backfilling) would be avoided in the top-down method. The top slab would instead be supported by the bottom slab and skin walls during backfilling, resulting in a less critical load-situation. To summarize, using a bottom-up method would most likely result in smaller crack widths if additional struts are used to minimize the horizontal deformations of the D-wall.

The three types of models used, 2D plane strain, 2D beam model and the local model can also be described as elastoplastic, elastic and non-linear. The first and second model kept the structure fully elastic while the soil in the plane strain model was assumed to be elastoplastic assuming a yield surface following Mohr-coulomb. The assumption of a fully elastic behavior in the structure means neglecting redistribution of loads due to plasticity, thus giving higher loads than if plastic behavior of the structure had been considered. The assumption might thereby lead to an overestimation of loads acting in the connection. A way to include the plastic behavior of the structure in the first model could have been to also model the concrete by a Mohr-Coulomb material model or a concrete damage plasticity model. As a result, redistribution of loads would have been included in the global analysis and the load transferred to the local model could have been reduced and the resulting crack width smaller.

Although the result regarding deformations and stresses corresponded well between the plane strain model and beam model is an estimate as the final load applied to the beam model was larger than the earth pressure subjected to the structure in the plane strain analysis. The section forces and moments in the beam model were consequently probably too high, resulting in too wide cracks in the connection. It can be argued that a beam model with partly mobilized earth pressure according to Eurocode 7 is accurate enough to use in early design. However, a plane strain model, or equivalent, including the soil is preferable during detailed design.

The very large crack width (1.89mm) in the corner in between the D-wall and top slab indicates that some additional measures to reduce the crack widths are needed. It should be considered that the crack is an overestimation due to the assumed elastic behavior, and the larger mobilized earth pressure. Still, the crack-width in the corner is much larger than the allowable crack widths and would most probably not meet the requirements even without the overestimations. One possible alternative to reduce the crack width would be to strengthen the corner by a haunch, to increase the thickness of the top slab near the connection. Another alternative would be to have additional strut-levels which would reduce the deformation of the D-wall and thus the mobilization of passive earth pressure.

7

Conclusion

This master thesis aimed to investigate the structural behavior of the connection between the tunnel roof and D-walls at Korsvågen, a sub-project of the West Link Project. The conclusions of the work are listed below:

- A tunnel located at a large depth, built with a top-down method results in a critical situation with respect to the connection. The situation in Korsvågen is thus more critical than the other sub-projects in the West Link project.
- The earth pressure developed in the plane strain model, including the non-linear behavior of the soil, showed less mobilization of passive earth pressure than the analyses using a simplified beam model. One reason may be because the soil-structure interaction was included in the plane strain model.
- The assumption of elastic structure, and not including the soil-structure interaction in the simplified beam-model analyses result in too high mobilization of passive earth pressure, and thus the crack widths in the connection were overestimated.
- The FE-analyses indicated that the design of the connection at Korsvågen is not sufficient regarding allowable crack widths. Additional measures such as a haunch, additional struts or lighter backfill, may be used to reduce the crack widths.

7.1 Further studies

There are several aspects that would be interesting to study further regarding D-walls and their connection to tunnels. A further study that would be interesting is to investigate the effect of having D-wall panels with varying length and the effect of the vertical connections between panels. This could be studied for example by performing a three dimensional-model of the tunnel structure and D-walls.

Further, it would be interesting to study the effect of several parameters on the connection. The parameters of interest might be:

- Foundation of D-wall: to bedrock or clay
- Building method
- Type of connection
- Depth of tunnel

From such studies, it would be possible to understand the interplay between the involved parameters, and to recommend suitable requirements regarding permanent D-walls and their connection to the tunnel. To get a full understanding and

7. Conclusion

overview of underground tunnels built with permanent D-walls, it would be interesting to conduct a further study regarding the environmental effects of such structures, especially, compared to other more traditional methods used in Sweden.

Bibliography

- Alén, Claes, Lindvall, Anders, Johansson, Morgan, Magnusson, Jonas, and Norén, Christer (2006). “Slitsmurar som permanenta konstruktioner”. In: *SBUF Utvecklingsprojekt* 11603.
- Bartlett, F. Steven (2012). “Mohr-Coulomb Model”. In: URL: <https://fdocument.org/document/mohr-coulomb-model-civil-bartlettveen6920mohr-coulomb-modelpdfsteven-f-bartlett.html?page=1>.
- Bertbau (2017). *File:Ausführung-Schlitzwand.png*. URL: <https://commons.wikimedia.org/wiki/File:Ausf%C3%BChrung-Schlitzwand.png>. (accessed: April 01, 2022).
- Caster, Rickard, Kendes, Antonio, and Thunström, Fredrik (Mar. 18, 2022). personal communication at study visit Kvarnberget.
- Chen, Xiaoqing, Ding, Wenqi, Zhao, Tianchi, Lu, Xingbang, and Wei, Lixin (2020). “Deformation characteristics of latticed diaphragm wall in revetment foundation trench for one immersed tunnel”. In: *IOP Conference Series: Materials Science and Engineering*. Vol. 741. 1. IOP Publishing, p. 012018.
- COWI (2019). *Redogörelse för konstruktionsarbetets förutsättningar och metoder (RKFM) – E02 – Station Centralen, Km 456+870 till Km 457+700*. Tech. rep. Trafikverket.
- (2021). *Västlänken: 5310-Liseberg, Stödkonstruktioner, Slitsmur Armering - Detaljer, Detaljritning (E05-16-360-5310-0₀ – 1743)*.
- Dausch, Gebhard (2020). “Diaphragm Wall Technique – Planning, Execution and Development over the Last 65 Years”. In: *Recent Developments of Soil Mechanics and Geotechnics in Theory and Practice*. Ed. by T Triantafyllidis. Springer Nature Switzerland AG, pp. 347–354.
- Al-Emrani, M, Björn, E, Johansson, M, and Johansson, P (2011). “Bärande konstruktioner del 2 (Rapport 2011: 1)”. In: *Göteborg: Chalmers university of technology*.
- Everaars, MJC and Peters, MGJM (2013). “Finite element modelling of D-wall supported excavations”. In: *Proceedings of the 18th International Conference on Soil Mechanics and Geotechnical Engineering*, pp. 711–714.
- Feng, Zheyuan, Xu, Qi, Xu, Xiangyang, Tang, Qiang, Li, Xuedong, and Liao, Xin (2022). “Deformation Characteristics of Soil Layers and Diaphragm Walls during Deep Foundation Pit Excavation: Simulation Verification and Parameter Analysis”. In: *Symmetry* 14.2, p. 254.
- fib special activity group, and Taerwe, Luc and Matthys, Stijn (2013). *fib model code for concrete structures 2010*. Ernst Sohn, Wiley. ISBN: 9783433604090. URL: <http://dx.doi.org/10.1002/9783433604090%7D>.

- Fleming, Ken, Weltman, Austin, Randolph, Mark, and Elson, Keith (2008). *Piling engineering*. CRC press.
- Helwany, Sam (2007). *Applied soil mechanics with ABAQUS applications*. John Wiley Sons, Inc. ISBN: 978-0-471-79107-2.
- Hibbitt, Karlsson, Sorensen (2011). *ABAQUS User's Manual*. 6:th Edition. Pawtucket.
- Jankowiak, Tomasz and Lodygowski, Tomasz (2005). "Identification of parameters of concrete damage plasticity constitutive model". In: *Foundations of civil and environmental engineering* 6.1, pp. 53–69.
- Jansson, Anette and Wikström, Johanna (2006). "Load Effects on Permanent Diaphragm Walls. Interaction between soil and concrete structure". MA thesis.
- Knappett, Jonathan (2012). *Craig's soil mechanics*. Vol. 8. spon press London.
- Lubliner, Jacob, Oliver, Javier, Oller, Sand, and Oñate, Eugenio (1989). "A plastic-damage model for concrete". In: *International Journal of solids and structures* 25.3, pp. 299–326.
- Malm, Richard (2009). "Predicting shear type crack initiation and growth in concrete with non-linear finite element method". PhD thesis. KTH.
- Mortier, Hans, Doorn, Emile van, Zwart, Walther, and Sluis, Hans van der (2013). "Detailing Concrete Structures of a Top-Down Built Urban Tunnel Using Diaphragm Walls". In: *Structural Engineering International* 23.4, pp. 479–488.
- OpenStreetMaps (2015). *OpenStreetMaps of central Gothenburg in Sweden, including layer of Västlänken train tunnel*. URL: https://commons.wikimedia.org/wiki/File:Vastlanken_train_tunnel_in_Gothenburg_Sweden_map_based_on_OpenStreetMaps.png. (accessed: February 07, 2022).
- Scholz, Christian (2021). *Course on planning, execution and quality assurance of D-Walls*.
- SGS (2020). *Main Excavation and Concrete Tunnel km 458+100 to 458+260*. Tech. rep. Trafikverket.
- (2021). *Västlänken: E05-Kvarnberget-Betongtunnlar, Konstruktionsredovisning, Detalj Skjuvbox, Betongform Mittenplatta (E03-18-110-3300-0₀ – 0507)*.
- SIMULIA (2022). *Abaqus Analysis User's Guide (6.14) - 130.149.89.49:2080*. URL: <http://130.149.89.49:2080/v6.14/books/usb/default.htm>. (accessed: May 29, 2022).
- SIS (2005a). "Eurocode 2: Design of concrete structures - Part 1-1: General rules and rules for buildings". In.
- (2005b). "Eurocode 7: Geotechnical design - Part 1: General rules". In.
- Steffensen, Mette Baaring (2020). *Redogörelse för konstruktionsarbetets förutsättningar och metoder (RKFM), Stödkonstruktioner, geoteknik och grundvatten*. Tech. rep. Trafikverket.
- Swedish Standards Institute (2015). "Execution of special geotechnical work – Diaphragm walls". In.
- Taka2san (2012). *Mohr-coulomb2*. URL: <https://commons.wikimedia.org/wiki/File:Mohr-coulomb2.jpg>. (accessed: February 14, 2022).
- Technical Committee on Performance of Structures during Construction (2000). *Effective Analysis of Diaphragm Walls*. <https://books.google.se/books?id=Qepax7sIcqEC&pg=PA1&dq=diaphragm+wall&hl=sv&sa=X&ved=2ahUKewjitzvz->

- 3dv1AhV6QvEDHalwBGUQ6AF6BAgFEAI#v=onepage&q=diaphragm(visited 2022-02-10). ASCE Publications. ISBN: 0784474877, 9780784474877.
- Teike, Anna (Mar. 9, 2022a). personal communication at study visit Korsvägen.
- (Mar. 16, 2022b). personal communication at study visit Centralen.
- Trafikverket (2011). “TRV Geo, Trafikverkets tekniska krav för geokonstruktioner”. In.
- (2016a). *Krav Tunnelbyggande*. Tech. rep. Trafikverket.
- (2016b). *Råd Tunnelbyggande*. Tech. rep. Trafikverket.
- (2021a). *Krav med Rådstext TRVINFRA-00227, Bro och broliknande konstruktion, Byggande*. Tech. rep. Trafikverket.
- (2021b). *Krav TRVINFRA-00227, Bro och broliknande konstruktion, Byggande*. Tech. rep. Trafikverket.
- (2022). *Krav TRVINFRA-00230, Geokonstruktion, Dimensionering och utformning*. Tech. rep. Trafikverket.
- (n.d.). *The West Link Project (Västlanken)*. URL: <https://www.trafikverket.se/en/startpage/projects/Railway-construction-projects/The-West-Link-ProjectVastlanken/>. (accessed: January 24, 2022).
- Wahalathantri, Buddhi, Thambiratnam, David, Chan, Tommy, and Fawzia, Sabrina (2011). “A material model for flexural crack simulation in reinforced concrete elements using ABAQUS”. In: *Proceedings of the first international conference on engineering, designing and developing the built environment for sustainable wellbeing*. Queensland University of Technology, pp. 260–264.
- Xu, Ri-qing, Zhu, Yi-hong, and Ding, Pan (2021). “Performance of a Large-Scale Excavation by Bottom-Up Technique in Hangzhou Soft Clay”. In: *Advances in Civil Engineering* 2021.
- Zangeneh Kamali, Abbas (2012). *Shear strength of reinforced concrete beams subjected to blast loading: Non-linear dynamic analysis*.

A

Appendix A

Table A.1: National and international standards treating D-walls

National	Requirements
Krav TRVINFRA-00227 (Trafikverket 2021b)	Chapter 6.3.3.4 and 7.3.4.3: <ul style="list-style-type: none"> • D-walls should be designed with special regard to durability. • D-walls should be designed and dimensioned according to SS-EN 1538. • A D-wall subjected to bending moments should be reinforced. • For calculations regarding earth pressure, movements and consideration of geotechnical conditions, see TK Geo (Krav TRVINFRA-00230). • In case the D-wall should be used in a tunnel-construction and the requirements regarding tunnels are stricter, they should be followed.
Additional advises to TRVINFRA-00227 (Trafikverket 2021a)	Chapter 6.3.3.4: <ul style="list-style-type: none"> • The concrete in the D-wall cannot be expected to have sufficient durability against frost, chloride or fire. • D-walls subjected to these kinds of impacts should be designed as a twopart-construction with an inner wall.
Krav TRVINFRA-00230 (Trafikverket 2022)	Chapter 10.2: <ul style="list-style-type: none"> • The construction should be designed for loads from above construction and arising earth, and water pressure both in temporary and permanent stages. • For permanent constructions the earth pressure at rest might be recreated behind the D-wall over time. The effect of settlements which increase the active soil pressure behind the D-wall should be taken into consideration. • ULS: At design the following things should be considered: the total stability and load transferring between support constructions and underground. The D-wall should be designed such that progressive failure is avoided. • SLS: Design in SLS should show that allowable deformations are not exceeded and should be verified by measurements. • Partial safety factors: should be chosen as $\gamma_{G,g} = 1.1\gamma_d$ when the resultant of the active and passive earth pressure is >0. When the resultant is <0 the coefficient should be $\gamma_G = 1.0$. • The effect of permanent and variable loads should be separated. • If the result from calculations based on total-stability and rotation-stability contradict, the most conservative should be used, see Appendix A. • Characteristic values: when designing with a FE-analysis that considers the interaction between the soil and concrete, the forces should be multiplied with at least 1.4 at ductile and 1.5 at brittle failure.
International	
SS-EN 1538:2010 (Swedish Standards Institute 2015)	<ul style="list-style-type: none"> • Geotechnical investigation: General and specific requirements. • Materials and products: Constituents, general, bentonite, Polymers, Cement, Aggregates, Water, additions, admixtures, support fluids, bentonite suspensions, polymer solutions, fresh hardening slurries, concrete etc. • Considerations related to design: panel stability, reinforcement cage, design principles, vertical and horizontal reinforcement, multiple cages and joints etc. • Execution: construction phases, construction tolerances, excavation, forming the joints, concreting and trimming etc. • Supervision, testing and monitoring. • Records. • Special requirements.

A.1 Calculation methods

According to TRVINFRA 00230, if the two methods, total stability and rotational stability, contradict one another the most conservative result should be used henceforth in the dimensioning. To know which one is the most critical, the two methods are explained further.

A.1.1 Total stability method

The total stability can be calculated in both undrained and drained soils when investigating the slope-stability (Knappett 2012). In the undrained situation, right after construction, when the soil is assumed to be fully saturated the failure surface is illustrated as a circular arc. In addition to the assumption that the soil is fully saturated it is also assumed to be homogenous and cohesionless. In the total stability method, only moment equilibrium is considered and the moments that are considered are the moment from the weight of the soil and the resisting moment (Knappett 2012).

$$M_a = W * d \quad (\text{A.1})$$

$$M_r = c_u * r * L \quad (\text{A.2})$$

To control the safety with regard to total stability can then be calculated as:

$$F = M_r / M_a \quad (\text{A.3})$$

such that if F is larger than one, the slope is considered safe. Since the overturning moment is M_a , the weight of the soil above the failure surface is the governing factor of instability.

If the soil is drained, the method is slightly different. Then the area above the failure surface is divided into slices, see Figure A.1. Each slice has a base that is a straight line and assumed to have the same safety factor. In other words, there will be some inter-slice forces acting on each slice (Knappett 2012). The forces are shear forces on the sides and at the base, normal forces on the sides and at the base and the weight of the slice. The safety factor is in this case the available shear strength divided by the shear strength required to keep limiting equilibrium at the slip surface. In the drained analysis it is also possible to estimate the safety factors of inhomogeneous soil profiles as:

$$F = \frac{\sum_i (c_i + \sigma_i * \tan \phi) * l_i}{\sum_i W_i * \sin \alpha_i} \quad (\text{A.4})$$

Where W_i is the weight of each slice, c_i is the shear strength, σ_i is the vertical stress in each soil slice, ϕ_i is the friction angle and l_i is the length of the base. The method is statically indeterminate and require some assumptions about the inter-slice forces to be able to calculate the safety factor. Depending on the soil, if it is homogeneous or not, the slip surface has different shapes (Knappett 2012).

A.1.2 Rotation stability method

The rotational stability of the structure also has to be controlled. This is done by analyzing the effect of the earth pressure on the rotation of the D-wall (Fleming et al.

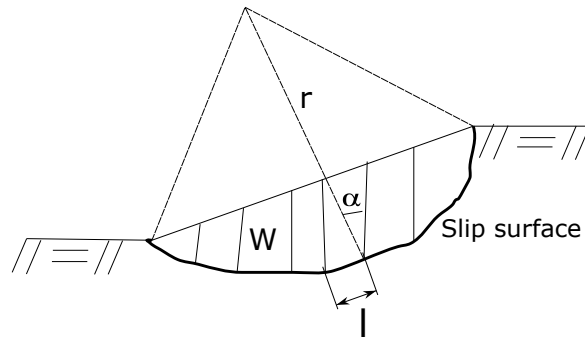


Figure A.1: Figure of failure surface and slices in the total stability method

2008). The soil behind the D-wall from a pressure that increases with depth acting towards the D-wall, see Figure A.2. At the excavation side, a similar pressure is acting in the other direction against the D-wall. To establish if active or passive earth pressure will develop, the maximum horizontal deflection of the D-wall subjected to the initial earth pressure have to be investigated (SIS 2005b). If the maximum horizontal deflection is 7-25%, in loose soil, or 5-10%, in dense soil, of the height of the D-wall, passive pressure is developed. If the maximum horizontal deflection is 0,4-0,5%, in loose soil, or 0,1-0,2%, in dense soil, active pressure is developed (SIS 2005b).

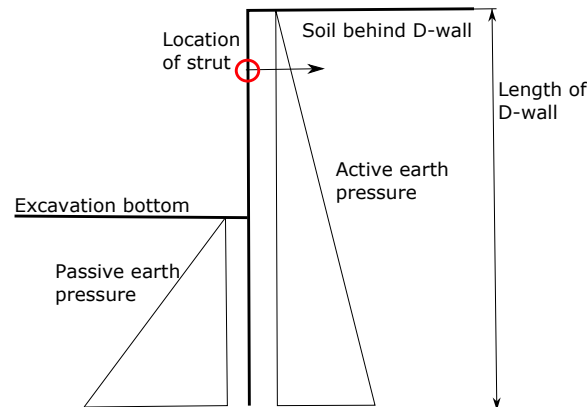


Figure A.2: Calculation properties of the rotational stability check

When the distribution of earth pressure is established a moment equilibrium is set up (Fleming et al. 2008). If the wall has a strut or anchor, the moment equilibrium should be taken about the location of this. From the moment equilibrium, the necessary length of the D-wall can be calculated and from that the resulting force in the strut. Similarly to the total stability method, a safety factor F can be found as the ratio between the restoring moment and the disturbing moment. If a specific safety factor is wanted, the procedure of calculating pressure distribution, moment equilibrium, length of D-wall and force in strut is repeated until it is reached (Fleming et al. 2008). Recommended values for the safety factor vary for different friction angles and if the construction is temporary or permanent. In general it increases with the friction angle and is higher when the construction is permanent.

B

Appendix B

B.1 Earth pressure and load calculations

Material	γ [N/m ³]	ϕ [°]	ψ [°]	Cohesion yield stress [Pa]
Fill	18000	28,3	0	100
Cl1	14700	35	5	1000
Cl2	15000	35	5	1000
Cl3	15000	35	5	1000
Sicl	18700	35	5	1000
Sisa	19000	32	2	100
D-wall	25000			
Top slab	25000			
Cross-wall	24000			

Backfill (LW)	11000	40	10	
Backfill standard	21000	35	5	
Reinforcement	78500			

Material	E [Pa]	ν
Fill	2,50E+07	0,3
Cl1	2,50E+07	0,2
Cl2	2,50E+07	0,2
Cl3	2,50E+07	0,2
Sicl	2,50E+07	0,2
Sisa	1,70E+07	0,3
D-wall	2,38E+10	0,15
Top slab	3,40E+10	0,15
CW	2,38E+10	0,2

Backfill (LW)	2,00E+07	0,3
Backfill standard	2,50E+07	0,3

$$K_0 = 1 - \sin\phi$$

$$K_a = (1 - \sin\phi)/(1 + \sin\phi)$$

$$K_p = (1 + \sin\phi)/(1 - \sin\phi)$$

	K0	Ka	Kp
Fill	0,526	0,357	2,803
Cl1	0,426	0,271	3,690
Cl2	0,426	0,271	3,690
Cl3	0,426	0,271	3,690
Sicl	0,426	0,271	3,690
Sisa	0,470	0,307	3,255
Backfill (LW)	0,357	0,217	4,599
Backfill standard	0,426	0,271	3,690

	Depth (z) [m]	Y [N/m ³]	$\sigma_v = Y * z$ [Pa]	$\sigma_h = K0 * \sigma_v$ [Pa]
Fill	1,5	18000	27000	14200
Clay 1	1,5	18000	27000	11513
Level of strut	3,5	14700	56400	24050
Clay 1	7	14700	107850	45990
Top of top slab	9,2	15000	140850	60062
Bottom of top slab	11	15000	167850	71575
Clay 2	15	15000	227850	97161
Clay 3	18	15000	272850	116350
Top of bottom slab	19,3	18700	297160	126716
Bottom of bottom slab	20,7	18700	323340	137880
SiCl	23	18700	366350	156220
SiSa	23	18700	366350	172214
Bottom of cross-wall	23,7	19000	379650	178466
SiSa	29	19000	480350	225803

Depth (z) [m]	Passive σ_p [Pa]	Active σ_a [Pa]
1,5	75679	9633
1,5	99635	7317
3,5	208126	15284
7	397985	29226
9,2	519761	38169
11	619395	45486
15	840806	61745
18	1006864	73940
19,3	1096572	80527
20,7	1193180	87622
23	1192318	99277
23	1351895	112564
23,7	1400974	116651
29	1772574	147592

Backfill

Depth (z) [m]	$\sigma_v = Y * z$ [Pa]	$\sigma_h = K0 * \sigma_v$ [Pa]	Passive σ_p [Pa]	Active σ_a [Pa]
1,5	31500	13432	116240	8536
3,5	73500	31342	271228	19918
3,5	73500	26255	338020	15982
7	112000	40008	515078	24354
9,2	136200	48652	626372	29616

Horizontal earth pressure [Pa]

Construction phase 1

Depth (z) [m]	Excavation side	Behind D-wall
0	0	0
1,5	0	14200
1,5	0	11513
3,5	0	24050
7	21939	45990
9,2	36011	60062
11	47525	71575
15	73110	97161
18	92299	116350
19,3	102666	126716
20,7	113830	137880
23	132170	156220
23	145702	172214
23,7	151954	178466
29	199291	225803

Construction phase 2

Depth (z) [m]	Excavation side	Behind D-wall
0	0	0
1,5	0	14200
1,5	0	11513
3,5	0	24050
7	0	45990
9,2	0	60062
11	0	71575
15	25585	97161
18	44774	116350
19,3	55141	126716
20,7	66305	137880
23	84645	156220
23	84645	172214
23,7	90317	178466
29	133257	225803

Construction phase 3

Depth (z) [m]	Excavation side	Behind D-wall
0	0	0
1,5	0	14200
1,5	0	11513
3,5	0	24050
7	0	45990
9,2	0	60062
11	0	71575
15	25585	97161
18	44774	116350
19,3	55141	126716
20,7	66305	137880
23	84645	156220
23	84645	172214
23,7	90317	178466
29	133257	225803

Construction phase 4

Depth (z) [m]	Excavation side	Behind D-wall
0	0	0
1,5	13432	14200
1,5	13432	11513
3,5	26255	24050
7	40008	45990
9,2	48652	60062
11	0	71575
15	25585	97161
18	44774	116350
19,3	55141	126716
20,7	66305	137880
23	84645	156220
23	84645	172214
23,7	90317	178466
29	133257	225803

Construction phase 5 and 6

Depth (z) [m]	Excavation side	Behind D-wall
0	0	0
1,5	13432	14200
1,5	13432	11513
3,5	26255	24050
7	40008	45990
9,2	48652	60062
11	0	71575
15	0	97161
18	0	116350
19,3	0	126716
20,7	0	137880
23	18340	156220
23	20218	172214
23,7	26470	178466
29	73807	225803

Construction phase 7

Depth (z) [m]	Excavation side	Behind D-wall
0	0	0
1,5	13432	14200
1,5	13432	11513
3,5	26255	24050
7	40008	45990
9,2	48652	60062
11	0	71575
15	0	97161
18	0	116350
19,3	0	126716
20,7	0	137880
23	18340	156220
23	20218	172214
23,7	26470	178466
29	73807	225803

Water pressure [Pa]

Construction phase 1

Depth (z) [m]	Excavation side	Behind D-wall
0	0	0
1,5	0	15000
3,5	0	35000
7	35000	70000
9,2	57000	92000
11	75000	110000
15	115000	150000
18	145000	180000
19,3	158000	193000
20,7	172000	207000
23	195000	230000
23,7	202000	237000
29	255000	290000

Construction phase 2

Depth (z) [m]	Excavation side	Behind D-wall
0	0	0
1,5	0	15000
3,5	0	35000
7	0	70000
9,2	0	92000
11	0	110000
15	40000	150000
18	70000	180000
19,3	83000	193000
20,7	97000	207000
23	120000	230000
23,7	127000	237000
29	180000	290000

Construction phase 3 and 4

Depth (z) [m]	Excavation side	Behind D-wall
0	0	0
1,5	0	15000
3,5	0	35000
7	0	70000
9,2	0	92000
11	0	110000
15	40000	150000
18	70000	180000
19,3	83000	193000
20,7	97000	207000
23	120000	230000
23,7	127000	237000
29	180000	290000

Construction phase 5 and 6

Depth (z) [m]	Excavation side	Behind D-wall
0	0	0
1,5	0	15000
3,5	0	35000
7	0	70000
9,2	0	92000
11	0	110000
15	0	150000
18	0	180000
19,3	0	193000
20,7	0	207000
23	23000	230000
23,7	30000	237000
29	83000	290000

Construction phase 7

Depth (z) [m]	Excavation side	Behind D-wall
0	0	0
1,5	15000	15000
3,5	35000	35000
7	70000	70000
9,2	92000	92000
11	0	110000
15	0	150000
18	0	180000
19,3	0	193000
20,7	0	207000
23	230000	230000
23,7	237000	237000
29	290000	290000

Uplift and weight of water below and above cross-wall, bottom slab and top slab

	Constr. Phase 1	Constr. Phase 2-4	Const. Phase 5-6	Permanent
Under Cross-wall	202000	127000	30000	237000
Over Cross-Wall	-172000	-97000	0	0
Under Botom slab	0	0	0	207000
Over Top slab	0	0	0	-92000

B.2 Water pressure in plane strain model

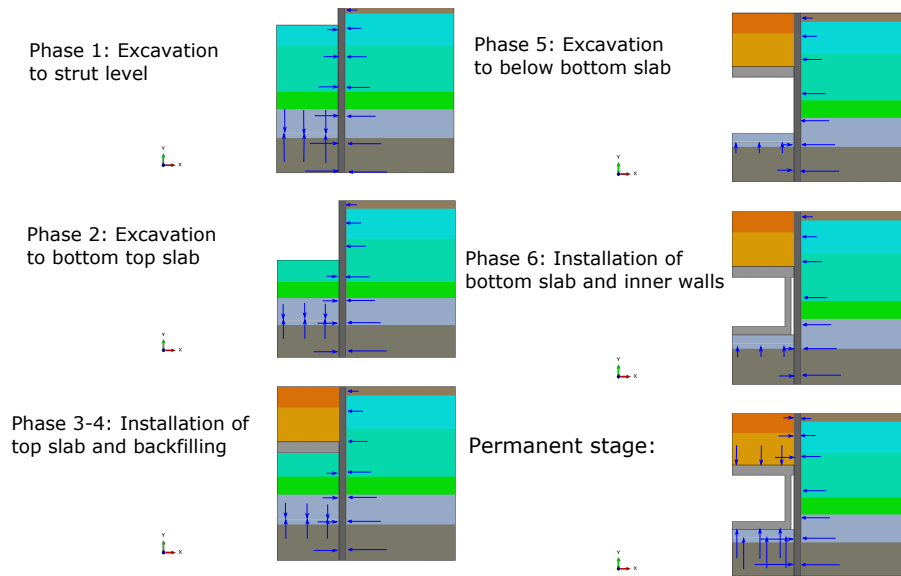


Figure B.1: Calculations steps in soil model with varying water pressure

C

Appendix C

C.1 Control of horizontal reaction forces in plane strain model

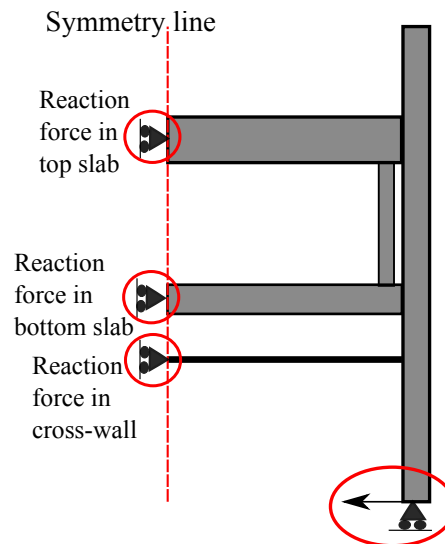


Figure C.1: The different reaction forces and force at the bottom of the D-wall used for the control

Step	CW	Top slab	Bottom slab
Step 3	0.1%	-	-
Step 4	0.3%	-	-
Step 5	0.3%	2.2%	-
Step 9	0.4%	0.7%	-
Step 10	0.7%	1.4%	-
Step 11	0.7%	1.4%	9.0%
Step 12	0.2%	0.1%	0.2%

Table C.1: Ratio between the horizontal force at the bottom of the D-wall and the different horizontal reaction forces along the symmetry line in the plane strain model

C.2 Mesh convergence study of plain strain model

The final mesh used in the 2D plane strain model is listed in Chapter 4.2.4 and the mesh convergence study of the D-wall, tunnel and soil is presented in Figure C.2. The mesh convergence of the soil was controlled both inside and outside the D-wall. The result used to study the convergence was the maximum deformation in the D-wall and top slab and the maximum vertical stress in the soil.

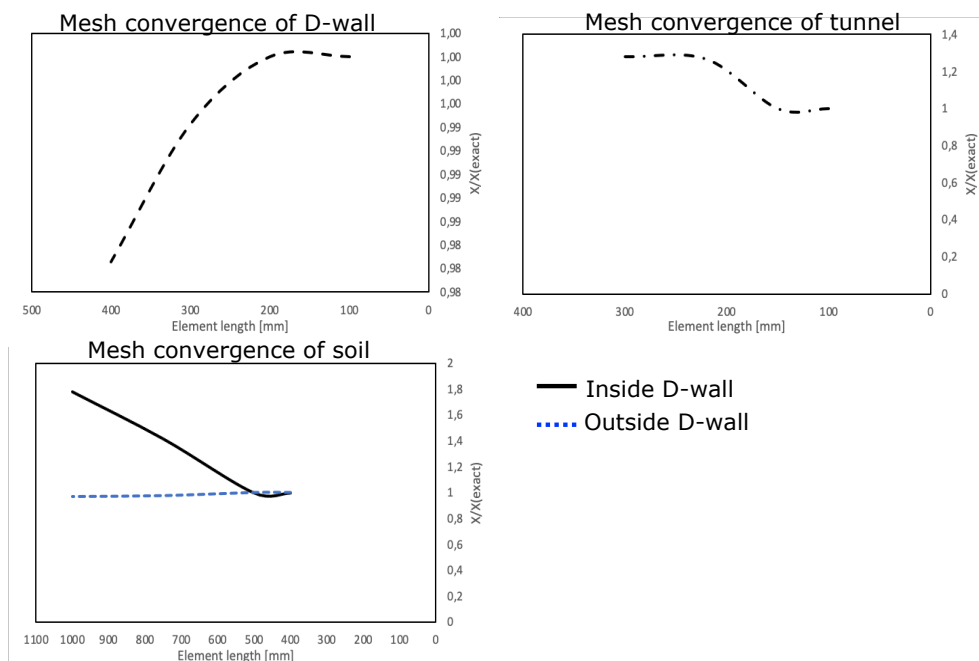


Figure C.2: Convergence study of different element-lengths in the D-wall, tunnel and soil

C.3 Complete verification of plane strain model

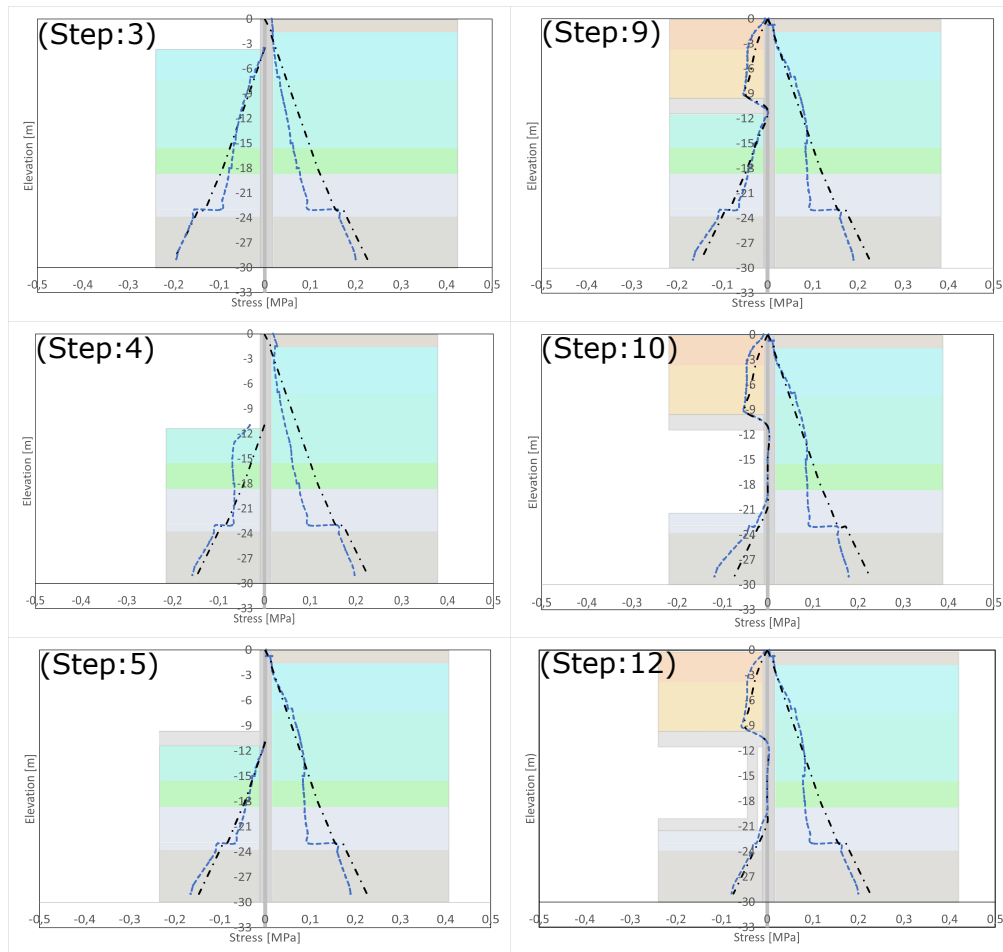


Figure C.3: Complete verification of the horizontal earth pressure

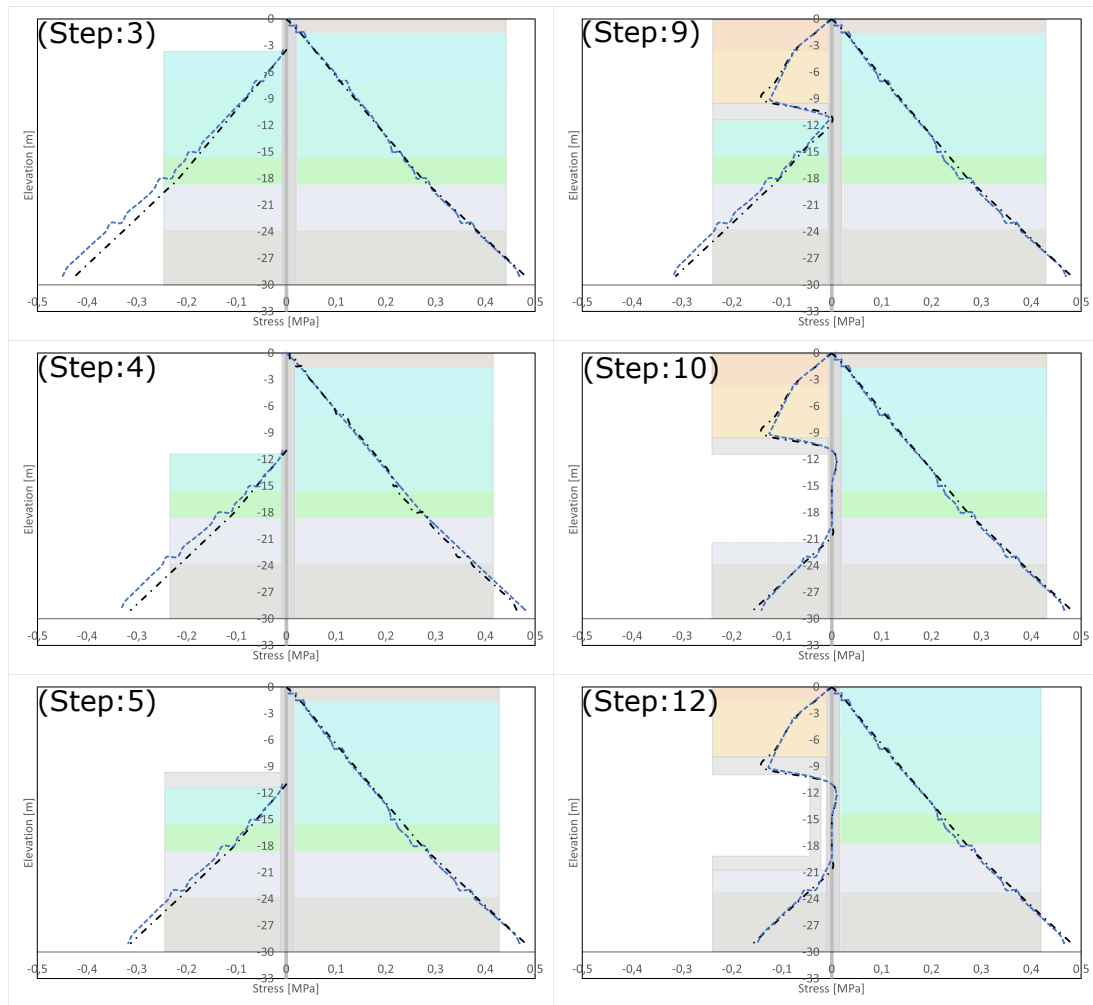


Figure C.4: Complete verification of the vertical earth pressure

D

Appendix D

D.1 Control of horizontal reaction forces in the beam model

Step	CW	Top slab	Bottom slab
Step 2	0.2%	-	-
Step 3	0.04%	-	-
Step 4	0.1%	2.5%	-
Step 5	0.3%	1.4%	-
Step 6	0.4%	10.4%	-
Step 7	0.4%	54.5%	20.4%
Step 8	0.05%	1.2%	0.3%

Table D.1: Comparison between the horizontal force at the bottom of the D-wall and the different horizontal reaction forces along the symmetry line in the beam model

D.2 Mesh convergence study of beam model

The mesh convergence study of the beam model was conducted comparing the deformation in the bottom of the D-wall and the outer field moment in the top slab. The result is shown in Figure D.1.

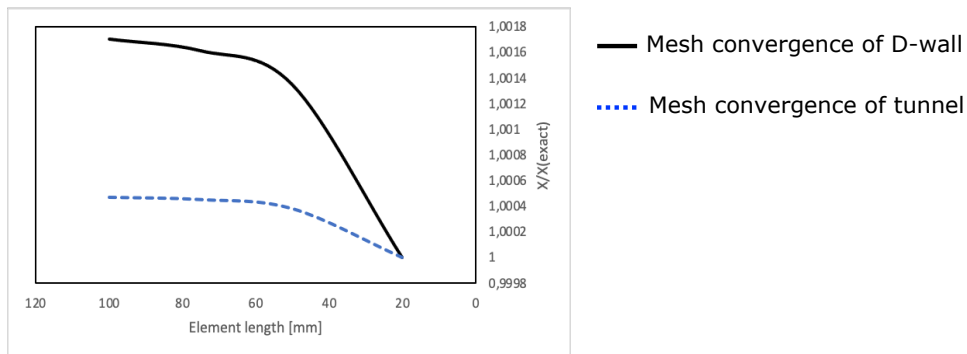


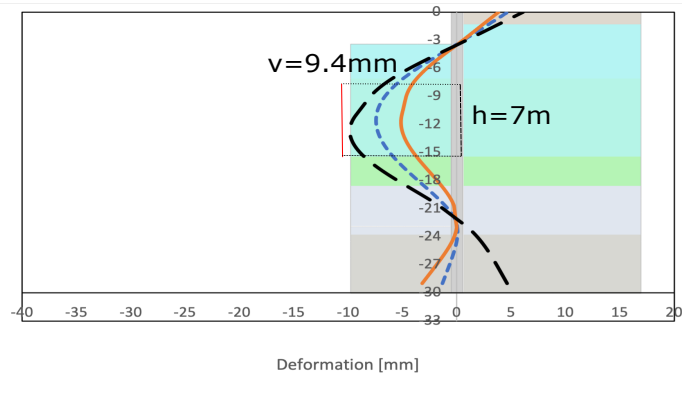
Figure D.1: Convergence study of the 2D beam model

D.3 Complete verification of beam model

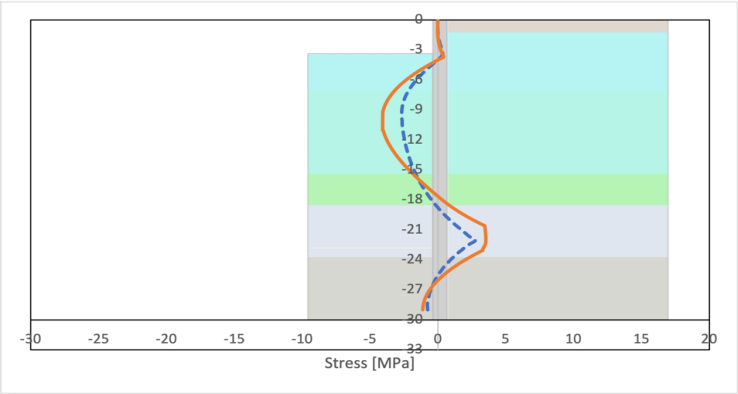
Construction phase 1

Depth (z) [m]	At rest at exc. Side [Pa]	Behind D-wall [Pa]	Partly mob passive [Pa]
0	0	0	0
1,5	0	14200	0
1,5	0	11513	0
3,5	0	24050	0
7	21939	45990	37972
9,2	36011	60062	62327
11	47525	71575	82254
15	73110	97161	126536
18	92299	116350	159748
19,3	102666	126716	102666
20,7	113830	137880	113830
23	132170	156220	132170
23	145702	172214	145702
23,7	151954	178466	151954
29	199291	225803	199291

Deformations of the D-wall



Vertical stresses along the D-wall



..... Plane strain Model - - - Beam model (at rest) — Beam model (partly mob)

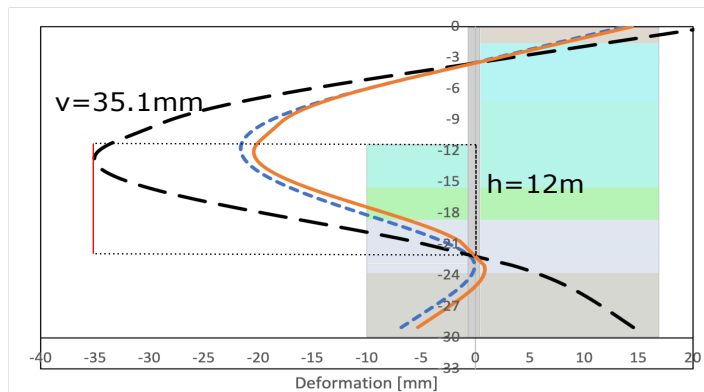
Max def [mm]	h [m]	v/h	Soil layer	Mob passive	Shape
9.84	7	0.141%	Clay 2	20%	b
			Clay 3	20%	b

Construction phase 2

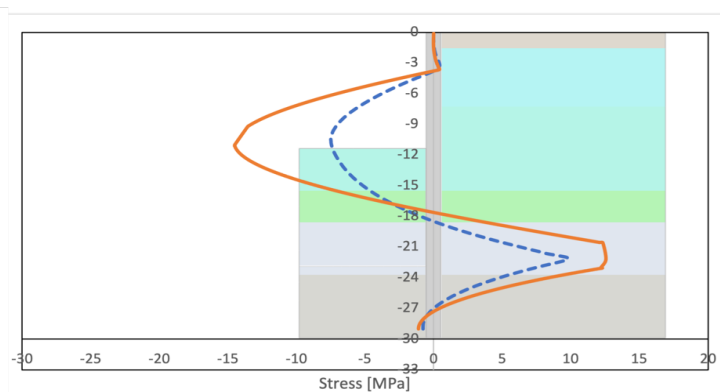
Depth (z) [m]	At rest at exc. Side [Pa]	Behind D-wall [Pa]	Partly mob passive [Pa]
0	0	0	0
1,5	0	14200	0
1,5	0	11513	0
3,5	0	24050	0
7	0	45990	0
9,2	0	60062	0
11	0	71575	0
15	25585	97161	88564
18	44774	116350	154987
19,3	55141	126716	190870
20,7	66305	137880	229514
23	84645	156220	293000
23	93311	172214	93311
23,7	99563	178466	99563
29	146900	225803	146900

Max def [mm]	h [m]	v/h	Soil layer	Mob passive	Shape
35.1	12	0.292%	Clay 2	40%	b
			Clay 3	40%	b
			SiCl	40%	b

Deformations of the D-wall



Vertical stresses along the D-wall

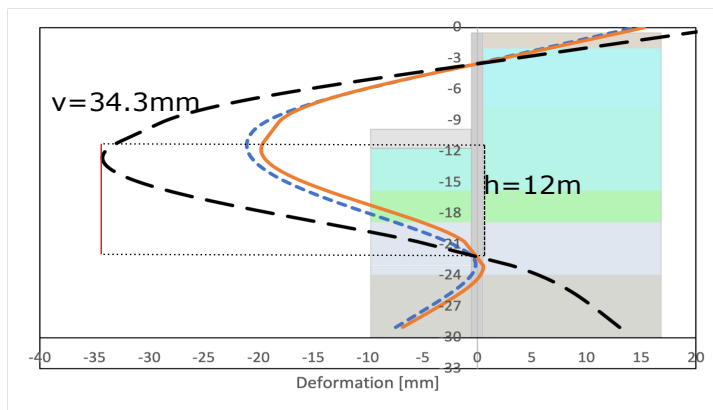


Construction phase 3

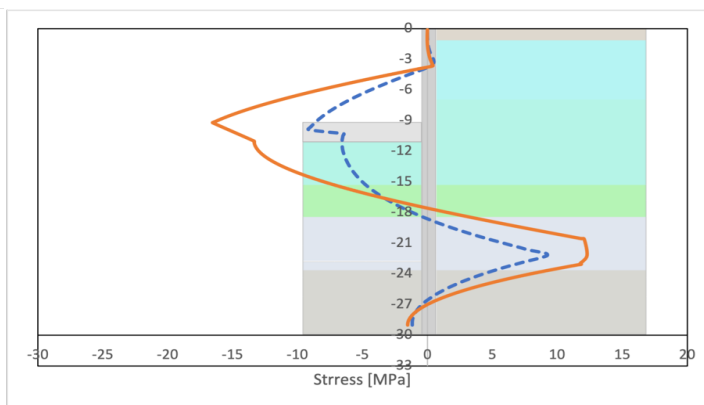
Depth (z) [m]	At rest at exc. Side [Pa]	Behind D-wall [Pa]	Partly mob passive [Pa]
0	0	0	0
1,5	0	14200	0
1,5	0	11513	0
3,5	0	24050	0
7	0	45990	0
9,2	0	60062	0
11	0	71575	0
15	25585	97161	88564
18	44774	116350	154987
19,3	55141	126716	190870
20,7	66305	137880	229514
23	84645	156220	293000
23	93311	172214	93311
23,7	99563	178466	99563
29	146900	225803	146900

Max def [mm]	h [m]	v/h	Soil layer	Mob passive	Shape
34.3	12	0.286%	Clay 2	40%	b
			Clay 3	40%	b
			SiCl	40%	b

Deformations of the D-wall



Vertical stresses along the D-wall

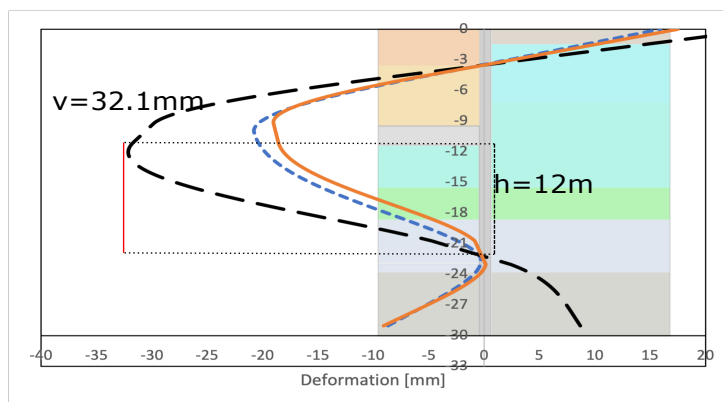


Construction phase 4

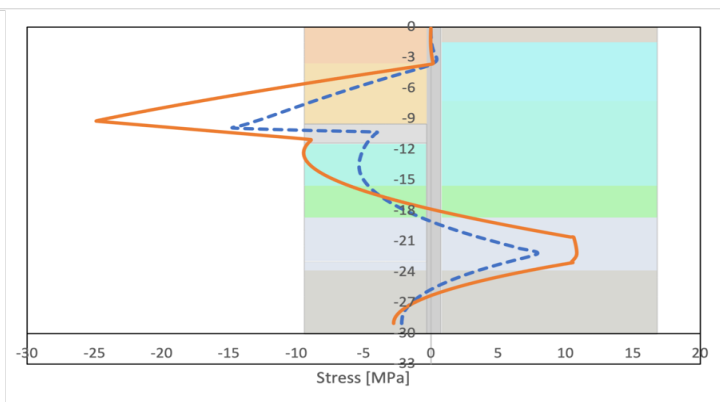
Depth (z) [m]	At rest at exc. Side [Pa]	Behind D-wall [Pa]	Partly mob passive [Pa]
0	0	0	0
1,5	13432	14200	13432
1,5	13432	11513	13432
3,5	26255	24050	26255
7	40008	45990	40008
9,2	48652	60062	48652
11	0	71575	0
15	25585	97161	66423
18	44774	116350	116240
19,3	55141	126716	143153
20,7	66305	137880	172135
23	84645	156220	219750
23	93311	172214	93311
23,7	99563	178466	99563
29	146900	225803	146900

Max def [mm]	h [m]	v/h	Soil layer	Mob passive	Shape
32.1	12	0.267%	Clay 2	30%	b
			Clay 3	30%	b
			SiCl	30%	b

Deformations of the D-wall



Vertical stresses along the D-wall

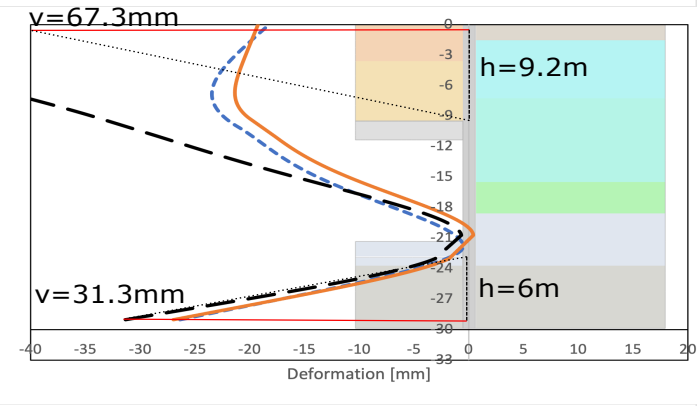


Construction phase 5

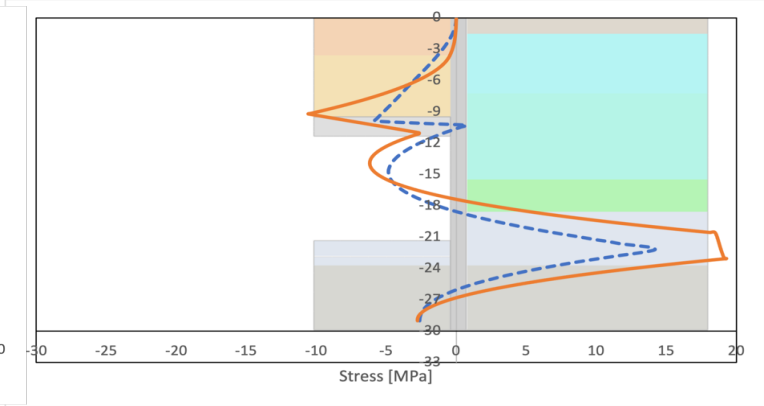
Depth (z) [m]	At rest at exc. Side [Pa]	Behind D-wall [Pa]	Partly mob passive [Pa]
0	0	0	0
1,5	13432	14200	46496
1,5	13432	11513	46496
3,5	26255	24050	118307
7	40008	45990	180277
9,2	48652	60062	219230
11	0	71575	0
15	0	97161	0
18	0	116350	0
19,3	0	126716	0
20,7	0	137880	0
23	18340	156220	18340
23	20218	172214	41994
23,7	26470	178466	54980
29	73807	225803	153301

Max def [mm]	h [m]	v/h	Soil layer	Mob passive	Shape
67.3	9.2	0.732%	BF standard	40%	a
			BF Lightweight	35%	a
31.3	6	0.34%	SiSa	30%	c

Deformations of the D-wall



Vertical stresses along the D-wall

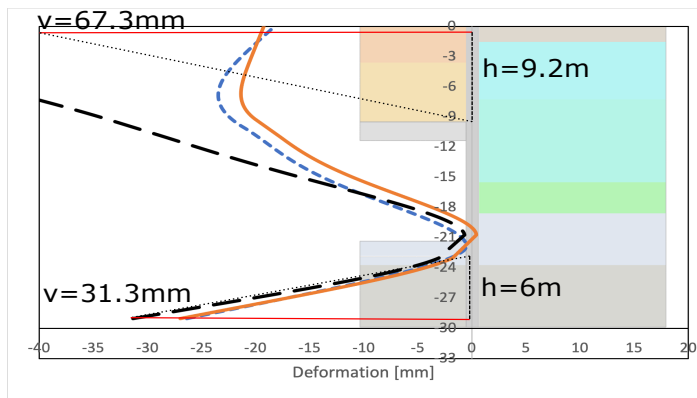


Construction phase 6

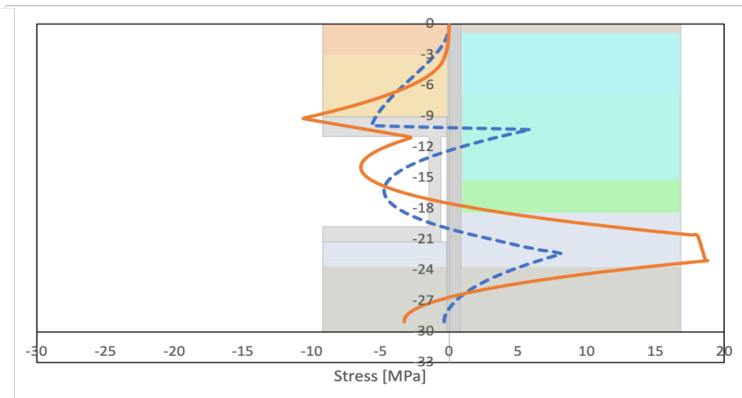
Depth (z) [m]	At rest at exc. Side [Pa]	Behind D-wall [Pa]	Partly mob passive [Pa]
0	0	0	0
1,5	13432	14200	46496
1,5	13432	11513	46496
3,5	26255	24050	118307
7	40008	45990	180277
9,2	48652	60062	219230
11	0	71575	0
15	0	97161	0
18	0	116350	0
19,3	0	126716	0
20,7	0	137880	0
23	18340	156220	18340
23	20218	172214	41994
23,7	26470	178466	54980
29	73807	225803	153301

Max def [mm]	h [m]	v/h	Soil layer	Mob passive	Shape
67.3	9.2	0.732%	BF standard	40%	a
			BF Lightweight	35%	a
31.3	6	0.34%	SiSa	30%	c

Deformations of the D-wall



Vertical stresses along the D-wall

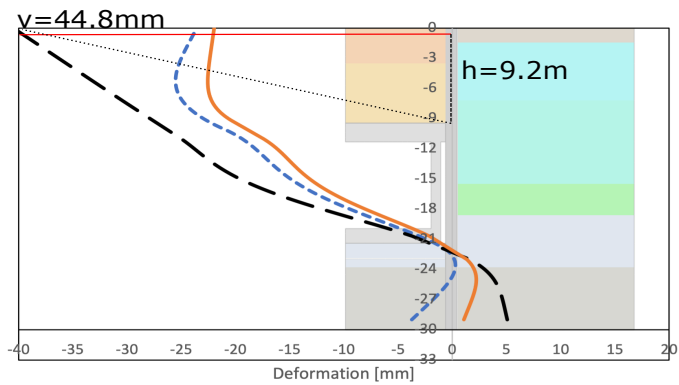


Permanent stage

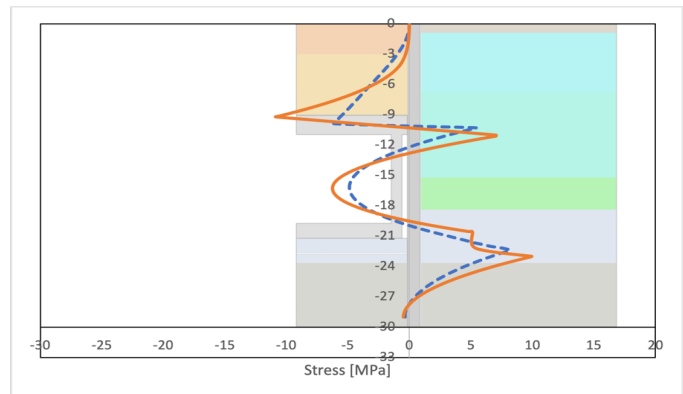
Depth (z) [m]	At rest at exc. Side [Pa]	Behind D-wall [Pa]	Partly mob passive [Pa]
0	0	0	0
1,5	13432	14200	34872
1,5	13432	11513	34872
3,5	26255	24050	84505
7	40008	45990	128769
9,2	48652	60062	156593
11	0	71575	0
15	0	97161	0
18	0	116350	0
19,3	0	126716	0
20,7	0	137880	0
23	18340	156220	18340
23	20218	172214	20218
23,7	26470	178466	26470
29	73807	225803	73807

Max def [mm]	h [m]	v/h	Soil layer	Mob passive	Shape
44.8	9.2	0.487%	BF standard	30%	a
			BF Lightweight	25%	a

Deformations of the D-wall



Vertical stresses along the D-wall

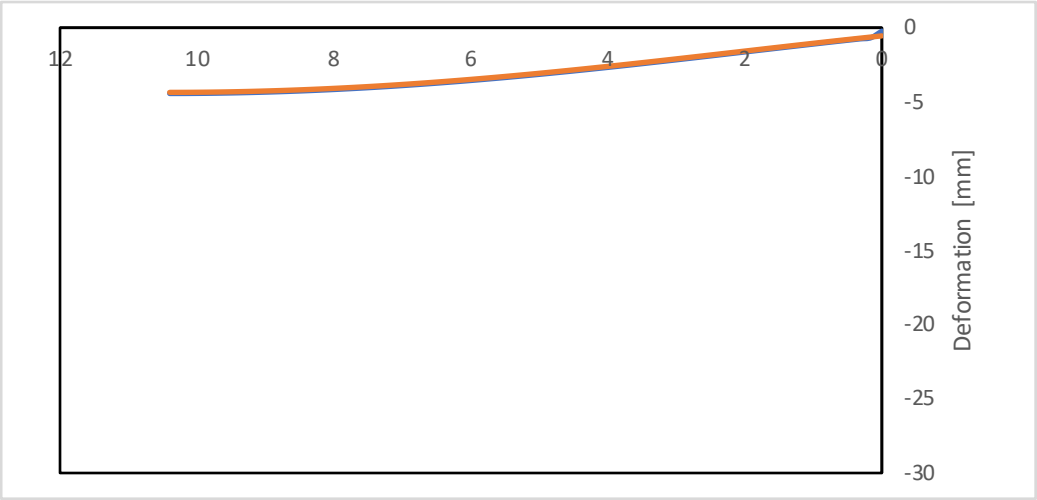


Comparison of deformations and horizontal stresses in top slab

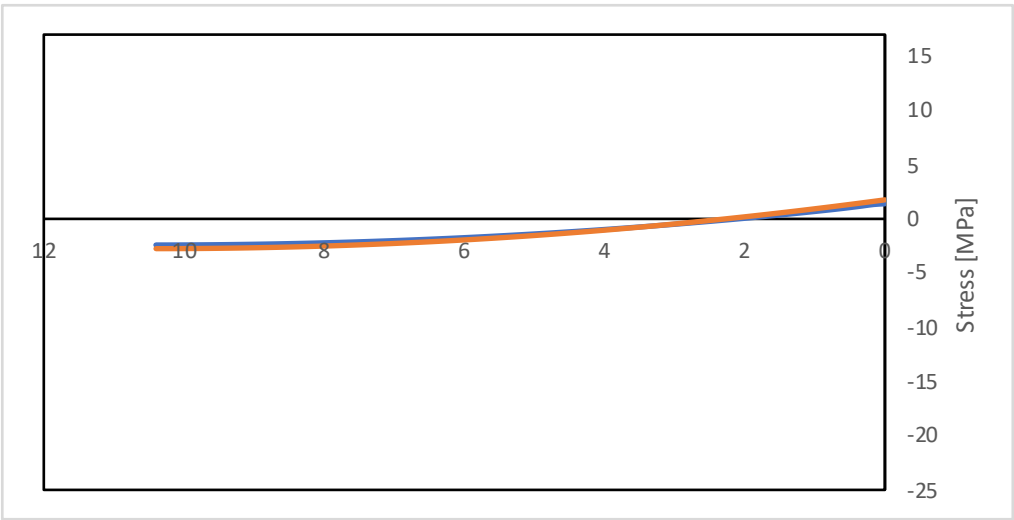
Construction phase 3

..... Plane strain model — Beam model (partly pass)

Deformation in top slab

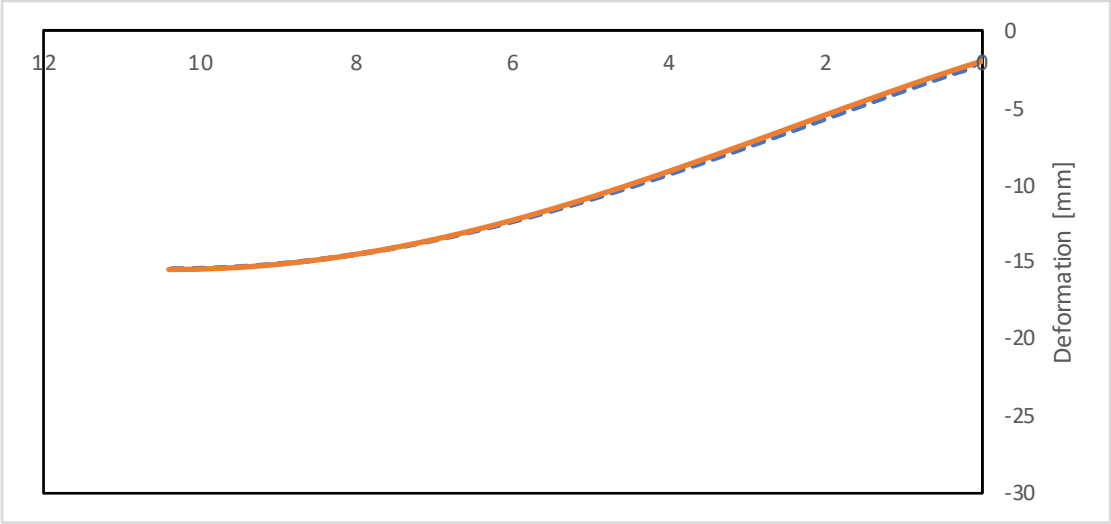


Horizontal stress along upper edge of top slab

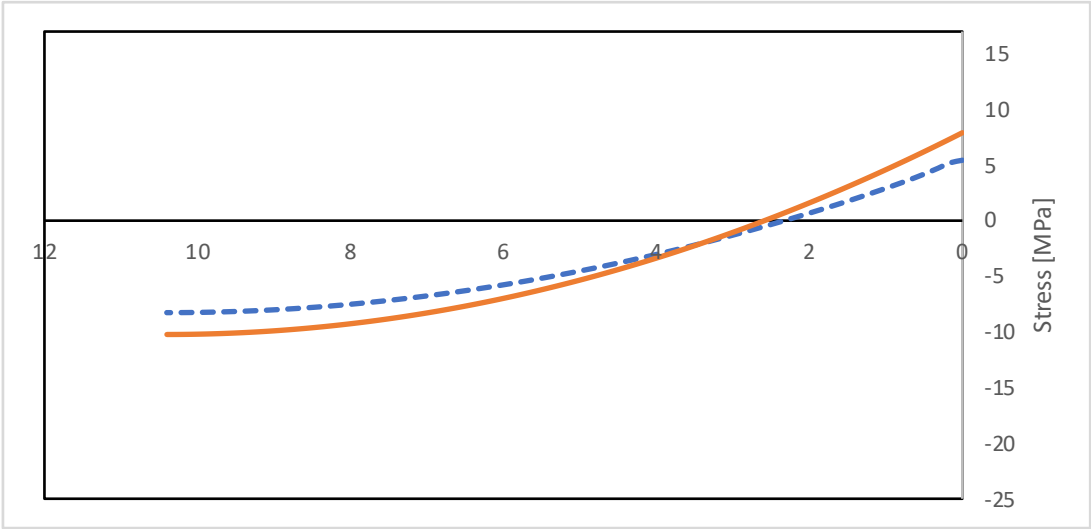


Construction phase 4

Deformation in top slab

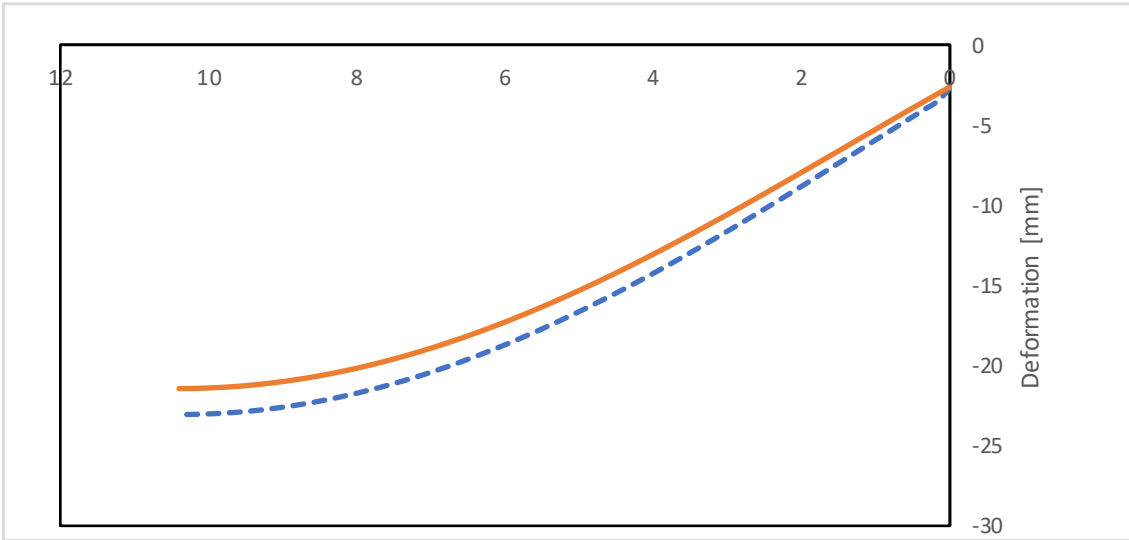


Horizontal stress along upper edge of top slab

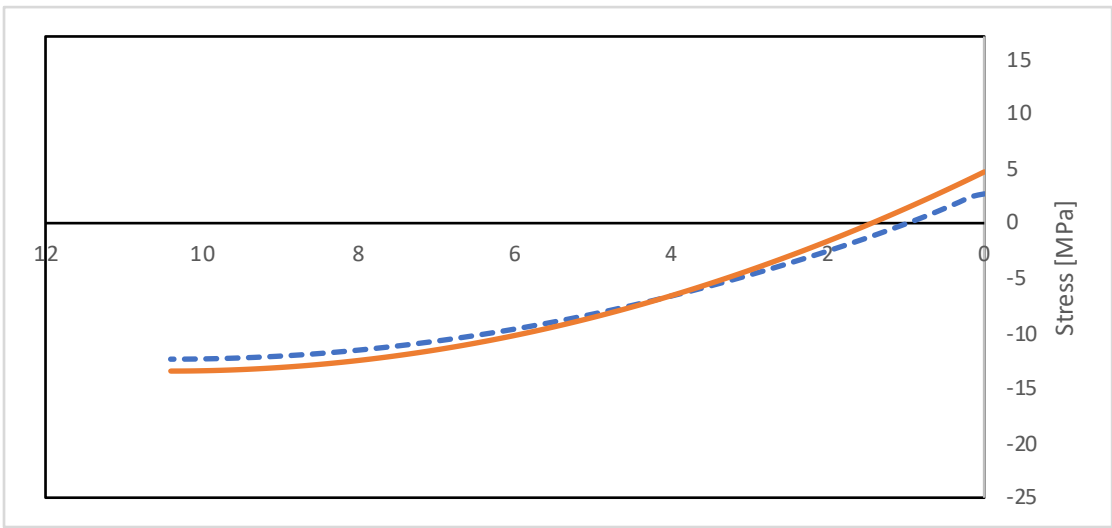


Construction phase 5

Deformation in top slab

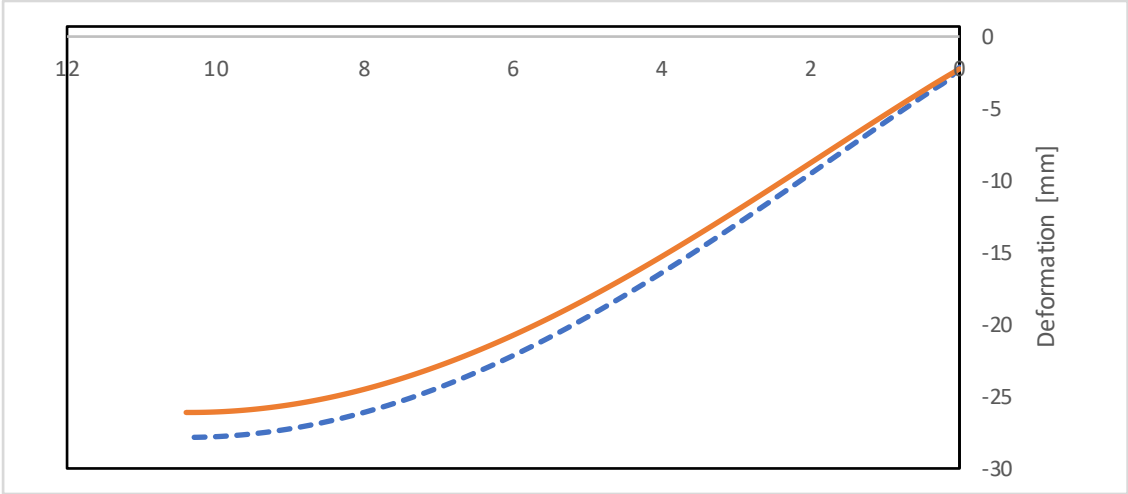


Horizontal stress along upper edge of top slab

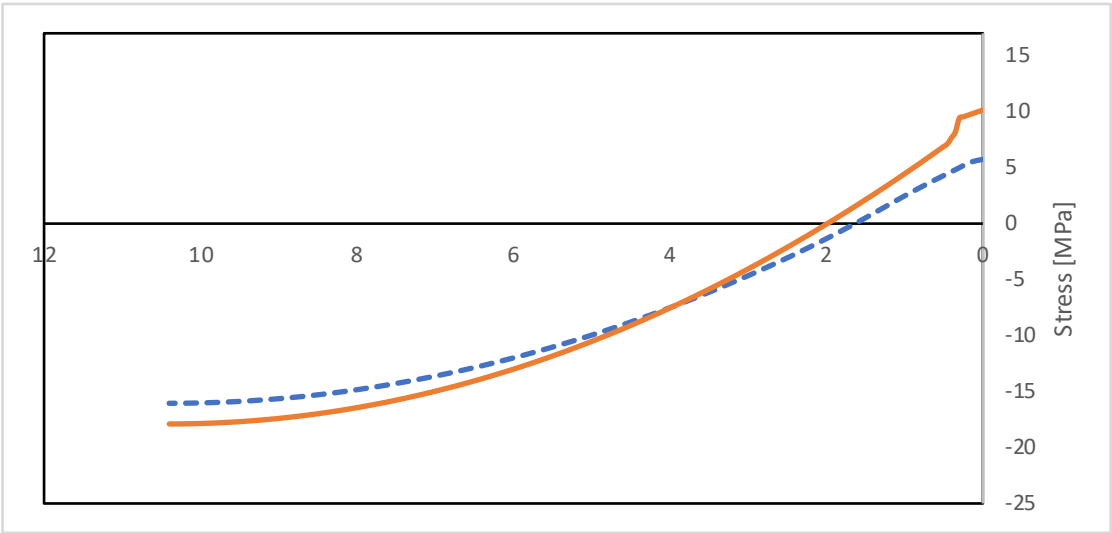


Permanent stage

Deformation in top slab



Horizontal stress along upper edge of top slab



E

Appendix E

E.1 Material and element type of local model

Calculation of tension softening parameters

According to Hordjik (Zangeneh Kamali 2012)

$$\sigma_t(w) = \left(\left(1 + \left(c_1 * \frac{w}{w_c} \right)^3 \right) * e^{-c_2 * \frac{w}{w_c}} - \frac{w}{w_c} * (1 + c_1^3) * e^{-c_2} \right) * f_{ctm}$$

$$c_1 = 3 \quad c_2 = 6$$

W is the crack opening displacement

Wc is the maximum crack opening displacement at zero tension

According to model code 2010

Fracture energy of concrete:

$$G_f = 73 * f_{cm}^{0.18} \left[\frac{N}{m} \right] \quad W_c = 5.14 * \left(\frac{G_f}{f_{ctm}} \right) [mm]$$

D-wall C40/50
f _{cm} = 48 Mpa
f _{ctm} = 3,5 Mpa
G _f = 146.54 N/m
W _c = 0,215 mm

Top slab C35/45
f _{cm} = 43 MPa
f _{ctm} = 3,2 MPa
G _f = 143.66 N/m
W _c = 0,231 mm

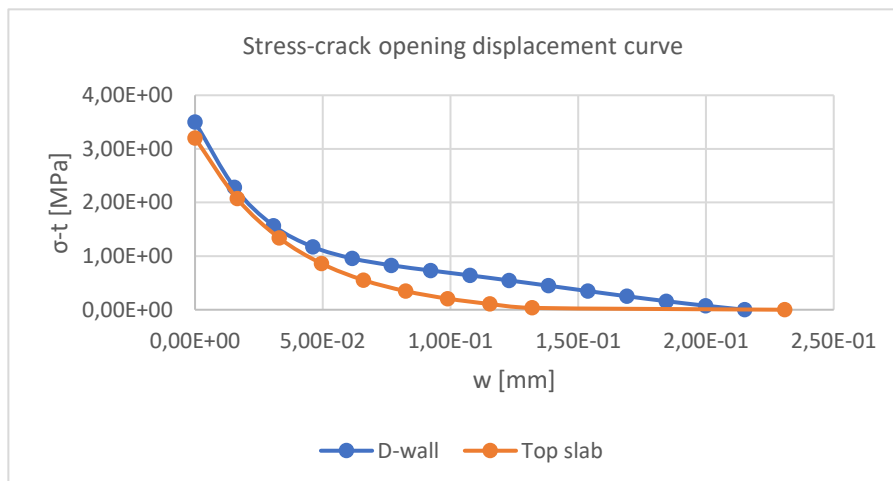
The peak tension stress will be used as input in the FE analysis in the submodel to express the tension softening behaviour after cracking

D-wall

f _{ctm} [Mpa]	w [mm]
3,50E+00	0,00E+00
2,29E+00	1,54E-02
1,57E+00	3,07E-02
1,17E+00	4,61E-02
9,58E-01	6,15E-02
8,29E-01	7,69E-02
7,32E-01	9,22E-02
6,41E-01	1,08E-01
5,47E-01	1,23E-01
4,48E-01	1,38E-01
3,49E-01	1,54E-01
2,52E-01	1,69E-01
1,60E-01	1,84E-01
7,56E-02	2,00E-01
0,00E+00	2,15E-01

Top slab

f _{ctm} [Mpa]	w [mm]
3,20E+00	0,00E+00
2,07E+00	1,65E-02
1,34E+00	3,30E-02
8,63E-01	4,95E-02
5,53E-01	6,59E-02
3,47E-01	8,24E-02
2,07E-01	9,89E-02
1,08E-01	1,15E-01
3,50E-02	1,32E-01
0,00E+00	2,31E-01



E.2 Material and element type of local model

Damage evolution parameters and stiffness recovery

According to Hordjik (Zangeneh Kamali 2012)

D-wall	C40/50 [Pa]
f _{cm}	4,80E+07
f _{ctm}	3,50E+06
E	2,38E+10

Top slab	C35/45 [Pa]
f _{cm}	4,30E+07
f _{ctm}	3,20E+06
E	3,40E+10

$$\varepsilon_t = \frac{f_{ctm}}{E}$$

$$\varepsilon_t = 1.47E-04$$

$$\varepsilon_t = 9.41E-5$$

$$\varepsilon_t^{ck} = \varepsilon_t - \left(\frac{\sigma_t}{E} \right)$$

$$\varepsilon_t^{pl} = bt * \varepsilon_t^{ck}$$

$$bt = 0.7$$

$$dt = 1 - \left(\frac{\sigma_t * E^{-1}}{\sigma_t * E^{-1}} + \varepsilon_t^{ck} * (1 - bt) \right)$$

D-wall			
σ_t [Pa]	ε_t^{ck}	dt	ε_t^{pl}
3,50E+06	0,00E+00	0,00E+00	0,00E+00
2,29E+06	5,10E-05	1,38E-01	3,57E-05
1,57E+06	8,12E-05	2,70E-01	5,68E-05
1,17E+06	9,78E-05	3,73E-01	6,85E-05
9,58E+05	1,07E-04	4,43E-01	7,48E-05
8,29E+05	1,12E-04	4,92E-01	7,86E-05
7,32E+05	1,16E-04	5,32E-01	8,14E-05
6,41E+05	1,20E-04	5,72E-01	8,41E-05
5,47E+05	1,24E-04	6,18E-01	8,69E-05
4,48E+05	1,28E-04	6,71E-01	8,98E-05
3,49E+05	1,32E-04	7,31E-01	9,27E-05
2,52E+05	1,36E-04	7,95E-01	9,55E-05
1,60E+05	1,40E-04	8,62E-01	9,82E-05
7,56E+04	1,44E-04	9,31E-01	1,01E-04

Top slab			
σ_t [Pa]	ε_t^{ck}	dt	ε_t^{pl}
3,20E+06	0,00E+00	0,00E+00	0,00E+00
2,07E+06	3,32E-05	1,41E-01	2,32E-05
1,34E+06	5,48E-05	2,94E-01	3,83E-05
8,63E+05	6,87E-05	4,48E-01	4,81E-05
5,53E+05	7,78E-05	5,89E-01	5,45E-05
3,47E+05	8,39E-05	7,11E-01	5,87E-05
2,07E+05	8,80E-05	8,13E-01	6,16E-05
1,08E+05	9,09E-05	8,96E-01	6,37E-05
3,50E+04	9,31E-05	9,64E-01	6,52E-05

F

Appendix F

F.1 Loads applied to local model

Table F.1: Section forces/moments inserted at the upper reference point in the D-wall

Step	X-direction	Y-direction	Moment
Step 1	548725	-239990	-3365390
Step 2	924436	-239970	-4643890
Step 3	793874	-240000	-2660820
Step 4	774626	-239996	-2091910
Step 5	665844	-240068	-1775700

Table F.2: Section forces/moments inserted at the reference point in the top slab

Step	X-direction	Y-direction	Moment
Step 1	-157382	-300466	-266478
Step 2	-323415	-1243550	-603106
Step 3	-211555	-1344880	-2011930
Step 4	-90345	-1345100	-2267460
Step 5	96252	-2014440	-2376880

Table F.3: Section forces/moments inserted at the reference point in the inner wall

Step	X-direction	Y-direction	Moment
Step 4	-494309	-100008	166318
Step 5	1519860	427697	-201989

F.2 Mesh convergence study of local model

The mesh convergence study of the local model was done by varying the mesh and comparing the vertical and horizontal reaction force with the assumed exact value, see Figure F.1. The final mesh had an element length of 20 mm.

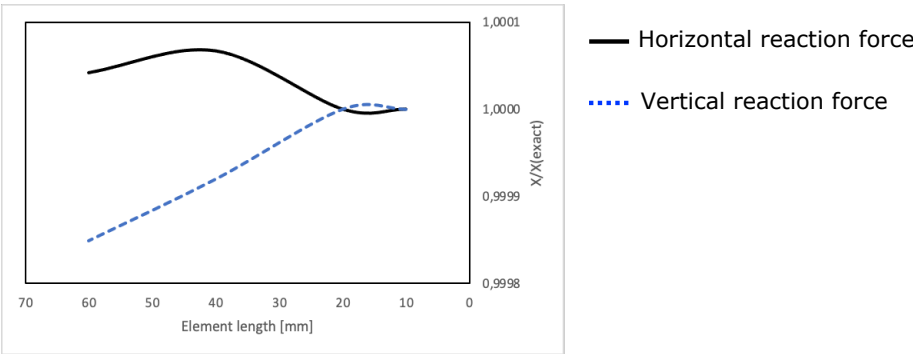


Figure F.1: Convergence study of the 2D local model of the connection

G

Appendix G

G.1 Verification of crack widths and steel stress at top slab

Calculation of crack width at Top slab:

According to EC2 and RKFM-E05

Top slab C35/45

f _{cm} [Mpa]	f _{ctm} [Mpa]	E _c [Gpa]	b x h [m]	E _s [Gpa]
4,30E+01	3,20E+01	3,40E+01	1 x 1,8	2,00E+02

Reinforcement

Bottom (5 x 3)

Ø 32	s150	B161
Ø 32	s150	B163
Ø 32	s150	B166

Top (5 x 1)

Ø 32	s150	A164
------	------	------

X-c [m]	9,00E-01
d1 [m]	1,63E+00
d2 [m]	1,50E+00
d3 [m]	1,37E+00
d-ave [m]	1,50E+00
d' [m]	2,46E-01

Asi [m^2]	A'-Ø32 [m^2]	A-Ø32 [m^2]
8,04E-04	4,02E-03	1,21E-02

Assume uncracked section:

α _s	Ac [m^2]	A-I [m^2]	X-I [m]	I-c [m^4]
5,88E+00	1,80E+00	1,88E+00	9,12E-01	4,86E-01
			I-I [m^4]	M-cr [KNm]
			5,15E-01	1,86E+03

Where:

$$A_I = A_c + (\alpha_s - 1) * A'_s + (\alpha_s - 1) * A_s$$

$$\alpha_s = E_s / E_c$$

$$x_I = \frac{A_c * X_c + (\alpha_s - 1) * A'_s * d' + (\alpha_s - 1) * A_s * d}{A_I}$$

$$I_I = I_c + A_c * (x_I - x_c)^2 + (\alpha_s - 1) * A'_s * (x_I - d')^2 + (\alpha_s - 1) * A_s * (d - x_I)^2$$

$$M_{cr} = f_{ctm} * \frac{I_I}{h - x_I}$$

The extracted force and moment from the beam model:

SF1 [KN]	SM [KNm]
6,25E+02	5,74E+03

M-cr < SM => the section is in stage 2

Guess a new x:

x [m]	x-tp [m]	A-II [m^2]	I-II [m^4]	e [m]
3,66E-01	3,91E-01	4,57E-01	1,08E-01	5,09E-01

$$A_{II} = b * x + (\alpha_s - 1) * A'_s + \alpha_s * A_s$$

$$x_{tp} = \frac{b * x * \frac{x}{2} + (\alpha_s - 1) * A'_s * d' + \alpha_s * A_s * d}{A_{II}}$$

$$I_{II} = b * \frac{x^3}{12} + b * x * \left(\frac{x}{2} - x_{tp}\right)^2 + (\alpha_s - 1) * A'_s * (x_{tp} - d')^2 + \alpha_s * A_s * (d - x_{tp})^2$$

occ (x-ttp) [Mpa]	occ (d ave - ttp) [Mpa]	occ (-ttp) [Mpa]	os [Mpa]
5,63E-03	6,37E+01	-2,06E+01	3,75E+02

Where:

$$\sigma_{cc}(z) = \frac{N}{A} + \frac{N * e + M}{I} * z$$

$$\sigma_s = \alpha_s * \sigma_{cc}(d_{ave} - x_{tp})$$

$$w_k = s_{r,max} * (\epsilon_{sm} - \epsilon_{cm})$$

$$s_{r,max} = K_3 * C + K_1 * K_2 * K_4 * \Theta / \rho_{p,eff}$$

$$\epsilon_{sm} - \epsilon_{cm} = \frac{\left(\sigma_s - K_t * \left(\frac{f_{ctmeff}}{\rho_{peff}}\right) * (1 - \sigma_s * \rho_{peff})\right)}{E_s} > 0,6 * \sigma_s * E_s$$

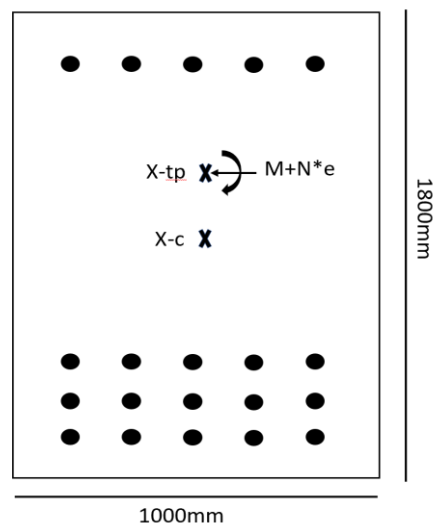
k1	k2	k3	k4
8,00E-01	5,00E-01	1,49E+00	4,25E-01

$$h_{eff} = \min\left(2,5 * (h - d), \frac{h - x_{tp}}{3}, \frac{h}{2}\right)$$

h-eff [m]	c [m]	Θ [m]	ρ-p,eff	Ac,eff [m^2]
4,70E-01	1,50E-01	3,20E-02	2,57E-02	4,70E-01

fctm,eff [Mpa]	kt	ε,sm - ε,cm	Wk [mm]
3,20E+00	4,00E-01	1,59E-03	6,92E-01

$$\epsilon_{sm} - \epsilon_{cm} > 0,6 * \sigma_s * E_s \quad \text{ok}$$



G.2 Verification of crack widths and steel stress at D-wall

Calculation of crack width at D-wall:

According to EC2 and RKFM-E05

D-wall C40/50

f _{cm} [Mpa]	f _{ctm} [Mpa]	E _c [Gpa]	b x h [m]	E _s [Gpa]
4,80E+01	3,50E+00	2,38E+01	1 x 1,2	2,00E+02

Reinforcement

Bottom (4 x 3)

Ø 20	s150	A101
Ø 40	s150	A105
Ø 40	s150	A106

Top (4 x 2)

Ø 40	s150	A130
Ø 40	s150	A137

X-c [m]	6,00E-01
d1 [m]	1,06E+00
d2 [m]	9,15E-01
d3 [m]	7,85E-01
d-ave [m]	9,45E-01
d-ave Ø40 [m]	9,85E-01

d1' [m]	1,45E-01
d2' [m]	2,85E-01
d'-ave [m]	2,15E-01

Asi [m^2]	A'-Ø40 [m^2]	A-Ø40 [m^2]	A-Ø20 [m^2]
1,26E-03	1,01E-02	1,01E-02	1,26E-03

Assume uncracked section:

α-s	Ac [m^2]	A-I [m^2]	X-I [m]	I-c [m^4]
8,40E+00	1,20E+00	1,36E+00	6,01E-01	1,44E-01
			I-I [m^4]	M-cr [KNm]
			1,66E-01	9,73E+02

Where:

$$A_I = A_c + (\alpha_s - 1) * A'_s + (\alpha_s - 1) * A_s$$

$$\alpha_s = E_s / E_c$$

$$x_I = \frac{A_c * X_c + (\alpha_s - 1) * A'_s * d' + (\alpha_s - 1) * A_s * d}{A_I}$$

$$I_I = I_c + A_c * (x_I - x_c)^2 + (\alpha_s - 1) * A'_s * (x_I - d')^2 + (\alpha_s - 1) * A_s * (d - x_I)^2$$

$$M_{cr} = f_{ctm} * \frac{I_I}{h - x_I}$$

The extracted force and moment from the beam model:

SF1 [KN]	SM [KNm]
2,75E+02	2,55E+03

M-cr < SM => the section is in stage 2

Guess a new x:

x [m]	x-tp [m]	A-II [m^2]	I-II [m^4]	e [m]
3,13E-01	3,24E-01	4,83E-01	5,14E-02	2,76E-01

$$A_{II} = b * x + (\alpha_s - 1) * A'_s + \alpha_s * A_s$$

$$x_{tp} = \frac{b * x * \frac{x}{2} + (\alpha_s - 1) * A'_s * d' + \alpha_s * A_s * d}{A_{II}}$$

$$I_{II} = b * \frac{x^3}{12} + b * x * \left(\frac{x}{2} - x_{tp}\right)^2 + (\alpha_s - 1) * A'_s * (x_{tp} - d')^2 + \alpha_s * A_s * (d - x_{tp})^2$$

occ (x-ttp) [Mpa]	occ (d ave - xtp) [Mpa]	occ (-xtp) [Mpa]	os [Mpa]
3,46E-03	3,23E+01	-1,60E+01	2,72E+02

Where:

$$\sigma_{cc}(z) = \frac{N}{A} + \frac{N * e + M}{I} * z$$

$$\sigma_s = \alpha_s * \sigma_{cc}(d_{ave} - x_{tp})$$

$$w_k = s_{r,max} * (\epsilon_{sm} - \epsilon_{cm})$$

$$s_{r,max} = K_3 * C + K_1 * K_2 * K_4 * \Theta / \rho_{p,eff}$$

$$\epsilon_{sm} - \epsilon_{cm} = \frac{\left(\sigma_s - K_t * \left(\frac{f_{ctmeff}}{\rho_{peff}}\right) * (1 - \sigma_s * \rho_{peff})\right)}{E_s} > 0,6 * \sigma_s * E_s$$

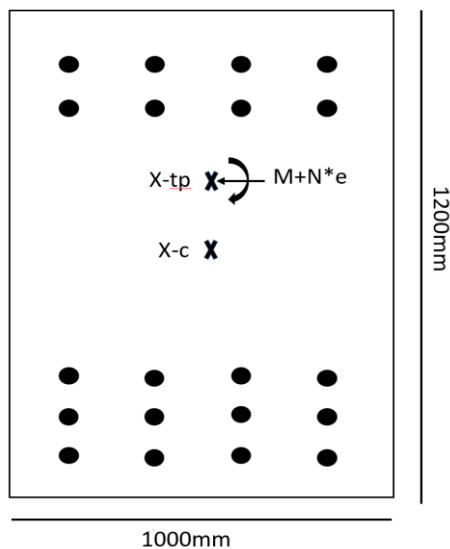
k1	k2	k3	k4
8,00E-01	5,00E-01	2,24E+00	4,25E-01

$$h_{eff} = \min\left(2,5 * (h - d), \frac{h - x_{tp}}{3}, \frac{h}{2}\right)$$

h-eff [m]	c [m]	Θ [m]	ρ-p,eff	Ac,eff [m^2]
2,92E-01	1,25E-01	4,00E-02	3,87E-02	2,92E-01

fctm,eff [Mpa]	kt	ε,sm - ε,cm	Wk [mm]
3,50E+00	4,00E-01	1,12E-03	5,10E-01

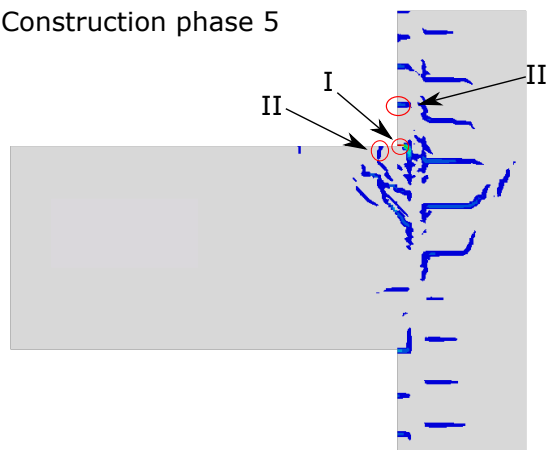
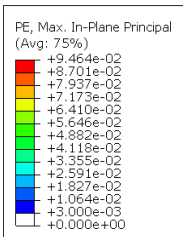
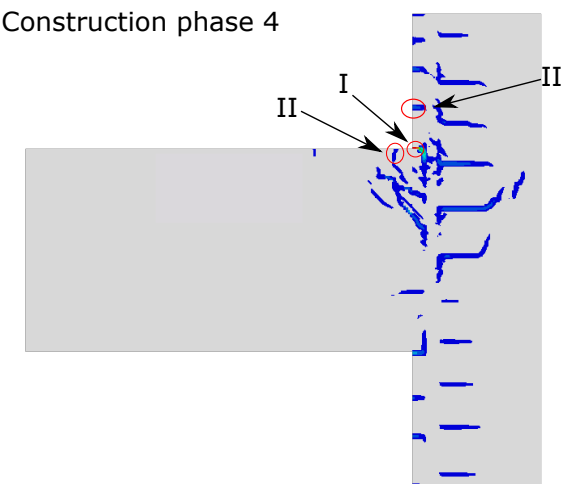
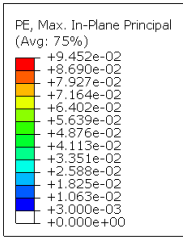
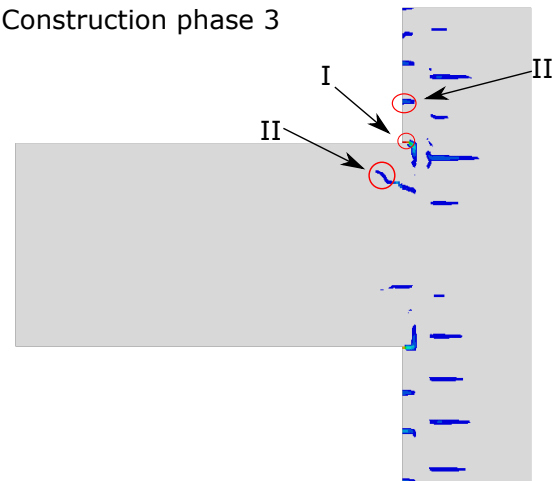
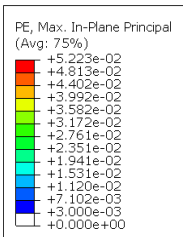
$$\epsilon_{sm} - \epsilon_{cm} > 0,6 * \sigma_s * E_s \quad \text{ok}$$



H

Appendix H

H.1 Plastic strain in local model



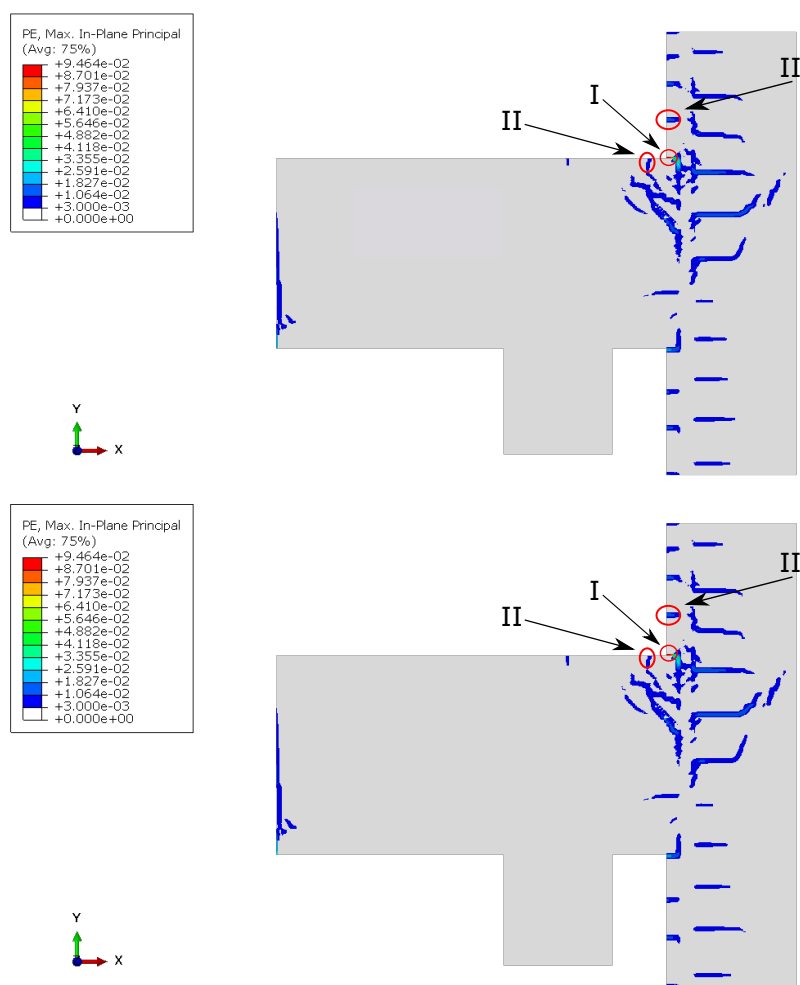


Figure H.2: Plastic strain in submodel in construction phase 6-7

H.2 Compression stress in concrete in local model

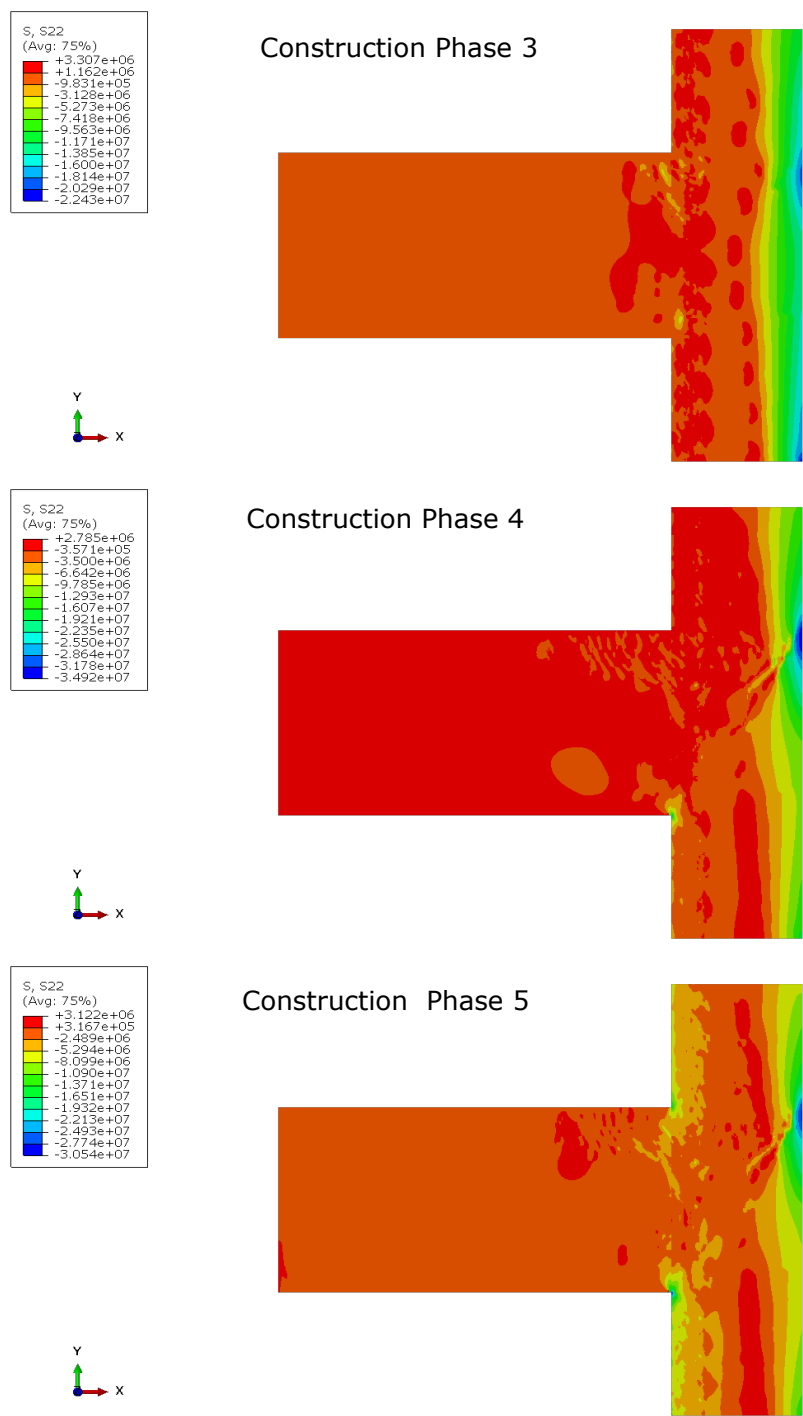


Figure H.3: Compression stress in concrete in construction phase 3-5

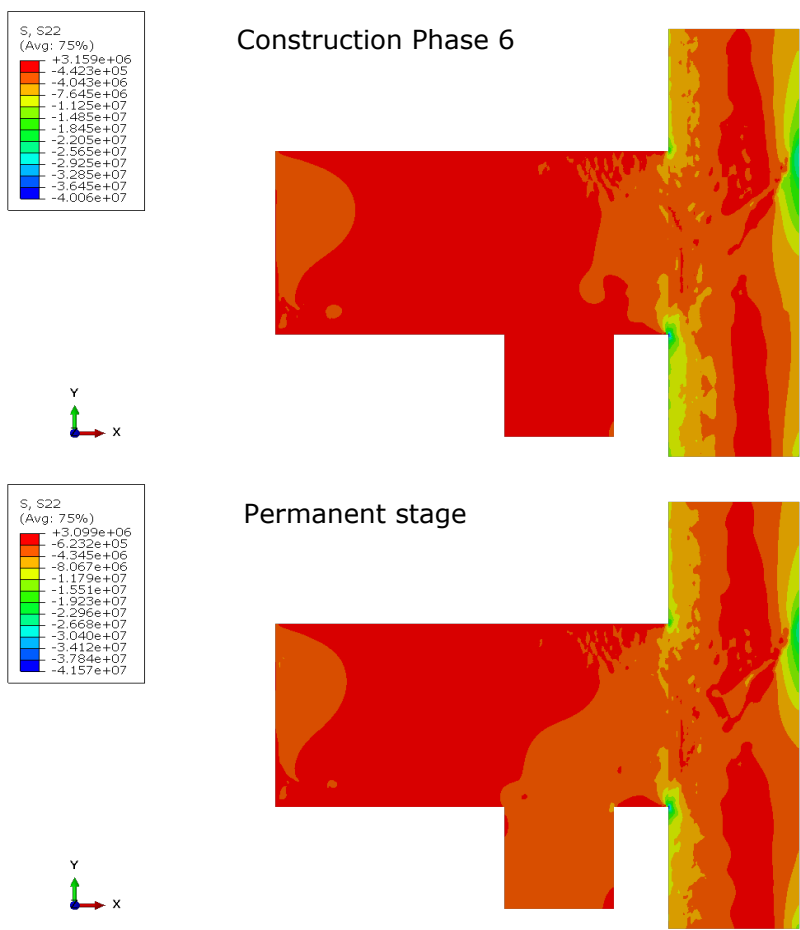


Figure H.4: Compression stress in concrete in construction phase 6-7

H.3 Tensile stress in reinforcement in local model

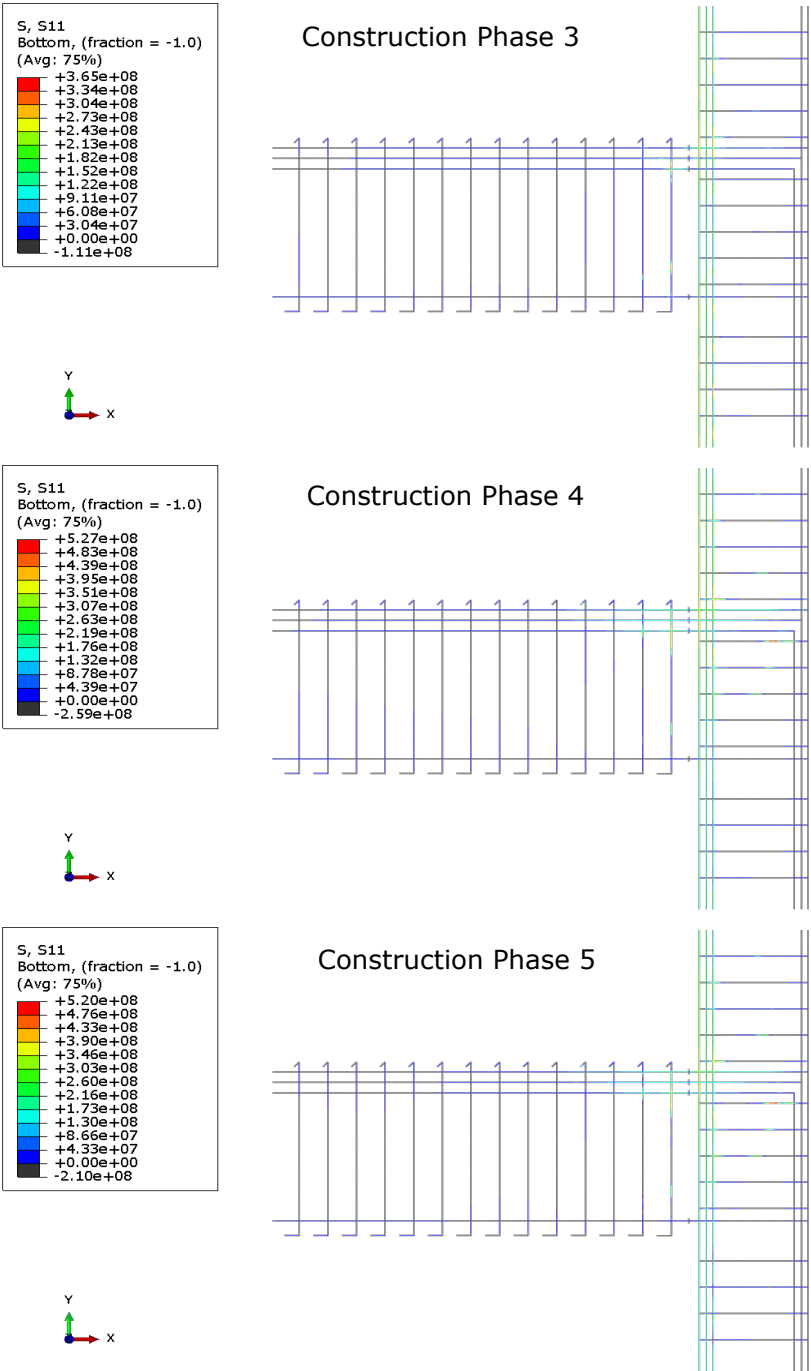


Figure H.5: Tensile stress in reinforcement in construction phase 3-5

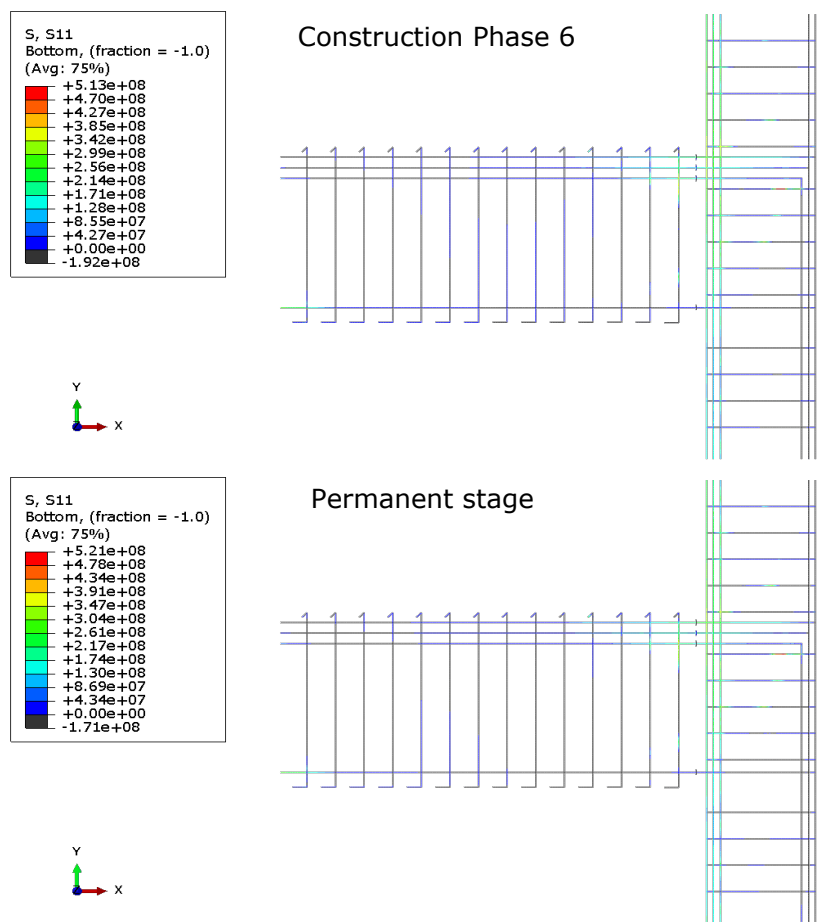


Figure H.6: Tensile stress in reinforcement in construction phase 6-7